The semiconducting properties of HgTe – In(_2)Te(_3) and related alloys

Peter.M. Spencer

The Semiconducting Properties of HgTe - In_2Te_3

and Related Alloys

by

Peter M. Spencer, B.A. (Oxon).

Thesis submitted for the degree of Doctor of Philosophy

Faculty of Science

University of Durham

1963

Copy number 5.

Contents

Chapter II

Previous Studies on Materials

Chapter III

Apparatus and Experimental Technique

Chapter IV

The Properties of HgTe - In_2Te_3 and Related Alloys

Acknowledgements

The work presented in this thesis forms part of a programme of research carried out under contract from A.E.R.E. Harwell, whose staff have allowed much freedom in the choice of subject matter. I am grateful to Professor D.A. Wright for his continued guidance and encouragement, and for the use of the facilities in the Department of Applied Physics.

I have drawn greatly on the knowledge and experience of members of the Department, all of whom have made themselves readily available. Dr. B.R. Pamplin provided many of the initial ideas and saw to the construction of much of the apparatus. During the final year I have had many interesting and useful discussions with Dr. W. Giriat of the Institute of Physics, Polish Academy of Sciences, who also performed the electrical measurements at low temperature.

The greater part of the apparatus was constructed in the department workshop under the direction of Frank Spence, without whose care and skill the work would not have been possible. The thesis was typed by Miss Patricia Hall and duplicated by the dye line process in the Department of Geography.

Introduction

The thesis is concerned with the effects of alloying the defect structure semiconducting compound indium sesquitelluride, In_2Te_3, which has a low electronic mobility and an energy gap of about 1.1 eV., with the zinc blende semi-metal, mercury telluride, HgTe. A phase diagram is proposed for the alloy system and the electrical, optical and thermal properties for the main phases are discussed with reference to the structural ordering which occurs at some of the compositions.

A comprehensive review of the properties of HgTe is presented in the second chapter. Single crystals of this compound have been produced using the standard techniques, but the electrical properties are peculiarly sensitive to the previous heat treatment in mercury vapour to which the samples have been subjected. Electronic mobilities of up to 73,000 $cm^2/V.sec.$ at 77^oK have been recorded recently in appropriately annealed samples. The high number of carriers at room temperature and at 4.2^oK have led several workers to believe that HgTe is a semi-metal with an overlap in energy between the conduction band and a valence band. Effective mass data obtained from cyclotron resonance and other experiments have been interpreted on the basis of this band structure which includes a non-parabolic conduction band. Many of the results quoted in the literature on this compound are open to query on the grounds that the material had not been annealed to produce stoichiometry. Until the measurements have been repeated on single crystals in which the electronic mobility is at the maximal value, the results must be considered tentative.

In comparison, far less work has been performed on In_2Te_3. Large single crystals have not been obtained and there is considerable disagreement between the results quoted for different samples. Subjected to the correct heat treatment the vacancies form an ordered superstructure. This ordering produces changes in the energy gap, the electronic mobility and the thermal conductivity.

Chapter II also contains a review of previous work on the system HgTe - In_2Te_3, and includes a copy of a paper presented at the Exeter Conference on the Physics of Semiconductors which forms part of the original work of the thesis. In this paper the preliminary measurements on an early batch of samples are given but are not sufficiently complete to enable any conclusions to be drawn.

The greater part of the original work of the thesis is presented in chapter VI. After a short discussion of the ternary phase diagram Hg-Te-In/Ga, a phase diagram for the pseudo-binary system Hg_3Te_3 - In_2Te_3 is proposed on the basis of X-ray and optical examination of the samples, which were made up every 5 molecular per cent (mpc) variation in composition and annealed for 60 days at 600°C. The HgTe - type phase changes at about 15 mpc. In_2Te_3 to a semiconducting phase of the same structure, which is often obtained p-type, with an energy gap of 0.3 eV. Ordered compounds, possibly peritectic, occur at $Hg_5In_2Te_8$ and $HgIn_2Te_4$, and there is a disordered compound $Hg_3In_2Te_6$, corresponding to the 50 mpc. composition, which may represent the maximum in the solidus.

The results of the optical, electrical and thermal measurements are discussed in terms of this phase diagram. Since both p- and n-type

materials were produced, values for the mobilities, effective masses and intrinsic carrier concentration have been calculated using the model of the simple energy band semiconductor which is discussed in chapter I. The effects of ordering in the system are considered and the thesis ends with a discussion of compounds of the type $II_5 III_2 Te_8$ some of which have the ordered structure.

The third chapter contains a description of the apparatus, much of which was constructed on the premises, and the experimental techniques. The accuracy of the measurements is also considered. The thesis opens with a review of the relevant chemical and semiconductor physics.

Group Period	I	II	III	IV	V	VI	VII	VIII
1	H							He
2	Li	Be	B	C	N	O	F	Ne
3	Na	Mg	Aℓ	Si	P	S	Cℓ	Ar
4	Cu	Zn	Ga	Ge	As	Se	Br	Kr
5	Ag	Cd	In	Sn	Sb	Te	I	Xe
6	Au	Hg	Tℓ	Pb	Bi	Po	At	Rn

Table 1.

The B Sub-group of the Periodic Table of Elements.

CHAPTER I

RELEVANT SEMICONDUCTOR PHYSICS

1.0 Chemical Bonding and Structure of Semiconductors

The fundamental tendency in the binding of atoms into solids is to form closed shells of electrons similar to those of the inert gases. It is largely therefore the numbers of electrons in the outermost shells of the free atoms which determine the nature of the bonds in the solid state. Of the four types of bond (1), the two which play important, though not exclusive, roles in the structure of semiconductors are the ionic and the covalent or homopolar bond. The van der Waals or residual bond is found in certain anisotropic semiconductors, for instance Te and Bi_2Te_3 (2).

1.1 The Ionic Bond

To achieve the stable configuration of eight electrons in the outer shell it is common for atoms of group I in the periodic table of elements to yield their outermost electrons to atoms of group VII, thus creating ions whose electrostatic attractions provide the binding forces. The types of crystal structure associated with ionic bonds are typified by Caesium Chloride, bodycentred cubic, where the ions are of similar size, and Sodium Chloride whose unequal ions must form the more open structure of the simple cube. The latter structure is found in some semiconductors notably the sulphide, selenide and telluride of lead which in this context

behaves as a group II element. The bonding for these compounds is not completely ionic, the effective charges being about 1.5e (3).

1.2 The Covalent Bond

The structures of the majority of semiconductors indicate that the bond is predominantly of a different nature. An atom may also obtain the inert gas configuration by matching its unpaired electrons to valence electrons of the opposite spin belonging to similar atoms. Thus there is a covalent bond between the two atoms in the chlorine molecule, in which the third 3p electrons are shared to form the closed shell configuration similar to that of Argon. The total number of such bonds that an atom can make is 8 - N where N is the group number.

The ground state of the group IV atoms has only two unpaired electrons, but the atoms form four bonds when in the slightly higher sp^3 hybrid state where there is one unpaired electron in the s state and three in the p state. The atom binds itself to four other atoms situated at the corners of a regular tetrahedron as in figure 1.

The covalent crystal formed by such bonds is best thought of as two interpenetrant face centred cubic sublattices shown in figure 2.

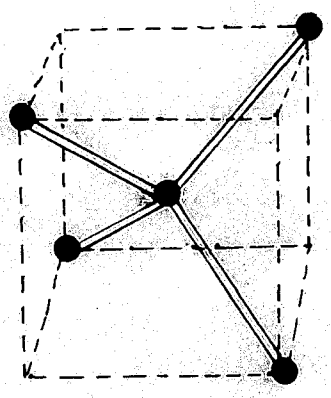

Fig.1. Covalent Bonds in a Group IV Solid.

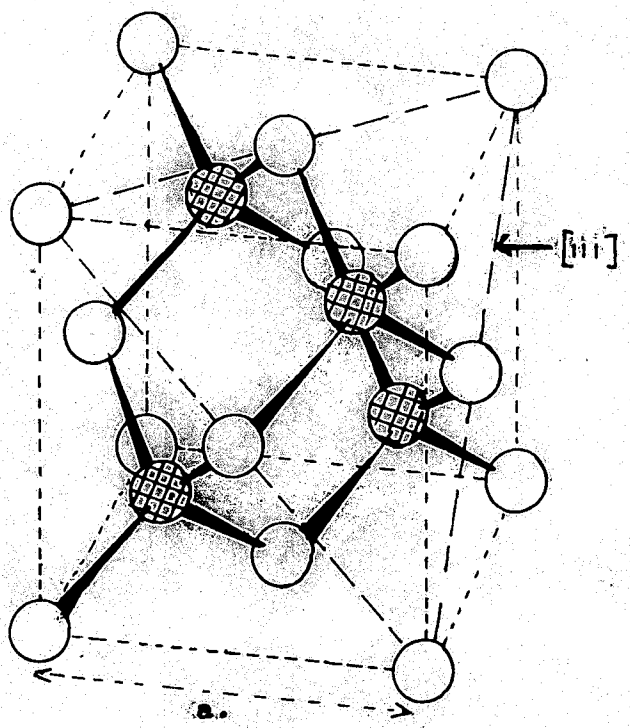

Fig.2. The Zinc Blende Structure.

This structure is formed by diamond, silicon, germanium, and the grey phase of tin, all of which may be classed as semiconductors, though diamond appears as an insulator at ordinary temperatures.

1.3 Mixed Bonds

The zinc blende or sphalerite structure, Figure 2, derived from that of diamond, is found in a large number of semiconducting

compounds in which the number of electrons per crystal site, averaged throughout the lattice, is four. Compounds obeying this rule may be of the type AB where A and B may be elements from groups III and V, II and VI or I and VII respectively, or of the more complicated type $III_2 \square VI_3$ where $\square$ denotes a lattice site not occupied by an atom. In general, each of the two face centred sublattices are occupied by atoms from different groups though for the defect type of compound one in three of the metallic sublattice sites is vacant.

The character of the bonds in the zinc blende structure is partly ionic and partly covalent. In order to maintain the sp^3 hybrid configuration necessary to the covalent bond in this context, the appropriate number of p electrons must be transferred from one type of atom to the other, thus introducing a degree of ionicity into the bond.

A structure closely related to zinc blende is hexagonal wurtzite. This is formed by a number of II-VI and V-III compounds notably ZnS and CdS, both of which are polymorphous, having the zinc blende structure in the low temperature phase. The two polymorphs of such a compound have similar interatomic separations and binding energies so that the semiconducting properties are also similar. The difference between the two structures lies mainly in the number of second nearest neighbours. The bond in wurtzite is also slightly more ionic in character.

The particular structure assumed by this type of compound depends mainly on two factors: the removal of the group of either element away from group IV in the periodic table and the radius of the ions involved (1). It must be stressed, however, that in semiconductors the nature of the bond is of greater importance than the crystal structure. Mooser and Pearson define a type of bond which appears to be necessary to semiconductors (4). It is predominantly covalent in character, but only anions need acquire filled valence subshells provided that cation-cation bonds do not run continuously through the crystal. A generalisation of the eight electron rule provides a means of predicting new semiconducting compounds more successfully than band calculations in which the emphasis is on crystal symmetry.

Recent work, reported by Kleinman (5), concerning the charge density of bonds in diamond and the bending of bonds in Si, gives considerable insight into the nature of the covalent bond.

2.0 The Chemical Approach to Energy Gap

When all the valence electrons are used to form covalent bonds in a semiconductor, the valence band is said to be filled and no electrons are available for conduction. This is represented diagrammatically in figure 3(a), where the double lines indicate covalent bonds. However, although the energy needed to free a bonding electron may be large compared to the thermal energy kT, quantum mechanical considerations show that, at any temperature

some bonds will be broken. The freed electron may then migrate through the crystal under the influence of an applied electric field and give the appearance of a moving negative ion, and the vacancy in the bond may be filled successively to give the appearance of a moving positive ion as in figure 3(b). Thus conduction is possible and the energy needed to break a bond represents the energy gap between the valence and conduction bands.

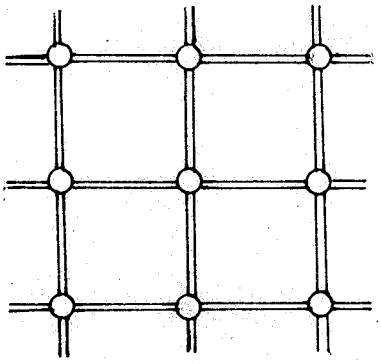

Fig.3(a). Schematic Representation of Covalent Bonds in a Group IV Solid.

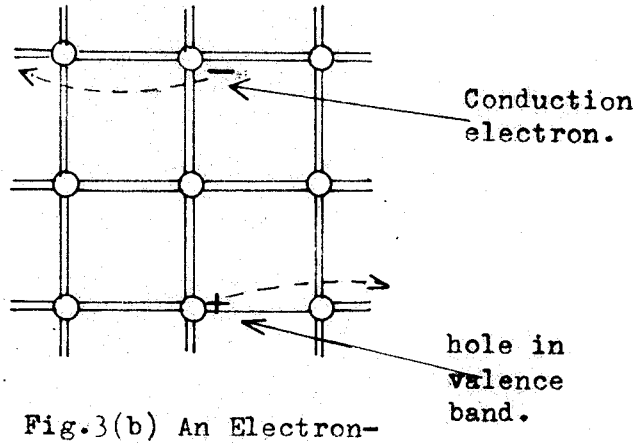

Fig.3(b) An Electron-hole pair.

Another view of the energy band structure is obtained by considering the bringing together of mutually independent atoms to form a solid. This is shown diagrammatically in figure 4 for a hypothetical element.

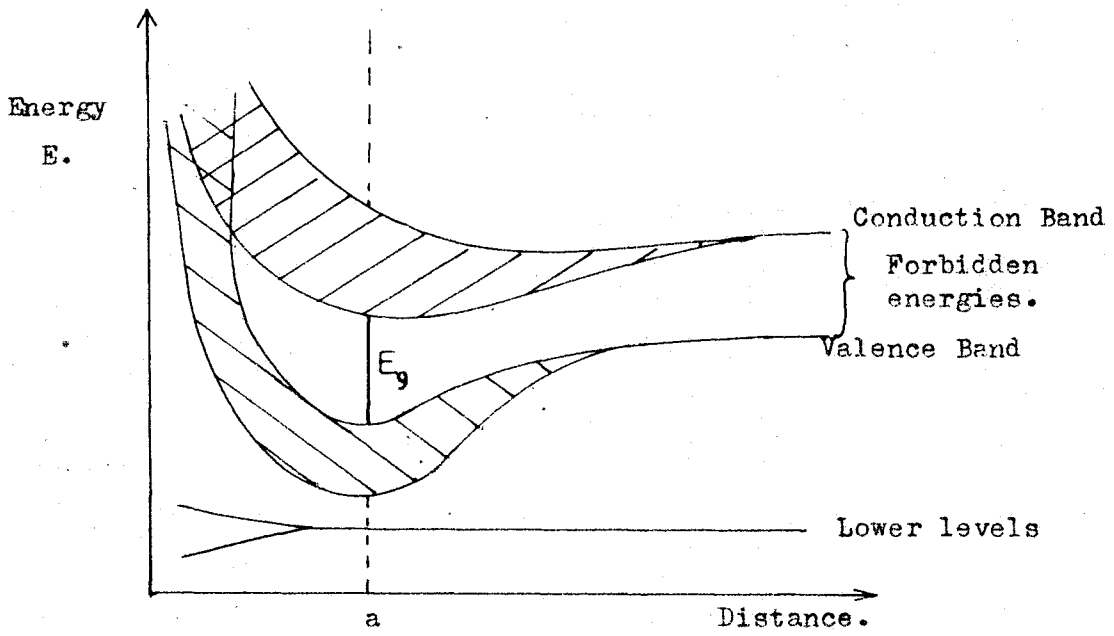

Fig.4. Energy Levels v. Interatomic Distance.

The discrete energy levels of electrons in the independent atoms must be split into bands each of which contain 2N separate energy states, where N is the number of atoms in the crystal. These bands of allowed energy levels widen with decreasing interatomic distance but will, at first, be separated by an energy gap. Where the valence band contains 2N electrons and the next band is unoccupied except for electrons exited from the valence band, the crystal that is in equilibrium at this separation, will be a semiconductor or an insulator depending on the magnitude of the energy gap. At a smaller separation the bands may overlap so that electrons from the valence band may remain permanently in the upper band. Such a material is a

semi-metal. In metals such as the alkali metals one band is only half filled with electrons and the upper bands also overlap. Diagrams similar to that of figure 4 have been computed for a number of elements and are discussed by Slater (6) with particular reference to sodium and diamond.

2.1 The Chemical Approach to Impurities

The properties of semiconductors are greatly influenced by defects from the perfect lattice. They may be of substitutional or interstitial atoms, vacancies in the lattice, surface atoms, or dislocations. The weakened bonds thus introduced provide more electrons for conduction at a given temperature than the perfect lattice. A well known example is provided by the substitution of group V atoms in germanium and silicon. Because of the high dielectric constant of these materials, the extra electron on such an impurity is easily removed and becomes a conduction electron without leaving a vacancy in the covalent bond, although the impurity atom, now ionised, remains a scattering centre in the lattice. Similarly, group III impurities create vacancies in the valence band.

It is common to represent such impurities as introducing energy levels within the energy gap in the manner of figure 5 in which energy is plotted against distance through the crystal.

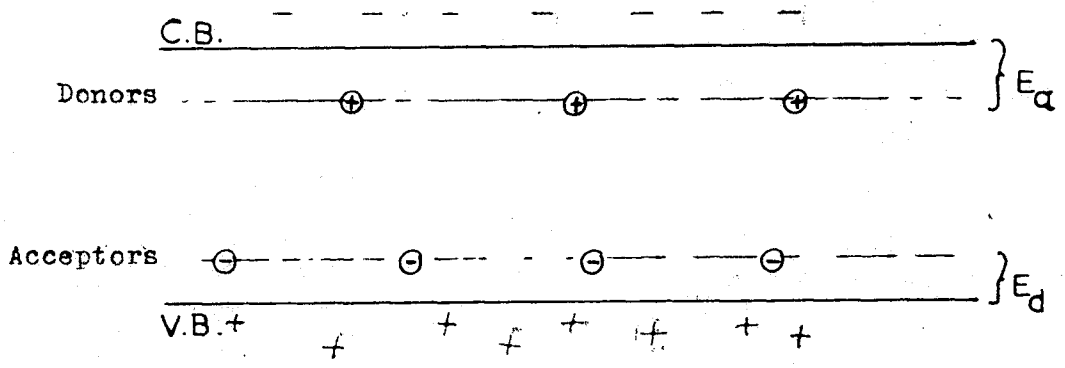

Fig.5. Impurity Energy Levels in a Semiconductor.

A survey of semiconductor chemistry, containing a discussion of the effects of departures from the perfect crystal lattice, is presented by several authors in reference 7.

3.0 Band Structure

Semiconducting properties are generally described in terms of the energy levels allowed to the outermost electrons of the atoms in the solid. The quantum mechanical theory of these levels becomes extremely complicated for even the simplest crystal structure so that the general approach to the energy band structure is empirical. In this section, however, it will be necessary to outline the fundamentals of the theory and introduce terms that will be used later in the text. Fuller treatment of the problem particularly for semiconductors is found in reference 8.

The model of the solid used for the simple theory is one in which the electrons are considered as moving independently of each other in a perfect periodic lattice. The motion of each electron is governed by the Schrödinger equation

$$\nabla^2\psi + \frac{8\pi^2 m}{h^2}[E - V]\psi = 0 \qquad \ldots\ldots 1.$$

where ψ is the wave function for an electron of mass m and energy E, and V is the potential energy due to the crystal lattice. In the model used by Sommerfeld (3.P23) the crystalline potential was averaged out so that electrons were bounded only by the surface of the solid. Considerable understanding of the motion of electrons was gained from this approach and the idea that electrons are free to move independently of the crystal lattice was introduced into the model proposed by Bloch, which took into account the periodic nature of the crystal potential. V then becomes

$$V(\underline{x}) = V(\underline{x} + \underline{d}) \qquad \ldots\ldots 2.$$

where $\underline{x}$ is the vector position of the electron and $\underline{d}$ any vector whose components along any one of the three crystal axes X_r, $r = 1,2,3$, is an integral factor of the periodic spacing d_r along that axis.

Bloch showed that the solution of the Schrödinger equation could be written in the form

$$\psi(\underline{x}) = U_k(\underline{x}) \exp [i(\underline{k}.\underline{x})] \qquad \ldots\ldots 3.$$

where U_k is a function with periodicity of the lattice and $\underline{k}$ is a constant vector whose three components along the axes may be thought of as quantum numbers for the electron. The vector $h\underline{k}/2\pi$ is called the crystal momentum by analogy with the momentum $h\underline{k}/2\pi$ in the solution for the free electron. The energy E is an even function of $\underline{k}$ and is periodic such that the periodicity for any one component k_r is $2\pi/d_r$.

The components of $\underline{k}$ define k-space. Because of the periodic nature of E, it is usual to confine the discussion to the first Brillouin zone centred on the origin in k-space, which contains all non-equivalent values of $\underline{k}$. Distances in k-space are reciprocal to those in the crystal so that the zone is known in terms of the crystal structure.

The exact form of the energy function in general is too difficult to evaluate, but it is apparent from even the simplest form of a periodic potential, that of a square wave, that there are values of E which can be obtained only from imaginary values of k. This result corresponds to the idea of an energy gap from the chemical approach in section 2.0. It can also be shown (3.P30) that at the surface of a Brillouin zone the normal derivative $\partial E/\partial k_n$ is zero. Thus $E = f(\underline{k})$ may be represented schematically for a single direction in k-space as the curves in figure 6.

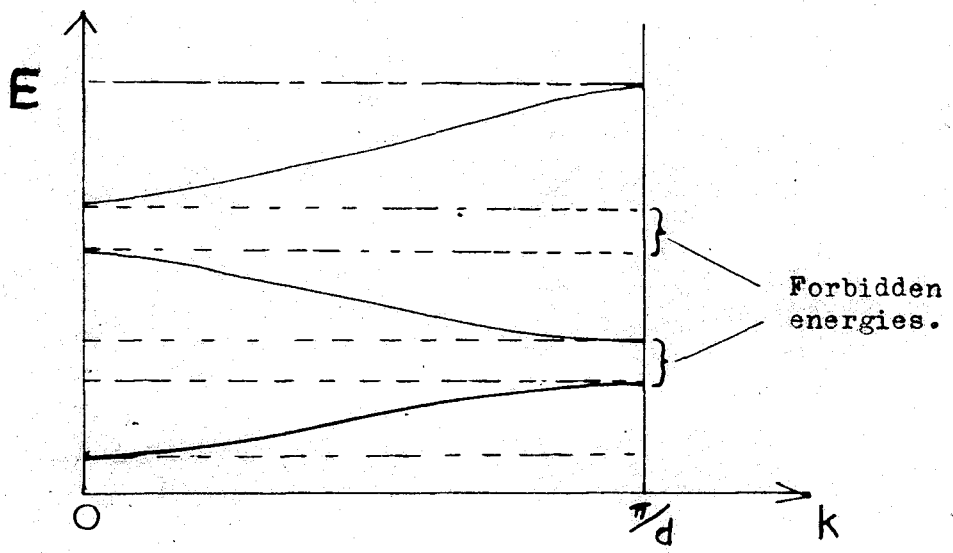

Fig. 6. Possible Variation of E with k.

Since E is an even function it is necessary to represent only one half of a period: the region to the left of the origin may be filled by the curves for some other direction in k-space.

The forms of the energy bands that have been empirically evaluated for actual semiconductors are generally complex. The following examples show some of the types that may arise.

In describing a large number of semiconducting properties it is necessary to know the form of the bands near their maximum or minimum only. Thus, if a minimum occurs at the origin of k-space in a cubic crystal the simplest form near the origin is

$$E(\underline{k}) = \frac{h^2}{8\pi^2 m_n} \Sigma\, k_r^2. \quad (r = 1,2,3) \qquad \ldots\ldots\ 4.$$

where m_n is a constant with the dimensions of mass and the zero for E is taken at the minimum.

This relationship differs from that for free electrons only in the magnitude of m_n. Bands of this nature are termed parabolic

and have spherical symmetry.

A maximum in a band is similarly represented by

$$E = -E_o - \frac{h^2}{8\pi^2 m_p} \Sigma k_r^2 \qquad \ldots\ldots 5.$$

In this situation the electrons behave as particles with negative mass. The combination of these two types of band in figure 7 gives the simplest possible configuration for the conduction and valence bands of a semiconductor.

No actual semiconductor has been found with this band structure, but it is usual to work on the basis of this simple energy band model until experimental results prove the contrary.

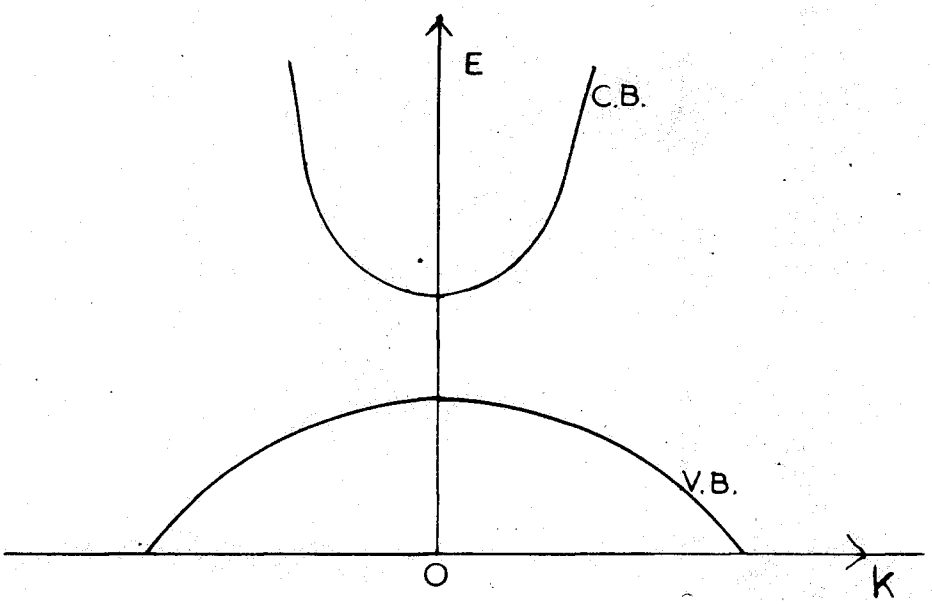

Fig.7. Model for Simple Energy Bands.

InSb is the only semiconductor in which it is well established that the minimum of the conduction band occurs above the maximum of the valence band at the centre of the zone. Its conduction band is however found to be non-parabolic.

Maxima or minima may also arise at other points in k-space, particularly at the zone boundary. The symmetry of the crystal then enables other extrema to be predicted. Expansions for E similar to equations 4 and 5 can be written down for each position where it may be necessary to use an effective mass m_n which varies with direction. Constant energy surfaces will in general no longer be spherical but ellipsoidal as in figure 8.

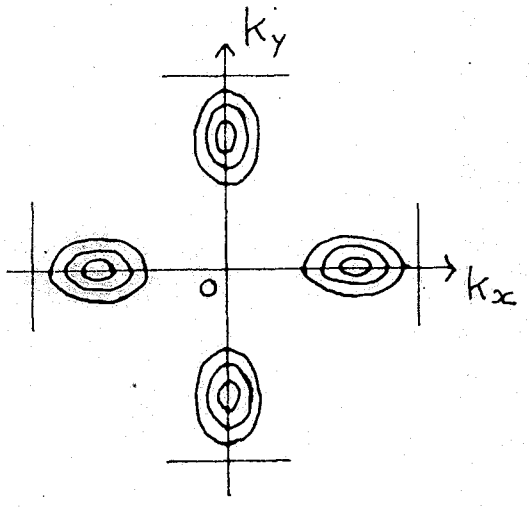

Fig.8. Ellipsoidal Energy Surfaces in k-space.

Where there are a number of such minima the band structure is termed multi-valley.

In the conduction band of germanium a minimum is believed to exist at the zone boundary in the <111> direction considerably below a subsidiary minimum at the centre of the zone above the valence band maximum. Predictions about the band structure for PbS (8.P291) show that the conduction band is lowest on the zone boundary in the <110> direction, but the valence band has a maximum at a point between the origin and the zone boundary. Band structures for other material are reported in references 3, 7, 9.

It is sometimes found that the valence band is not single but consists of two bands which are degenerate at their maxima at the centre of the zone. Different effective masses are ascribed to each degenerate band which may be termed the light and the heavy mass band respectively. Equation 5 indicates that the latter is the outermost band in the E(k) diagram.

In the band structure of true semiconductors the width of the energy gap between the valence and conduction bands determines many of the properties. Certain other material, notably the alkaline earth metals, HgTe and HgSe which will be discussed below, possess bands structure in which the valence band overlaps the conduction band in energy though the extrema may not occur at the same points in k-space. Under all conditions some electrons from the valence band will be in the conduction band and the material is termed a semi-metal.

Recent developments both in calculations on the band structure of materials and in experimental techniques are discussed in a review paper by Pincherle (10).

3.1 Effective Mass

The quantity m_n, the effective mass, introduced in equation 4 has become, due to the complicated nature of actual band structure, increasingly important in describing the motion of electrons. Moreover, deviations from the parabolic band are generally described in terms of variations in m_n whose value can be determined using the advanced technique of solid state cyclotron resonance.

The concept of effective mass arises by comparison with mass in Newton's second equation of motion. For a free electron moving with a velocity $\underline{v}$ and mass m_o

$$\underline{k} = \frac{2\pi m_o}{h} \underline{v} \qquad \ldots\ldots 6.$$

and in terms of the energy E of the electron the mass is given by

$$\frac{1}{m_o} = \frac{4\pi^2}{h^2} \frac{\partial^2 E}{\partial k^2} \qquad \ldots\ldots 7.$$

The effective mass for an electron in a crystal in general depends on the position in k-space and so is a second rank tensor defined by

$$\left|\left| \frac{1}{m_n} \right|\right| = \frac{4\pi^2}{h^2} \underline{\text{grad}}_k \cdot \underline{\text{grad}}_k \, E(k) \qquad \ldots\ldots 8.$$

For simple energy bands the quantity on the right reduces to that in equation 7. This implies that at the top of an energy band m_n is negative. However, since mass is conventionally positive and it is the transfer of energy in the conduction process which is important, the electrons at the top of the valence band are considered as having positive mass but positive charge. In the valence band, electrons can only move into sites made vacant by the excitation of other electrons to the conduction band or to impurity bands. These vacant sites appear to move through the crystal and give rise to the phenomena of positive hole conduction. A fuller consideration of the concept of effective mass particularly for deviations from the normal band structure is given by Krömer in reference 11.

The term effective mass arises in a number of other contexts where it is generally averaged over the three directions in k-space. The density of states effective mass for ellipsoidal constant energy surfaces is $m_d = (m_1 m_2 m_3)^{1/3}$ which must be multiplied by a factor $(N_V)^{2/3}$ where there are N_V similar valleys (12. P102). The conductivity mass m_c defined by

$$\frac{1}{m_c} = \frac{1}{3}\left(\frac{1}{m_1} + \frac{1}{m_2} + \frac{1}{m_3}\right) \quad (3.P99)$$

is also used under certain circumstances involving the relaxation time.

The effective mass may be determined from consideration of the Hall effect, or possibly the Seebeck effect, and the intrinsic carrier density. The theory used is generally that for simple energy bands where the effective mass is scalar.

By far the most accurate determination of both the effective mass tensor and the form of the band structure is obtained by observing cyclotron resonance. For very pure semiconductors, such as may be obtained in Ge and Si, with low carrier densities, the experiment is conducted at microwave frequencies. In order to overcome the short relaxation time due to impurity scattering in less pure materials, and the magneto-plasma effect due to high carrier densities, it is necessary to use infra-red radiation and strong magnetic fields. Measurements have been taken on a variety of semiconductors and metals, in particular on alloys of HgTe with other II-VI compounds which are discussed below.

A full account of the technique of cyclotron resonance is given by Lax and Mavroides (13), and a review of recent developments by Lax in reference 14.

4.0 Intrinsic Carrier Density

Assuming the existence of an energy gap it is then possible to calculate the number of electrons available for conduction. The problem is approached by the method of Fermi-Dirac statistics which is valid for particles obeying the Pauli Principle.

The probability that an energy level E will be occupied by an electron is given by

$$P(E) = f[(E - E_F)/kT] \quad (3\ P.74) \qquad \ldots\ldots 9.$$

where

$$f(x) = 1/(e^x + 1) \qquad \ldots\ldots 10.$$

is called the Fermi-Dirac function and E_F, known as the Fermi level, is equal to the value of the energy when the probability of occupancy is one half. For values of $x \gg 1$ the function approximates to e^{-x} and the probability approaches the classical value

$$P(E) = A \exp[-E/kT] \qquad \ldots\ldots 11.$$

where A is a constant.

In a simple energy band semiconductor it can be assumed that no electrons can occupy levels with energies in the forbidden gap E_g between the conduction band and the valence band. The lowest level in the conduction band may be conveniently taken as the zero of energy. If $N_c(E)dE$ is the density of allowed states between energy values E and E + dE for the conduction band then the density of electrons in the conduction band for the same energy range is given by

$$n(E).dE = 2\ N_c(E)\ P(E)\ dE \qquad \ldots\ldots 12.$$

where the factor 2 accounts for the degeneracy of electrons with opposite spins. The total number of conduction electrons is therefore

$$n = 2 \int N_c.(E).P(E)dE \qquad \ldots\ldots 13.$$

integrated between zero and the highest energy allowed in the conduction band. The function $N_c(E)\ dE$ is easily evaluated for the simple energy band structure (3 P.36) and is given by

$$N_c(E)\ dE = \frac{2\pi(2m_n)^{3/2}}{h^3} E^{1/2}\ dE \qquad \ldots\ldots 14.$$

The classical approximation may be used for the probability as in equation 11, provided $E - E_F \gg kT$, and ~~therefore~~ an upper integration limit of infinity ~~of impurity~~ is applicable.

$$n = 4\pi(2m_n kT/h^3)^{3/2} \exp\,[E_F/kT] \int_0^\infty x^{1/2}\ e^{-x}\ dx \qquad \ldots\ldots 15.$$

The integration is straightforward, giving

$$n = N_c \exp\,[E_F/kT] \qquad \ldots\ldots 16.$$

where

$$N_c = 2(2\pi m_n kT/h^2)^{3/2} \qquad \ldots\ldots 17.$$

A similar calculation for the valence band, the top of which has the energy $-E_g$, gives the number of holes as

$$p = N_v \exp\,[-(E_F + E_g)/kT] \qquad \ldots\ldots 18.$$

where

$$N_v = 2(2\pi m_p kT/h^2)^{3/2} \qquad \ldots\ldots 19.$$

Hence for intrinsic semiconductors where $p = n = n_i$ the Fermi level is given by

$$E_F = \frac{-E_g}{2} + \frac{3kT}{4} \ln[m_p/m_n] \quad \ldots\ldots 20.$$

Thus at low temperature the Fermi level is near half-way between the conduction band and the valence band but is displaced towards the lighter mass band at higher temperatures. The substitution of this value of E_F and the numerical constants in equations 16 and 18 gives

$$n_i = p_i = 4.82 \times 10^{15} T^{3/2} (m_n m_p/m_o^2)^{3/4} \exp[-E_g/2kT] \quad \ldots\ldots 21.$$

This equation may be used to determine the number of intrinsic carriers at a given temperature, although if little is known about the effective masses, only an estimate can be obtained. The variation of the intrinsic carrier density with temperature is of importance in the consideration of the electrical properties.

The integration of equation 13 cannot be performed for degenerate materials for which $E_F \gg -kT$ and the classical approximation is no longer valid. At room temperatures kT is about 0.025 eV which is considerably smaller than the gap for Ge, 0.67 eV, but of the same order as that for HgTe. An approximation for the integral has been proposed by Ehrenberg (15) which is valid up to about $E_F = 2kT$, above which it is necessary to use numerical methods (3 P.79).

4.1 Extrinsic Carrier Density

The presence of impurities in a semiconductor leads to energy levels within the energy gap. These may be of the donor or acceptor type depending on their positions relative to the bands: usually the effect of one type of impurity greatly exceeds that of any others. In figure 9 a possible distribution of energy states is shown.

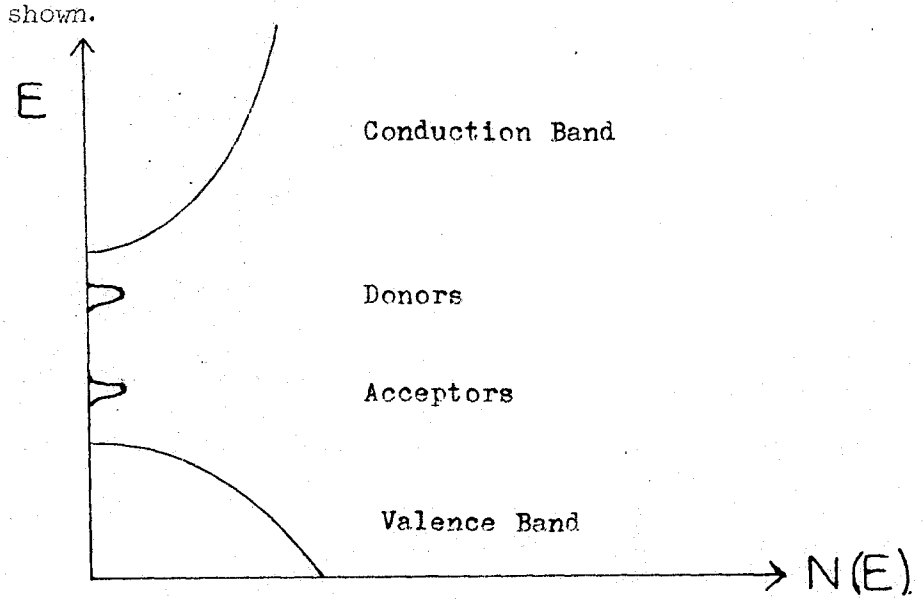

Fig.9 Density of States for an Impure Semiconductor.

Provided the electrons and holes in the material are not degenerate, the concentrations are still given by equations 16 and 18

$$n = N_c \exp [E_F/kT] \qquad \ldots\ldots 22.$$

and the product

$$np = N_c N_v \exp [-E_g/kT] \qquad \ldots\ldots 23.$$

is independent of the number of impurities and the Fermi level.

Since $n \neq p$, the Fermi level is no longer given by equation 20. If the number of carriers is measured, for instance by the Hall effect, then predictions concerning the Fermi level can be made. Assuming an effective mass ratio of unity, N_c at $T = 300^{\circ}K$ is about 2.5×10^{19} per cm^3. If E_F is more than kT below the conduction band, then n is less than 10^{19} per cm^3. This value of n may be taken as a criterion for non-degeneracy, although a small effective mass for a carrier naturally lowers the value of n.

The simplest example of doping may be considered when N_d donors per cm^3 lie at an energy E_d such that $E_d \ll E_g$. At low enough temperatures, electrons will be excited thermally from the donors to the conduction band according to

$$n = B \exp [-E_d/2kT] \qquad \ldots\ldots 24.$$

where B is a constant, until at a certain temperature all the donars are ionised. If n_i is still small compared to N_d then the number of carriers remains constant with temperature, as in a metal, until n_i becomes appreciable. This process is shown in figure 10.

The slope of the line at low temperature is $E_d/2kT$, and in the intrinsic range, $E_g/2kT$. A similar process is possible for p-type material with only acceptor impurities, N_a per cm^3.

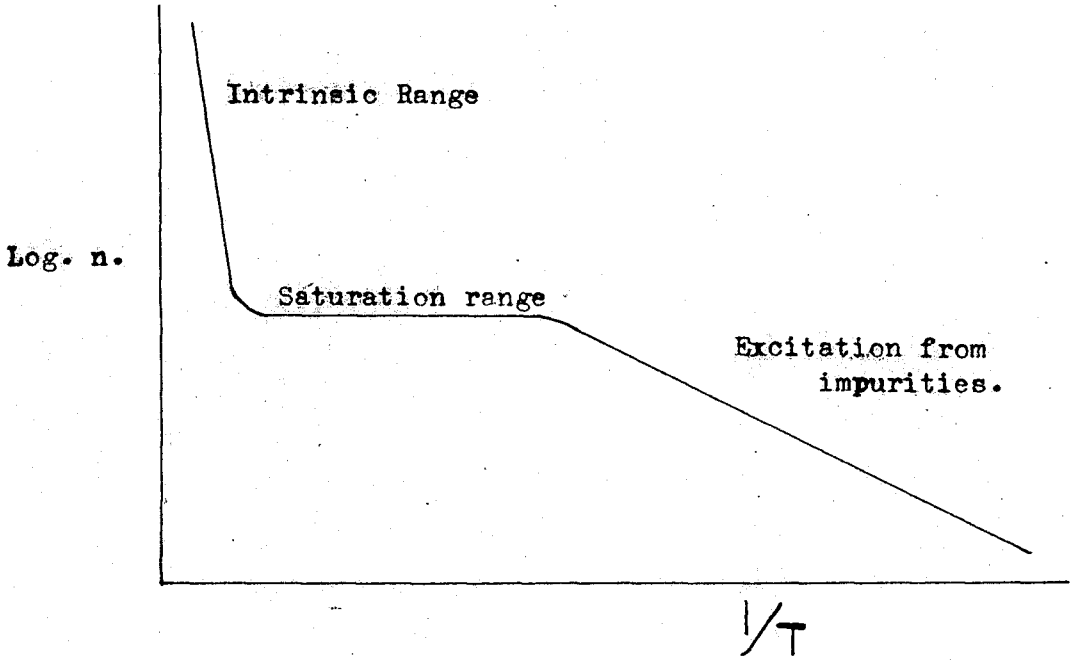

Fig.10 Variation of Carrier Density n with Temperature.

The Fermi level in an extrinsic semiconductor is a function of the difference between donor and acceptor concentrations and is shown in figure 11. (3 P.86).

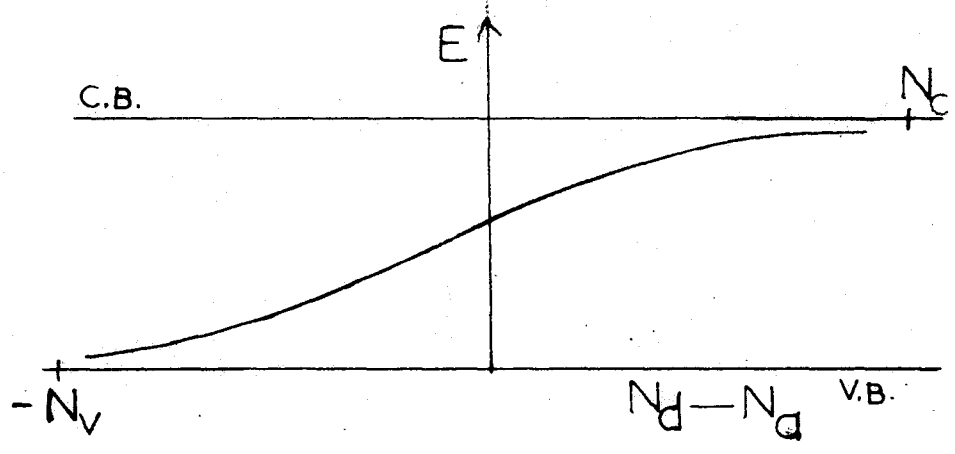

Fig. 11. Fermi Level v. Effective Impurity Concentration.

The above reference also provides a full discussion of the relations between the carrier densities and N_a, N_d and n_i.

A useful relation is easily obtained when the saturation carrier density q, of say p-type material, can be measured. For mixed conduction immediately before the intrinsic range, provided there is no other source of carriers, the number of holes is given by

$$p = q + n \qquad \ldots\ldots 25.$$

The product relation $pn = n_i^2$ is still valid.

5.0 Transport Phenomena in Semiconductors

The Pauli exclusion principle, applied to electrons in solids, implies that no two electrons of the same spin can occupy the same energy level within a band. Thus electrons can change their energy only if there are higher energy states vacant. A full valence band in a semiconductor, therefore, prohibits conduction unless some electrons have been excited into the conduction band or an impurity band, or electrons have been freed from other impurities, by a thermal or photo mechanism. Then all the holes in the valence band and all the electrons in the conduction band become current carriers.

The theory behind the various transport effects observed in semiconductors, generally derived from first principles, is available in standard texts. A concise account, together with extensive tables of formula is given by Putley (12). It is necessary to reproduce here the relevant expressions for mixed

and extrinsic conduction in simple energy band semiconductors and weak magnetic fields, and to indicate what can be obtained from them. The discussion will be restricted mainly to non-degenerate materials.

5.1 Conductivity and Hall Effect

The expression for the electrical conductivity is

$$\sigma = ne\mu_n + pe\mu_p \qquad \ldots\ldots 26.$$

where μ_n and μ_p are the mobilities of electrons and holes respectively, defined as the drift velocities per unit electric field.

If a magnetic field is set up perpendicular to the direction of the current flowing in a material, then an electric field is produced in the mutually perpendicular direction. This is known as the Hall effect. The Hall coefficient, R, is defined as the ratio of the Hall electric field to the product of the current density and the magnetic induction. In terms of the mobilities and carrier densities R is given by

$$eR = -r \frac{nb^2 - p}{(nb + p)^2} \qquad \ldots\ldots 27.$$

where the mobility ratio $b = \mu_n/\mu_p$ which is usually equal to or greater than unity, e the electronic charge and r a scattering factor that will be discussed below.

By convention, R is negative if electrons are the predominant carriers and positive for hole conduction.

For extrinsic conduction by electrons or where $b \gg 1$ in intrinsic material equation 27 may be approximated to

$$eR = -r/n \text{ or } n = -6.25r \times 10^{18}/R \quad \ldots\ldots 28.$$

There is a corresponding relation for holes.

The conductivity reduces to

$$\sigma = ne\mu_n \quad \ldots\ldots 29.$$

and the product

$$R\sigma = r\mu_n \quad \ldots\ldots 30.$$

is called the Hall mobility.

The intrinsic Hall coefficient is given by

$$eR = \frac{r(b - 1)}{n_i(b + 1)} \quad \ldots\ldots 31.$$

and the conductivity

$$\sigma = n_i e\mu_p (b + 1) \quad \ldots\ldots 32.$$

so that the product is

$$R\sigma = r(b - 1)\mu_p \quad \ldots\ldots 33.$$

If the value of n_i from equation 21 is substituted in equation 31 it is seen that

$$RT^{3/2} = D. \exp [-E_g/2kT] \quad \ldots\ldots 34.$$

where, provided b does not vary greatly, D is a constant. From the gradient of a graph of log $RT^{3/2}$ against 1/T the value of the energy gap is obtained.

Considerable information can be obtained from the variation of R with T for p-type material in the manner shown in figure 12.

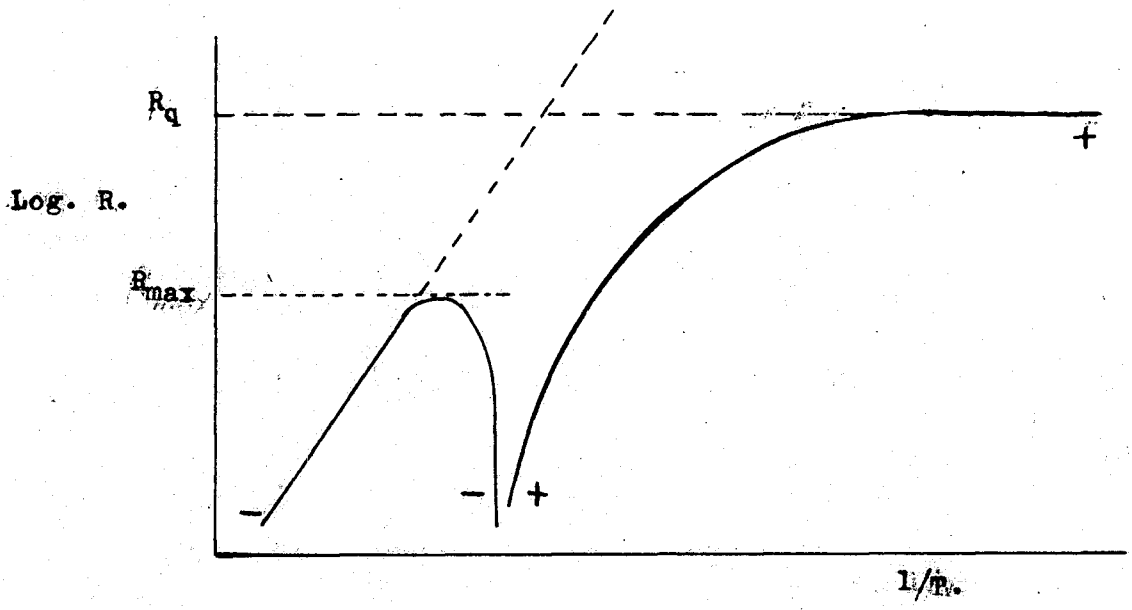

Fig.12. Hall Coefficient for p-type material.

The constant value of R_q at low temperatures yields the saturation carrier density q. In the intrinsic range R is negative since $b > 1$, and decreasing. The negative maximum in R can be shown by differentiation of equation 27 to occur when

$$(b - 1)n = q \qquad \ldots\ldots 35.$$

Hence the mobility ratio at the Hall maximum is obtained in terms of the two Hall coefficients from the relation

$$4bR_{max} = (b - 1)^2 R_q \qquad \ldots\ldots 36.$$

In the evaluation of the quadratic the positive sign is taken to obtain values of $b > 1$.

Assuming b does not vary much the values of the mobilities in the intrinsic range can be calculated from equation 33.

Since both n and p can be evaluated at the position of the Hall maximum, the intrinsic carrier concentration can be calculated and compared with that obtained from the energy gap by means of equation 23 to predict values of the effective mass product $m_n m_p / m_o^2$.

5.2 Variation of the Hall Effect with Induction

The exact expression for the Hall coefficient (12 P.119) indicates that in the region where the effect changes sign for p-type materials, there should be appreciable dependence on the magnetic induction, even if this is not large. The predicted effect has been observed for InSb (9.P.152). Disagreement between results and the simple theory for Ge led to the discovery of the lighter mass valence band (12.P.120).

5.3 Seebeck Effect

If two dissimilar materials A and B are joined in the sequence B-A-B and the two junctions so formed are maintained at temperature differing by $\delta T^{o}C$, then an open circuit voltage, known as the Seebeck voltage, is established across the two thermojunctions. The differential Seebeck coefficient α for the two materials is defined from the magnitude of the voltage δV, by the relation

$$\alpha = \delta V / \delta T$$

in the limit as δT approaches zero. In order to obtain the absolute Seebeck coefficient for material A it is necessary for that of B to be zero. This is so if B is in the superconducting state. Once absolute values have been obtained at low temperatures, it is possible to extend them to higher temperatures without the use of materials with zero Seebeck coefficient.

The absolute Seebeckcoefficient for semiconductors is usually much larger than that for metals. Therefore if B is a metal and A a semiconductor only a small correction is needed to account for the metallic component of the Seebeck coefficient. A good qualitative discussion of the Seebeck coefficient for metals and semiconductors is given by Ioffe (17.P.299).

For mixed conduction the Seebeck coefficient is given by (3.p.173)

$$\alpha = -\frac{k}{e}\left[\frac{nb(\frac{5}{2} - s + \eta) - p(\frac{5}{2} - s + \eta')}{nb + p}\right] \quad \ldots\ldots 37.$$

where η and η' are the reduced Fermi energies as shown in figure 13, and taken as positive quantities when the Fermi level lies in the energy gap.

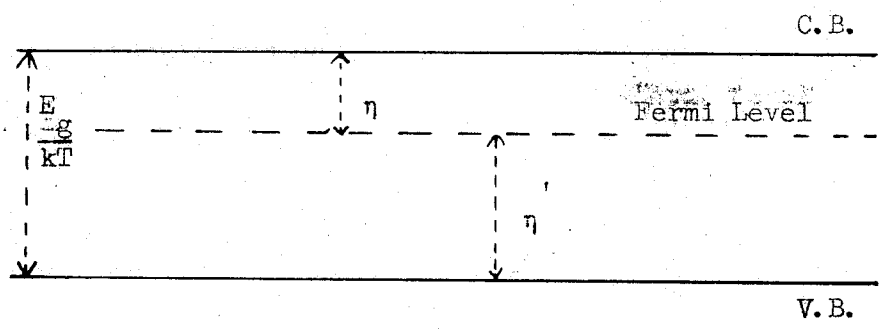

Fig. 13. Reduced Fermi Levels.

The Seebeck coefficient by convention is negative when electrons are the predominant carriers. The parameter s, which will be discussed below, has the value 1/2 for lattice scattering.

For extrinsic material α reduces to the simple relation

$$\alpha = -86.5\ (2 + \eta)\ \mu V/^{o}C \qquad \ldots\ldots\ 38.$$

where numerical values have been inserted. Hence the Fermi level may be calculated. Using equation 23 for the extrinsic carrier density, and the Hall coefficient, an idea of the effective mass can be obtained.

In p-type material the Seebeck coefficient changes sign when approximately $p = bn$ which is close to where the Hall effect is a maximum.

The intrinsic Seebeck effect may also be used to obtain further information about the effective mass ratio.

5.4 Relaxation Time, Mobility and Scattering Mechanisms

To account for the effects of scattering mechanisms transport phenomena are described formally in terms of a relaxation time and mean free path of electrons. According to the Bloch theory, the mean free path in perfect crystals is limited only by the dimensions of the crystal, so that in actual materials scattering is caused by departures from perfection in the lattice described in section 2.1 and by lattice vibrations. Most scattering processes have been considered in some detail in the literature. A good summary of the

theory is given by Smith (3) and a discussion by Putley (12). A summary of the relevant types of scattering is given below.

In general, the relaxation time τ, can be described by the equation

$$\tau = a\, E^{-s} \qquad \ldots\ldots 39.$$

where a is a constant and s is the scattering parameter. The conductivity mobility in terms of τ is

$$\mu_{ce} = \frac{e\langle\tau\rangle}{m_n} \quad (3.\ \text{P.111}) \qquad \ldots\ldots 40.$$

and the Hall mobility

$$\mu_H = \frac{e\langle\tau^2\rangle}{m_n\langle\tau\rangle} \qquad \ldots\ldots 41.$$

where $\langle\tau\rangle$ is the average relaxation time.

In order to evaluate these it is necessary to know the value of s. The relation between the two mobilities may be written $\mu_H = r\,\mu_{ce}$. Constant relaxation time is found in metals and highly degenerate semiconductors, where r = 1.

5.5 Lattice Scattering

If it is assumed that the energy lost in a collision is small, then interactions between electrons and phonons are restricted to the low energy of acoustic modes of vibration of the lattice. The problem has been considered from various approaches, all of which predict a value of 1/2 for s, r equal to $3\pi/8$ and a mobility proportional to $T^{-3/2}$. Lattice scattering is naturally predominant in extremely pure semiconductors and at high temperatures in less pure materials. It is generally assumed when there is no other information

available about the scattering. Departures from this variation for the mobility, as have been observed in pure Ge and Si, indicate that the multi-valley band structure must be taken into account. Scattering may also be affected by the more energetic optical modes of vibration, for which $s = -1/2$, or mutually by electrons.

5.6 Impurity Scattering.

The principal scattering mechanism due to physical defects in the crystal is that of ionised impurities, particularly so in doped materials. It is found that mobilities associated with this form of scattering vary as $T^{3/2}$. The value of s is $-3/2$ and that of r is 1.93.

Neutral or unionised impurities are found to have little effect on the temperature variation of the mobility, though in general, the addition of such impurities lowers the value of the mobility.

When several scattering mechanisms are combined, it is frequently assumed that a separate relaxation time can be calculated for each and the effective value found by reciprocal addition.

5.7 The Nernst Effect.

Of the thermomagnetic effects, the Nernst is usually the easiest to measure. It is the thermal analogue of the Hall effect: electrons tending to diffuse down a temperature gradient are deflected by a transverse magnetic field to produce a mutually perpendicular electric field. The sign of the Nernst coefficient

depends, not on the type of carrier, but on the scattering mechanism prevailing. It is positive for ionized impurity scattering and negative for lattice scattering.

5.8 Thermal Conductivity

The thermal conductivity K of a semiconductor consists of two major components such that

$$K = K_\ell + K_e \qquad \ldots\ldots 42.$$

where K_ℓ is the lattice component and K_e the component due to the current carriers. A full consideration of thermal conduction in semiconductors is given by Drabble and Goldsmit (18).

K_ℓ is a property of the lattice at the particular temperature and an expression for it is obtained by considering the propagation and scattering of phonons in the lattice.

For extrinsic semiconductors K_e is directly related to the electrical conductivity by an extension of the Wiedemann-Franz Law for metals

$$K_e = L \sigma T \qquad \ldots\ldots 43.$$

where the Lorenz number for non-degenerate materials is

$$L = (\frac{5}{2} - s)\ (k/e)^2 \qquad \ldots\ldots 44.$$

which for lattice scattering reduces to

$$L = 1.49 \times 10^{-8}\ \sigma T \qquad \ldots\ldots 45.$$

In the condition of complete degeneracy

$$L = \frac{\pi^2}{3}(k/e)^2 \qquad \ldots\ldots 46.$$

For mixed conduction an extra term arises in K_e. As

electrons and holes move under the influence of the temperature gradient, their tendency to accumulate at the cold end is counteracted by their recombination, in which process energy is given up to the surroundings. Thus the ionisation energy of the creation of electron-hole pairs at the hot end is transported in this process. The Lorenz number for mixed conduction and lattice scattering becomes

$$L = 2(k/e)^2 + \frac{k^2}{e^2}\frac{\sigma_1 \sigma_2}{(\sigma_1 + \sigma_2)}[4 + E_g/kT]^2 \qquad \ldots\ldots 47.$$

where σ_1 and σ_2 are the conductivities of electrons and holes respectively.

6.0 Optical Properties

The study of optical properties of semiconductors has become important in the determination of band structures over a wide range of energies, and has led to a number of important discoveries. A review of some aspects of recent progress is given by Tauc (19), although many developments have yet to be discussed in review literature. The basic theory, and background knowledge of photo effects in many semiconductors, is given by Moss (20). The two properties relevant to this thesis are the absorption and reflection of radiation.

6.1 Absorption Processes

The absorption spectrum of a semiconductor can be divided into three distinct wavelength ranges. Figure 14 shows typical

absorption in a semiconductor opaque to visible radiation.

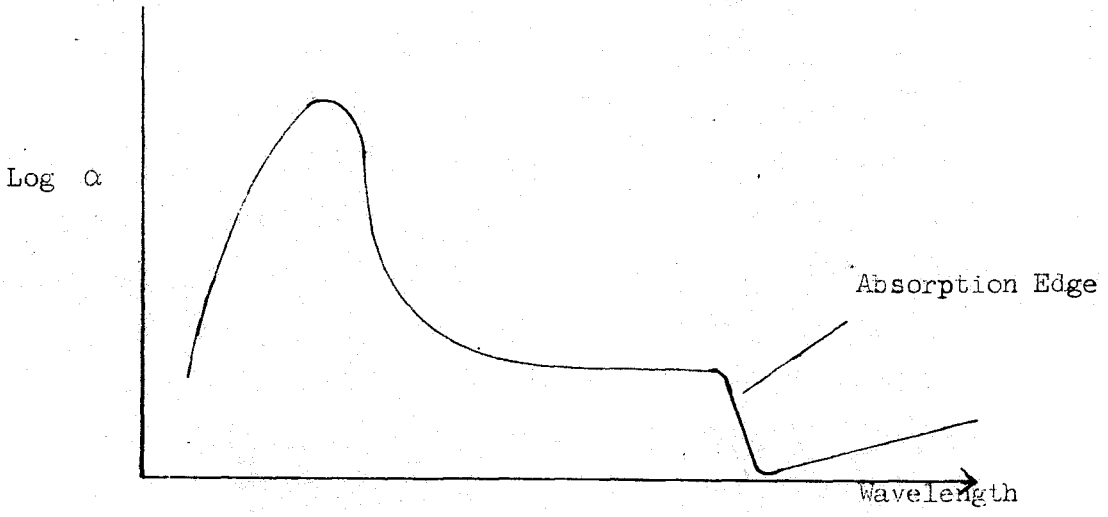

Fig. 14. Absorption Coefficient α v. Wavelength

At wavelengths lower than the absorption edge the energy of incident photons is absorbed strongly by valence band electrons which make the transition to the conduction band. In the infra-red region beyond the edge, radiation is absorbed by free carriers, holes as well as electrons. This can only happen by virtue of the perturbations due to the vibrations of the crystal lattice. The absorption, which is generally small near the edge, increases with wavelength.

Investigation of the absorption edge can lead to considerable knowledge about the energy gap.

Photon energy and wavelength are related by the equation

$E = \frac{1.24}{\lambda}$ eV. where λ is in microns.

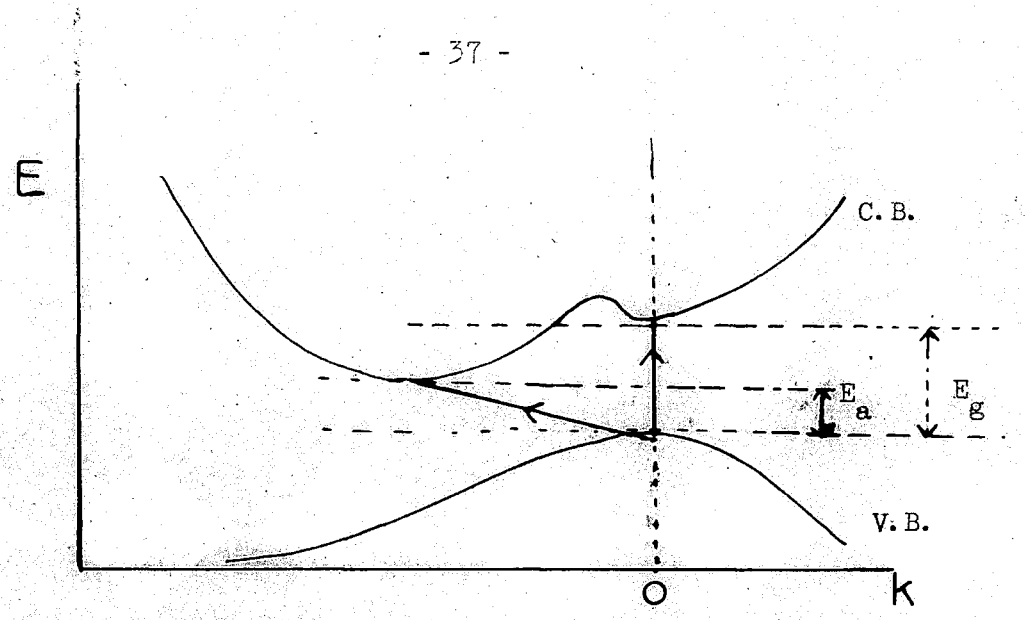

Fig. 15. Direct and Indirect Transitions.

Figure 15 shows a possible energy band scheme of the type calculated for Ge. The quantum mechanical allowed transitions from the valence band are those involving no change in k, i.e. vertical or direct transitions to the subsidiary minimum. The intense absorption stops sharply at $h\nu = E_g$. As the selection rules are generally relaxed to a certain extent, indirect transitions are permitted to the minimum in the conduction band. Momentum is conserved by interaction with phonons. In this way absorption continues down to $h\nu = E_a$. In a simple energy band semiconductor only direct transitions take place.

When the absorption edge has not been plotted in great detail it is possible to define the energy gap (20 P.40) as the wavelength where the slope is steepest. This corresponds to the point where the density of allowed states is changing most rapidly. In a simple energy band semiconductor this function is discontinuous.

However, any lattice disorders cause a tailing off of the states into the forbidden region, which has the effect of spreading out the observed absorption edge.

The exact form of the absorption edge has been discussed by a number of workers. Their results are reviewed in the standard texts (3, 20). In general, the absorption constant is proportional to $(h\nu - E_g)^n$, For direct transitions n has the value 1/2 for allowed, and 3/2 for forbidden transitions. For indirect allowed transitions n equals 2, and for those not allowed n has the value 3. Thus, from the relevant straight line plot the energy gap can be found by extrapolation, and also the nature of the transitions is determined.

For the majority of semiconductors the lowest unfilled states in the conduction band are very close to the bottom of the minimum, so that the intrinsic energy gap is measured in absorption experiments. Where the conduction band is non-parabolic as in InSb, or where, as in a semi-metal, the conduction band contains a considerable number of electrons, transitions can only take place to the lowest unfilled states in the band so that the apparent energy gap increases with carrier density.

6.2 Reflection Experiments

A powerful technique in the determination of band structures is the study of the reflectivity of semiconductors in the ultraviolet and visible wavelength regions where the absorption is too

high for good measurements to be made. The reflectivity presents a number of peaks which are believed to be associated with the onset of new interband transitions. The method is discussed in references 10, 20 and 21.

7.0 Semiconductor Alloys

The term alloy is used here to mean a disordered crystal in which two or more elements form solid substitutional solution. Ordered phases are regarded as compounds. Where two phases do not form solid solution the region is called a miscibility gap. The term binary system implies alloys of two elements but solid solution between two compounds is generally described as pseudo-binary.

Investigation of phase diagrams is best carried out by differential thermal analysis in which melting points and other changes of phase are readily observed. An apparatus, suitable for the materials discussed in this thesis, is described by Gasson (22). Where DTA is not available, and also for additional information, the limits of solid solution can be found by annealing the required proportions of the basic materials at various temperatures. The resulting mixtures are examined for homogeneity by X-ray analysis and, if solid, optical and infra-red microscopy. Two-phase regions are shown up by changes in reflectivity and absorption.

The energy gap of alloys is generally found to vary steadily with composition between the two end values: abrupt changes in gradient can be taken to indicate changes in band structure. The disorder in the lattice often has considerable effect on the scattering of both electrons and phonons and so the thermal conductivity and electron mobility of alloys fall below the end values.

Theoretical aspects of alloy systems are considered by Herman et al. (23).

CHAPTER II

Previous Studies on Materials

8.0 Introduction

In the first part of this chapter previous studies on the compound HgTe and its alloys with other group II-VI compounds are reviewed. A considerable amount of work has been performed on this material on the results of which a band structure of the semi-metal type has been proposed. It is apparent that the transport properties are peculiarly sensitive to the previous heat treatment of the material.

Less is known about the compound In_2Te_3, mainly because suitable single crystals have not been obtained. Some properties of the ordered and disordered phases have been obtained although the low values for the electron mobility and the carrier density further hinder experimental work.

The chapter ends with a review of previous work on some alloys between normal and defect zinc blende compounds.

9.0 The Mercury-Tellurium Binary Phase System

A detailed study of this system has not been carried out, although the principal features of the phase diagram are clear. Analysis of the Te-rich part of the system reported in ref. 24 shows that the only compound is HgTe which is sharply defined, and that there is a eutectic at 88 atomic per cent Te at a temperature of 410°C: the melting point of Te itself is 435°C. Delves and Lewis (25) agree

with these findings and further propose a phase diagram in the region of HgTe whose melting point is found to be 670°C. Using the techniques of differential thermal analysis and vapour phase equilibration, they find that there is considerably less than 2 atomic per cent solid solubility of Hg in HgTe but that Te may be soluble to about 2.5 at.p.c. The maximum in the liquidus occurs on the Te rich side, between 2.5 and 4 at.p.c., although they admit that the actual compositions of their samples could have been 2 at.p.c. deficient in Hg near the melting point. The phase diagram is reproduced in figure 16.

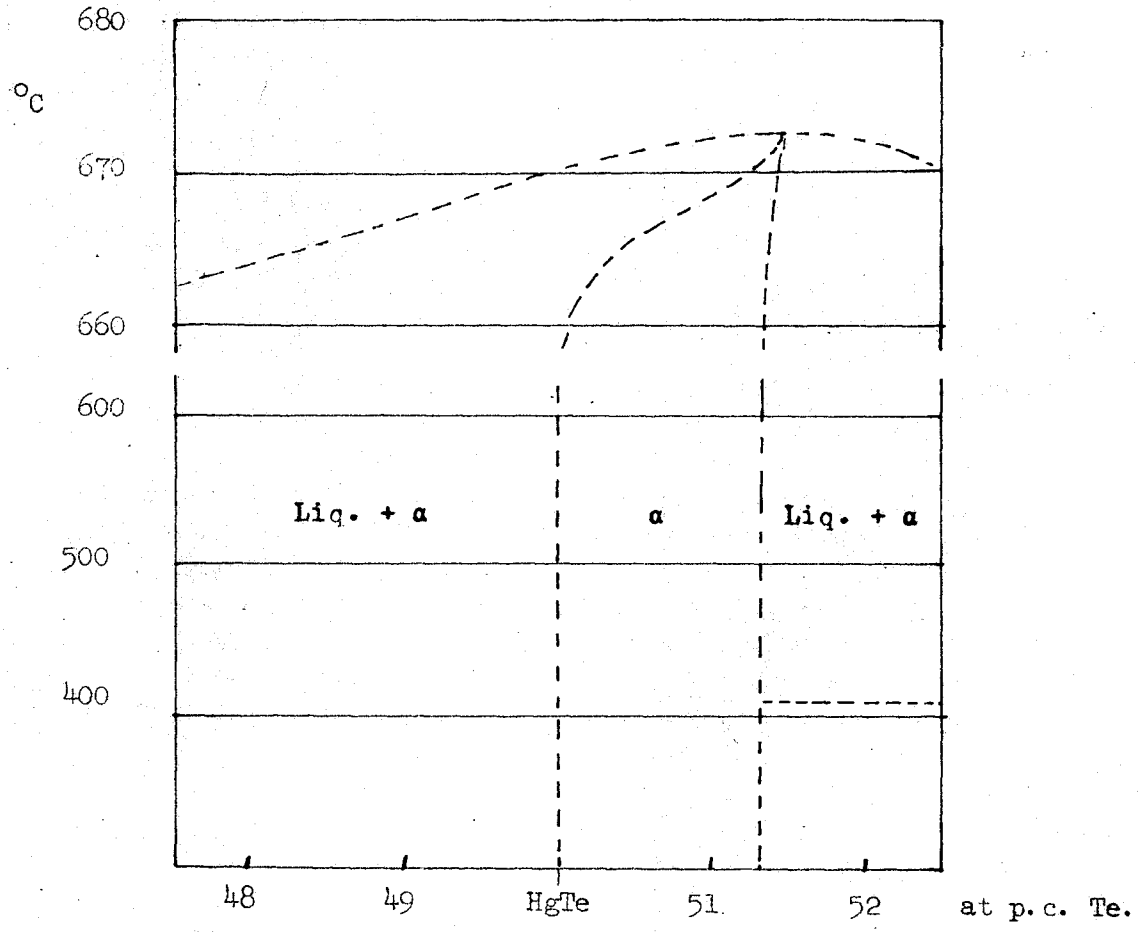

Fig. 16. Schematic Phase Diagram in the Region of HgTe (25).

The mineral form of HgTe, Coloradoite, was discovered in 1877 (26) in small impure deposits. Nearly all later work was performed on synthetic material of higher purity. In common with many other II-VI and III-V compounds, the structure is zinc blende, and the lattice parameter has been generally observed to lie between 6.460 and 6.462 A (27, 28) although lower values have been reported (24).

10.0 The Preparation and Electrical Properties of HgTe

Research into the electrical properties of the compound has been carried out recently in a number of countries, mainly Britain, France, Russia and the U.S.A. (27 - 56), but a comprehensive investigation has not yet been reported. At least two reasons may account for this. In the first place, without a full understanding of the phase diagram, difficulty has been encountered in forming the exact stoichiometric compound: most of the material worked on was p-type. Secondly, because of the narrow width of the forbidden energy gap, more advanced techniques than those used on other semiconductors have had to be employed to obtain any information of the band structure. These points will be expanded in the following review of the known properties of HgTe and its alloys with other II-VI compounds.

Early studies of the properties of HgTe, performed in Russia on sintered or pressed powders (29 - 32), were sufficient to indicate that conduction was mainly by electrons whose mobility

was fairly high, and that an energy gap of between 0.02 and 0.08 eV accounted for the variation of the Hall coefficient and conductivity with temperature. In 1958 Carlson in America (33) extended the measurements of Hall coefficient and conductivity down to liquid hydrogen temperatures and worked on some doped materials. His polycrystalline materials which were formed from stoichiometric quantities of the elements by the two furnace technique, were not annealed for any length of time, and he does not report the presence of free Hg in the ampoules after cooling. The Hall effect indicated that undoped samples were p-type, and that Cu acted as an acceptor and Zn as a donor. Electron mobilities at room temperature were about 10,000 $cm^2/V.sec.$ and the calculated values at $20^{\circ}K$ were similar. Figures of between 40 and 100 were estimated for the mobility ratio at the lower temperature. The Seebeck coefficient was observed to follow the standard p-type variation from -150 at room temperature to + +210 microvolts/$^{\circ}C$ at $50^{\circ}K$: Carlson also showed that below room temperature the Hall coefficient is strongly dependent on magnetic induction and suggests that a complicated conduction band may be the cause. Similar work to that of Carlson is reported by Lagrenaudie (34). Bell has examined the crystalline perfection of this and other single crystal compounds by X-ray techniques (35).

Some of the first large single crystals of HgTe were grown using the Bridgeman method by Black (36). He measured Hall coefficient, magnetoresistance and conductivity as functions of

temperature and concluded that the material, which was p-type, was intrinsic above 250°K, had an electronic effective mass ratio of 0.04 and an energy gap of 0.02 eV. The figure of 16,000 $cm^2/V.sec$ for the mobility is low for single crystal material, as is the value of 10 for the mobility ratio.

By zone refining some carefully prepared material, Lawson et al. (28) were able to produce both p- and n-type HgTe. Analysis of measurements on a p-type sample gave a mobility ratio of 70 and an intrinsic carrier density of 6.4×10^{17} per cm^3 at 174°K, and analysis of the Hall effect variation with magnetic induction gave similar values at 77°C. The electronic mobility varies between 19,000 at 300°K and 23,400 $cm^2/V.sec$ at 77°K. Single crystals of HgTe exhibiting similar properties were also prepared by Harman et al, (37).

High electron mobilities are recorded by Rodot and Triboulet (38) on material annealed in controlled mercury vapour pressure. Ingots made by the normal method and zone refined to remove foreign impurities were further annealed for 7 days at the same temperature (one group at 200°C and the other at 300°C) but under varying pressures of Hg vapour. High pressures produced n-type samples and low pressures p-type. In the intermediate pressure range, which was broader for the lower annealing temperature, samples were produced which were intrinsic down to at least 77°K. None of the

material prepared in this way showed any appreciable variation of the Hall coefficient with magnetic induction as had been observed in earlier experiments. It has been suggested (39) that samples made in the normal way may contain microheterogeneities, perhaps Hg precipitates, which are re-dissolved by annealing. Giriat has found that improved material can be obtained by annealing in vacuum (40) which also indicates that the hypothesis is correct.

The technique of annealing in Hg vapour has been extended by Giriat (40). He found that for a given vapour pressure, controlled by the temperature, there was an optimum time of anneal which gave the highest mobility. The materials prepared in this way were intrinsic down to 77°K and the highest mobility recorded at this temperature was 73,000 $cm^2/V.sec$. The Hall effect below room temperature was considerably dependent on the magnetic induction, which is in disagreement with the work of Rodot and Triboulet.

The change in properties by annealing in Hg vapour may also be partly explained with reference to the phase diagram proposed by Delves which is reproduced in section 9.0. As the compound that is formed from the melt probably contains excess Te it will be necessary to increase the Hg content to obtain stoichiometric material. On the other hand the work of Rodot and Triboulet (38) and Giriat (40) indicates that the solid solubility of Hg in HgTe is not negligible.

A summary of the properties of HgTe is given in section 10.4.

10.1 The Band Structure of HgTe

Investigations into the band structure of HgTe have mainly been coupled with studies of the alloy systems of CdTe and with HgSe.

Some work on the latter system has been performed by Rodot (41, 42). From measurements of the magnetoresistance, which is much greater in a field perpendicular to the current than one parallel, it is concluded that the conduction band for HgTe is of the standard isotropic form, whilst that for HgSe is a system of ellipsoids of revolution centred on the crystallographic direction <100>.

From studies of the properties of both alloy systems Harman et al. have arrived at a band structure for HgTe. In a paper published in 1961 (43) it is shown that HgSe and intermediate compositions in the alloy system with HgTe have electrical properties which cannot be explained on the basis of a conventional two band model. It is necessary to assume that these materials are semimetals, with an overlap in energy of one valence band with the conduction band. The schematic diagram for such a model is similar to that given in Fig. 17.

In two papers (44, 45) on the properties of $Cd_xHg_{1-x}Te$ a wide range of experimental evidence is analysed to show that HgTe

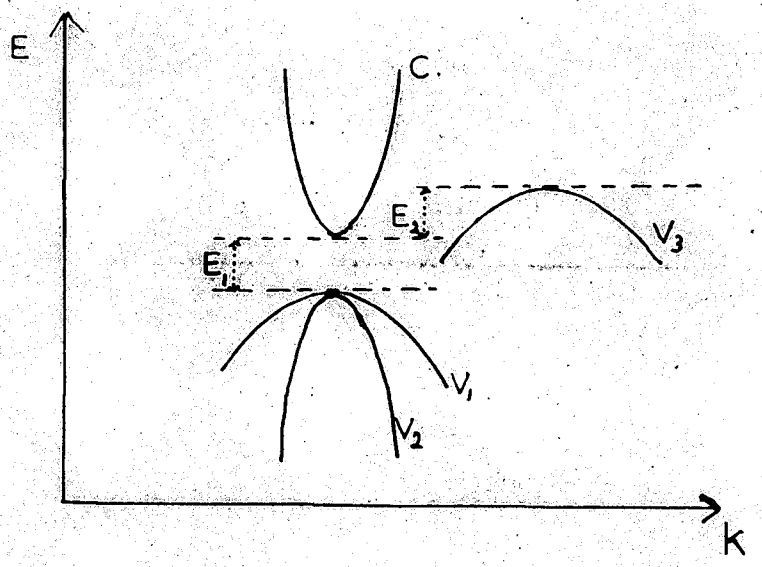

Fig. 17. Schematic E(k) Diagram for the Band Structure of HgTe. (After ~~Lehman~~ Harman).

and low Cd concentration alloys are also semimetals. The intrinsic carrier concentration at 4.2°K is estimated from the Hall coefficient and conductivity of both p- and n-type samples to be 2×10^{16} per cm^3. This value can only be accounted for by an overlap of the conduction and valence bands since the intrinsic carrier concentration for zero energy gap, with reasonable values of the effective masses, is only 10^{12} per cm^3 at 4.2°K. The Hall effect data at a temperature of 77°K was plotted against that for 4.2°K and the result compared with a theoretical curve obtained by assuming the high values for the intrinsic carrier concentration: the good agreement confirms the assumption.

Magnetoreflection measurements on low Cd content alloys, made in inductions of up to 70 kilogauss, indicate both interband transitions and cyclotron resonance within the conduction band and have been interpreted assuming the semimetal band structure and a non-parabolic conduction band similar to that proposed by Kane (46) for InSb. Satisfactory agreement is obtained between theory and experiment by adopting the value $E_{i,i} = 0.006$ eV. as the direct energy gap: the electronic effective mass ratio at the bottom of the conduction band is calculated to be 4×10^{-4}.

10.2 Scattering Mechanisms

From the measurement and interpretation of the magnetothermoelectric effect δQ with temperature, M. and H. Rodot (42) have determined the scattering mechanisms in operation in HgTe. At low temperatures the sign of δQ is positive which indicates ionised impurity scattering, but at room temperature the sign is negative showing that the majority of the scattering must be by lattice vibrations in the acoustic mode. The variation of s, the scattering parameter, is given in the summary in section 10.4.

In the region of room temperature the mobility of electrons is found to vary as $T^{-1/2}$ according to Tsidil'kovski (31), and as T^{-1} according to Harman et al. (37).

10.3 Other Studies of HgTe

It is worth recording some of the other effects observed in HgTe, not all of which are directly related to its semiconducting properties.

Blair and Smith (47) have observed that the resistivity of HgTe changes by a factor of about 10^4 under a pressure in the region of 15,000 Kg/cm^2. This is presumably due to a change in structure, but no other measurements are recorded. A similar effect has been observed in HgSe (48) for which the high pressure structure has been maintained at low temperatures in atmospheric pressure enabling X-ray photographs to be taken. The phase has a hexagonal structure best represented by a highly distorted NaCl structure in which the Hg atoms form only two strong bonds (as in the Hg halides) instead of the usual four in a zinc blende structure.

Photoelectron emission is reported by Sorokin (49). A smooth threshold to the emission at 4 eV is followed by a steep rise at 4.8 eV to a maximum at about 6 eV where the emission is considered high for this type of material. Examination of the data leads to an electron affinity of 4 eV and a forbidden zone of 0.45 eV.

Photoconductivity has been studied by Braithwaite (50) and by Kruse et al. (51) who also measured the thermal Nernst effect. The longwave threshold for photoconductivity in a thin film of HgTe at liquid oxygen temperatures is 3.1 microns i.e. 0.4 eV.

Measurements on the photo effects were made before any ideas concerning the band structure had been formulated and the interpretation of the results in terms of the complex semi-metal model would be difficult since nothing is known of the transition probabilities between the valence band and the conduction band or between the two valence bands. However, it seems possible that the photo effects may be due to electron transitions between the lower valence band and the lowest unfilled levels in the conduction band, with minimum energy change of 0.4 eV. This figure may be too high unless it is assumed that the material was strongly n-type and the Fermi level was well above the conduction band minimum.

Lawson et al. found that samples of HgTe were opaque to radiation as far as 38 microns (0.033 eV), the limit of the apparatus. Transmission through p-type samples has been observed by Quilliet et al. (52) in the range 3 to 15 microns. The square of the absorption constant is proportional to the energy of incident radiation, indicating direct transitions through an energy gap of 0.01 eV. This value is in agreement with the proposed band structure provided the Fermi level is not far above the conduction band minimum, which is probably the case for the p-type material obtained by annealing in Hg vapour. The energy gap as obtained from the absorption edge would naturally be the sum of the true energy gap and the Fermi level. Measurements in the far infra-red

are normally difficult to make and the effect may be further masked by free carrier absorption. An energy gap has been determined for HgSe (43), by this method. A minimum is observed between the inter-band absorption and the free carrier absorption which moves to higher energies with increasing free electron concentration.

The absorption spectrum of HgTe and other II-VI compounds in the form of thin films has been studied by Cardona and Harbeke (53). The L absorption edge and its spin-orbit splitting could be seen easily. The fundamental reflectivity and its bearing on the band structure has also been studied (54).

10.4 A Summary of the Properties of HgTe. Table 2.

Lattice Parameter $a_o = 6.461$ A° Melting Point 670°C

Electron Mobility

300°K	77°K	20°K	4.2°K	
22,000	31,000	18,000(38)	15,000[x](45)	$cm^2/V.sec$
19,000	23,000(28)	-	-	"
23,000	73,000(40)	-	-	"

Mobility Ratio

300°K	174°K	77°K	4.2°K
50[x](45)	70 (28)	50[x] (45)	100[x] (45)

[x] Values assumed by Harman et al.

Intrinsic Carrier Concentration

300°K	116°K	77°K	44.5°K	4.2°K	
5		1		0.2	x 10^{17} per cm^3 (45)
6.8	2.3		0.46		" (28)

Effective Mass Ratio for Electrons and Scattering Parameter r

	300°K	200°K	100°K	
carrier density per cm^3	5.0 x 10^{17}	3.9 x 10^{17}	3.4 x 10^{17}	(42)
m^x/m_o	0.031	0.027	0.007	"
S	+0.23	+0.012	-1.5	"

m_n/m_o at bottom of conduction band = 4 x 10^{-4} (45)

Thermal conductivity

	300°K	Remarks and References
K_{total}	27 mw/cm°C	varies at 1/T (33)
K_{phonon}	21 "	(56)
"	19 "	(55)

In the above summary of properties, the values quoted are thought to be typical of those found in the complete literature on HgTe, bearing in mind the degree of perfection of the materials used. Thus, though the early values for the electron mobility were about 10,000 $cm^2/V.sec$, continued improvement in the production of

single crystals has led to great increases in the mobility.

It must be realised that many of the properties depend not only on the lattice defects but also on the distance of the Fermi level above the conduction band, which is naturally affected by the foreign impurity concentration.

11.0 Alloys of HgTe

In this section will be considered the alloys of HgTe with the tellurides of Cd, Zn and Mn, and with HgSe, all of which, with the exception of MnTe, have the zinc blende structure. Previous work on the alloy of HgTe with In_2Te_3 will be reviewed in section 14.3.

11.1 HgTe - HgSe

Compositions in this system have been studied by a number of workers (30, 56 - 58). Solid solution exists throughout the system and the lattice parameter changes smoothly but not in a linear fashion between 6.46 $\mathring{A}$ for HgTe and 6,08 $\mathring{A}$ for HgSe (56).

Brach (57) obtained some good material by annealing the ingots at 500°C for 100 hours after which there was no trace of free Hg and then again for 200 hours at 200°C (homogenising anneal). Both the conductivity and the number of carriers rose to a maximum near the centre of the system, whilst the mobility dipped in the centre from 20,000 for HgSe and from 25,000 for HgTe. Values of the Seebeck coefficient and effective mass are given. The disagreement between the results and those of Nikol'skaya and Regel (30) is explained by the difference in heat treatment given to the two sets of samples.

A comprehensive table of properties for the complete range is given by Rodot et al. (56) for the temperatures 77°K, 293°K and 373°K. The electron mobility is found to be essentially characteristic of the lattice, and proportional to $1/T$ near HgTe and $1/T^2$ near HgSe. The values of the effective mass and lattice mobility seem to be little sensitive to the disorder of the lattice, but the value of the lattice thermal conductivity is seen to decrease appreciably from the extreme values as was also observed by Ioffe (55).

In two papers Harman and Wright et al. (43, 58) discuss the band structure. Detailed analysis of the Hall coefficient of HgTe and $HgSe_{0.5}$ $Te_{0.5}$ leads to the conclusion that these materials are semimetals with a band overlap of approximately 0.07 eV. The absorption coefficient for HgSe exhibits an edge which moves to higher energies with increasing free electron concentration. The electron effective mass is found to increase in a similar fashion, and thus it is concluded that the conduction band is non-parabolic.

11.2 HgTe - CdTe

The properties of this alloy system were first investigated by Lawson et al. (28) and later by Shneider and Gavrishchak (59), Woolley and Ray (60). It is well established that solid solution exists throughout the range and that the solidus, almost coincident with the liquidus, is practically linear. The lattice parameter (60) shows a slight curvature below the straight line joining the end values. The production of single crystals in the system is

described in detail by Blair and Newman (61).

The optical energy gap, plotted against composition to 90 mol.p.c. HgTe (28), presents a smooth curve from the value of 1.4 eV for CdTe. As HgTe is approached the absorption edge becomes less well defined and measurements more difficult.

Electrical measurements have been restricted to the range 40 to 100 mol.p.c. HgTe since CdTe has a low conductivity and a mobility much lower than that for HgTe. The work of Strauss et al. (45), already discussed in section 10.1 indicates that, at low Cd concentrations, the material is a semi-metal. It is estimated, from the sharp drop in intrinsic carrier concentration at both 300°K and 77°K, that the transformation to a semiconductor takes place at 80 mol.p.c. HgTe. There is a corresponding drop in the value of the mobility at this composition (28).

11.3 HgTe - ZnTe

This alloy system has been investigated by Woolley and Ray (60). Since molten ZnTe attacks quartz and the weakened ampoule explodes under the Hg pressure, the samples used were of annealed, compressed powders. The lattice parameter follows a curve very slightly below the line joining the two end values of 6.100 A° for ZnTe and 6.461 A° for HgTe. Also reported is the solidus curve, which exhibits a very steep rise from about 800°C at 75 mol.p.c. ZnTe to the melting point of ZnTe at 1240°C.

11.4 HgTe - MnTe

Delves and Lewis (25) have found that up to 80 p.c. of the Hg atoms can be replaced by Mn atoms in the zinc blende structure while the possible concentration of Te vacancies increases to 13 p.c. The interest in this system lies in the introduction of appreciable quantities of paramagnetic Mn ions into a crystal which has a high electron mobility.

11.5 HgTe - InAs

This system has been studied by Goryunova et al. (86). The formation of a continuous series of solid solutions was established in a wide concentration range with a zinc blende structure. The lattice parameter varied linearly with concentration.

12.0 The Indium-Tellurium Binary Plane System

An outline of the phase diagram of this system is given by Hansen (24 p.836). The principal compounds are InTe and In_2Te_3. In_2Te and In_2Te_5 are formed peritectically, and there is a eutectic at 90 at.p.c. Te at a temperature of 427°C. The phase diagram in the region of In_2Te_3 has been revised by Holmes et al. (62) to include the polymorphism of In_2Te_3 and the peritectic compound In_4Te_7. The revised diagram is reproduced in figure 18.

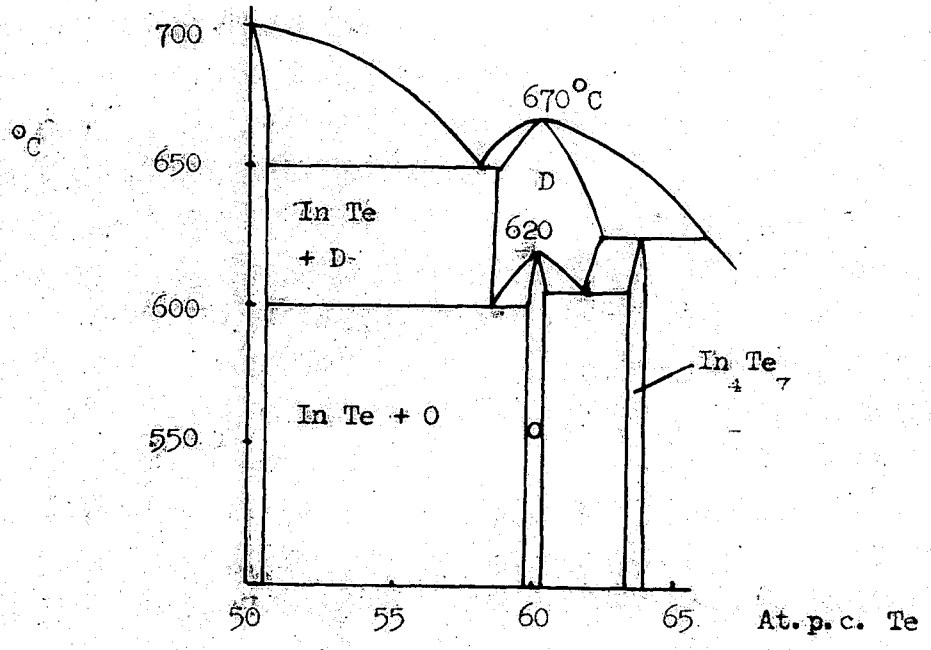

Fig. 18. Schematic Phase Diagram in the Region of In_2Te_3 (62).

13.0 The Compound In_2Te_3

Ingots have been prepared by the directional freezing technique (Woolley and Pamplin 63), by zone refining in a background temperature of 600°C (Holmes et al. 62) and by slow

cooling of the melt (Zhuze et al. 64). Good single crystals have not been obtained. The crystal grains are generally a few mm. in size though thin flakes up to 16mm^2 in area have been used (65).

By the use of infra-red microscopy, Holmes et al. have observed three types of inhomogeneity in their material. Opaque regions corresponding to grain boundaries have been shown by X-ray diffraction to consist of InTe. It seems likely that the other two, small random blobs and a needle-like pattern, are also InTe since Te may be lost by evaporation in the heat treatment of the material. The needles appear to be redissolved above 600°C where there is thought to be wider solid solution in the high temperature phase. This work throws doubt on the validity of measurements performed on material which has not been examined for a second phase by infra-red microscopy.

The transition temperature between the two phases is found to be 620°C and the transition is thought to be reversible, provided the stoichiometry is exact.

13.1 The structure of In_2Te_3

The structure of both phases of In_2Te_3 is discussed by Woolley et al. (66) on the basis of X-ray powder photographs alone. It is found that the structure could be either defect zinc blende or defect anti-fluorite on which is superimposed, for the low temperature phase, a pattern of ordering of the vacancies. Two possible structures are proposed for the supercell but the evidence is inconclusive.

Zaslavskii and Sergeeva (67) have interpreted Laue photographs of single crystals on the basis of the zinc blende structure. They conclude that, although quantitive comparison of intensities is extremely difficult, the results are best explained by a face-centred cubic lattice of space group $F\bar{4}3M$ with a three-fold increase in lattice parameter on the disordered parameter. The structure is based on nine-layer cubic packing with three patterns of ordering.

13.2 Optical and Photoelectric Properties

Samples used for infra-red transmission by Petrusevich and Sergeeva (65) were found to scatter the radiation strongly. When this had been allowed for, the absorption edge appeared sharp, though high absorption measurements were not made. This scattering, which probably accounts for the poor absorption curves produced by other workers, is not explained in the paper but in view of the work of Holmes et al. (62) may be due to the presence of small precipitates of InTe or other imhomogeneities. The measurements are interpreted using the formula for indirect transitions and the values of the energy gap obtained are 1.026 eV for the ordered and 1.02 eV for the disordered material.

Woolley et al. (68), defining the energy gap as the point where the absorption coefficient has changed by 300 cm^{-1} from the background value, obtain values of 1.16 eV and 1.10 eV for the ordered and disordered phases respectively.

The half maxima points in the photoconductivity curve (65) give values of 0.94 eV and 0.92 eV for ordered and disordered material respectively. These comparatively low values are explained in terms of the strong scattering observed.

13.3 Electrical measurements

The several sets of electrical measurements reported in the literature have all been made on polycrystalline material so that good agreement between results cannot be expected. It is unfortunate that single crystals of this interesting compound have not been obtained.

Most workers assumed that their material was stoichiometric, although this may not have been correct. The combination of low carrier density and low mobility in the intrinsic material, as is usually obtained by normal methods of preparation, make measurements of bulk properties below 250°C difficult and questionable. High temperature measurements are also of doubtful validity because of changes in the surface layer of samples and the redissolution of precipitates.

The interpretation of results is generally based on a simple semiconductor model, although Ioffe (69) has suggested that conduction may be better explained in terms of a hopping mechanism.

Woolley and Pamplin (63) together with earlier workers have observed, in the variation of conductivity and Hall effect with temperature, a change in activation energy at about 470°C. This effect was not reported by Zhuze et al. (64) who explained previous

results as probably being affected by irreversible changes in the material. They observed that when their results were not affected by conducting surface layers, the activation energy was constant up to the melting point and agreed well with the optical energy gap.

Variations with temperature of the product $R\sigma$, observed by Woolley and Pamplin for ordered material, were not found by Zhuze et al., although the room temperature values of 14 and 50 cm^2/V sec for the mobility of disordered and ordered material respectively are agreed upon. The constant mobility suggests that scattering is mainly by neutral impurities, probably cation vacancies. In doped material, the mobility was found to increase rapidly with temperature (64).

From the variation of the Seebeck coefficient with temperature, Zhuse et al. obtain a mobility ratio of about 4 and effective mass ratios of 0.7 for electrons and 1.2 for holes. The method used was, however, very approximate.

13.4 Thermal Conductivity

As with electron mobility, the thermal conductivity of In_2Te_3 is very much lower than that for normal zinc blende compounds in the same isoelectric series. Zaslavskii et al. (67) have measured the lattice thermal conductivity of cast and compressed In_2Te_3 subjected to various heat treatments. They conclude that for disordered material the very small value of 6.8 mw/cm^oC is due to the scattering of phonons by random vacancies. The value for ordered

material, 11.2 mw/cm ^{o}C at room temperature, rises considerably at lower temperatures.

Conclusion: The Effects of Ordering

Despite the difficulty in obtaining reliable measurements, it seems clear that the ordering of vacancies in In_2Te_3 has a considerable effect on the properties. Both the thermal conductivity and the electron mobility are greater in the ordered material. The energy gap is apparently wider and the number of carriers increased in a way that suggests changes in the band structure (63). Thermal conductivity results indicate that different scattering mechanisms exist for phonons in the two phases.

It is to be hoped that large enough single crystals of reliable stoichiometry will be obtained to enable this work to be completed.

14.0 In_2Te_3 Alloy Systems

Solid solution between defect and normal zinc blende structure compounds is found to exist for a number of combinations of elements. Thus In_2Te_3 can be successfully alloyed with compounds of the types In-V and II-Te. The principal interest in such alloys is the systematic introduction of vacancies into the normal structure. These vacancies naturally affect the electric and thermal properties of the materials.

14.1 The Systems In_2Te_3 in InSb and InAs

The range of solid solution of In_2Te_3 in InSb was found to be 15 molecular per cent by Woolley et al. (70) by X-ray analysis of annealed samples. Above this value the material was two phase, the second of which was shown to be possibly In_4SbTe_3 having the NaCl structure (71). The striking feature of the electrical results is the sharp increase in the number of carriers from 10^{16} per cm^3 for InSb to a maximum of almost 10^{19} per cm^3 at about 0.3 mol.p.c. This is due to the introduction of Te as an effective donor substituting for Sb. At higher percentages the added In_2Te_3 behaves in the expected alloying manner. The mobility of electrons falls rapidly with increasing vacancies. Where it is determined by the scattering of lattice vacancies, the mobility is found to be inversely proportional to the average distance between the vacancies. The variation of intrinsic energy gap is obscured by the Burstein-Moss effect due to the large carrier density.

In comparison with InSb, Woolley et al. (72) found that InAs formed a complete range of solid solution at high enough temperatures but that a closed miscibility gap existed in the range 10 to 35 mol.p.c. In_2Te_3. On the basis of differential thermal analysis, a phase diagram was proposed by Gasson et al. (73) who also found that the system was not truly pseudo-binary. The number of vacancies in the lattice was therefore smaller than expected. In order to oversome this drawback, samples for measurement were made

by pressed powder methods. The electrical results exhibit similar features for low percentages of In_2Te_3 as were observed in the InSb system, and as the range is complete, the decrease of the number of carriers and the mobility to the low values for In_2Te_3 could be followed. Gasson et al. find that a theory of defect interactions is capable of offering an adequate explanation of the variation of electron concentration with composition in this and similar alloys. Woolley et al. on the other hand explain the variation of the carrier density by the intervention of an upper conduction band of low mobility.

Greenaway and Cardona have investigated the reflectivity of etched samples from both systems. Their results are discussed with reference to possible band structures (74).

14.2 The Cd_3Te_3 - In_2Te_3 System

The original crystallographic work by Hahn et al. (75) on this system has been expanded by Woolley and Ray (76) who determined the range of solid solution by annealing ingots at 665°C. A miscibility gap exists between 50 and 70 mol.p.c. which is thought to correspond to a eutectic at 65 mol.p.c. The values of the optical energy gap plotted against composition for the single phase material, lie on two straight lines which meet at the 50 mol.p.c. composition considerably above the line joining the values for CdTe and In_2Te_3.

A phase diagram for the system has been proposed by Thomassen and Mason (77) which is not in complete agreement with the above work. In particular a peritectic compound at 50 mol. p.c. appears to form a two phase region with the CdTe phase. The central miscibility gap extends to 83 mol.p.c. with a peritectic compound at 75 mol.p.c. In_2Te_3. In a later paper Mason and Cook (78) reproduce the phase diagram and describe methods of preparing the peritectic compositions. The diagram is shown in figure 19.

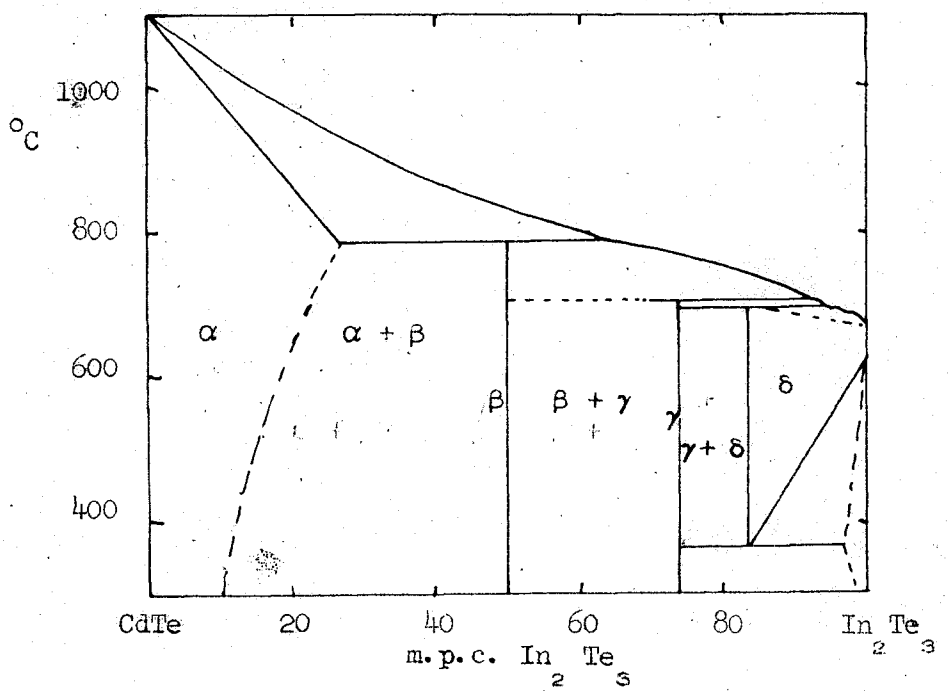

Fig. 19. Phase Diagram for CdTe-In_2Te_3 (78)

14.3 The Hg_3Te_3 - Ga_2Te_3 and Hg_3Te_3 - In_2Te_3 Systems

The lattice parameter and limits of solid solution of these two related systems have been described by Woolley and Ray (76,79). Their results are reproduced in figures 20a and 20b.

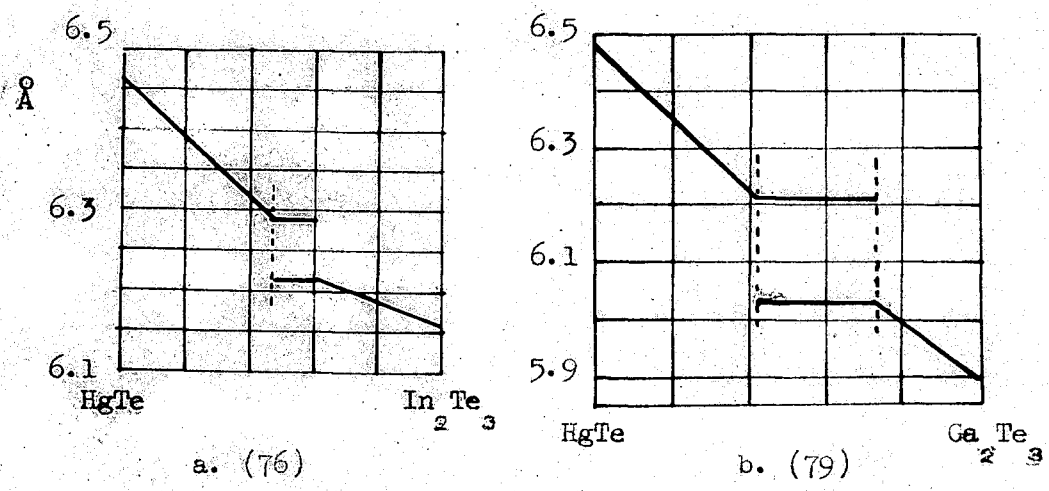

Fig. 20. Variation of Lattice Parameter with Composition in mol. p.c.

There appear two regions, one centred at about 40 mol.p.c. and the other at about 75 mol.p.c., where an ordered structure is superimposed on that of the zinc blende phase. These two compositions will be discussed in more detail below.

The Compound $AB_2\square Te_4$

The ordered defect compound $AB_2\square Te_4$, where A can be Zn, Cd or Hg and B can be Al, In or Ga, was first investigated by Hahn (75) and has been reported on by other workers in this field. The structure is tetragonal, being similar to that of chalcopyrite $CuFeS_2$. The c/s ratio is 2 so that a pseudo-cubic lattice parameter,

corresponding to that for the zinc blende structure, can be determined. This has been used in the above figures. Apart from the electrical work reported below and energy gaps for a few compounds no other research has been performed on these materials.

Busch et al. (80) have measured the electrical properties of $HgIn_2\square Te_4$ between 300°K and 800°K using both polycrystalline material and single crystals. The mobility ratio, calculated from the Seebeck effect, is 1.4. From the intrinsic Hall effect, the electron mobility is found to be 200 cm^2/V sec at 625°K falling to 110 cm^2/V sec at 770°K.

The Compound $Hg_5Ga_2\square Te_8$

Following the work of Woolley and Ray, Pamplin (81) investigated the ordered phase occurring at about 40 mol.p.c. Ga_2Te_3 in Hg_2Te_3. Material of the 40/60 mixture was prepared by the technique of directional freeze. The lattice parameter of both ends of the sample was 6.227 A°, and the density measurements corresponded almost exactly to $Hg_5Ga_2Te_8$. Both ends were p-type and the last end to freeze had a Hall coefficient of 1.5×10^4 cm/C and a conductivity of 6×10^{-3} mho/cm, giving a Hall mobility of 90 cm^2/V sec. The classification of the intensity of the ordered lines in the X-ray powder photograph is discussed but the structure is not identified.

15.0 The structure and properties of some adamantine compounds

P. M. SPENCER, B. R. PAMPLIN and D. A. WRIGHT
Department of Applied Physics, University of Durham, England

Abstract. Solid solutions have been investigated between HgTe or CdTe and In_2Te_3 or Ga_2Te_3, particularly in the neighbourhood of the composition $II_5III_2VI_8$. In x-ray powder photographs this composition shows superlattice lines characteristic of an ordered adamantine structure when Hg is the group II element. Ordering does not occur in the cadmium compound. Measurements have been made of lattice parameter, electrical conductivity, Hall effect, Seebeck coefficient and optical absorption.

Samples in the solid solutions $(Hg_xCd_{1-x})_5\ In_2Te_8$ and $(Hg_{1-x}Ag_{x/2}In_{x/2})_5\ In_2Te_8$ have also been prepared and studied, and some of their structural, electrical and optical properties are described.

Most of the compounds studied have low hole mobilities, but electron mobilities between 100 and 10 000 are encountered. Ordering tends in general to produce an increase in energy gap. Its effects on electrical properties have not yet been established.

1. Introduction

The object of the present work* was to investigate the relationship between structure and electrical and thermal properties in adamantine alloys exhibiting superlattice formation. The parameters studied include those which are relevant to thermoelectric applications, since the programme originated from an interest in this subject.

The spur to the work came from a study of In_2Te_3. This defect structure compound is capable of existing in a high symmetry disordered state and also in an ordered state of much lower symmetry. Even in its ordered state In_2Te_3 is quite useless for most semiconductor applications, including thermoelectricity, because of its very low mobility.

To obtain more useful properties attention is naturally drawn to alloys of III_2VI_3 compounds with isomorphous adamantine semiconductors with high mobilities such as III–V and II–VI compounds. It was decided to investigate certain solid solutions of HgTe and CdTe with In_2Te_3 and Ga_2Te_3. The work of Woolley and Ray (1960) had indicated that there were two ranges of superlattice formation in these systems, the well-known defect chalcopyrite region and a new region centred on the composition $II_5III_2VI_8$. As the former has been investigated to some extent, attention has been confined to the latter in the present work. Most of the work has been on $Hg_5In_2Te_8$ and $Cd_5In_2Te_8$ and their solid solutions, but the cross-substitution compounds $(Ag_{x/2}Hg_{1-x}In_{x/2})_5\ In_2Te_8$ have also been studied briefly.

It was found that some of these compositions occur normally in an ordered form, and others in a disordered form, and that heat treatment can transform some compositions

* Carried out under contract for A.E.R.E., Harwell.

from one to the other. Further information about the effects of ordering can therefore be obtained from studying these compounds.

The measurements to date have been confined to electrical conductivity, Hall coefficient, Seebeck coefficient and optical energy gap. It is hoped to add measurements of thermal conductivity in the near future. The work is at an early stage, and it is not yet possible to draw many conclusions as to the effects of ordering. §2 outlines some of the effects which are to be anticipated.

2. Superlattice formation in adamantine materials

The materials under investigation are all adamantine, having the diamond atomic lattice. In the disordered state at least some of the sites are randomly occupied. When ordering is complete one definite atomic species may be assigned to each atomic site, the randomness has disappeared and the entropy is reduced. The following effects may be expected when ordering occurs:

(i) The cubic isotropic symmetry of diamond (or zinc blende) is likely to be reduced to tetragonal, orthorhombic or rhombohedral. The properties of the ordered material would then be anisotropic.

(ii) The lowest minimum in the conduction band characteristic of the disordered material should separate more widely from the highest valence band maximum when ordering occurs, because of the reduction in entropy and the resulting increase in the strength of some of the bonds. Thus the direct effect should be for the energy gap to increase. This has been observed in In_2Te_3 and in certain solid solutions of III_2–VI_3 and II–VI compounds. However, other conduction band minima may fall towards the valence band since other bonds may decrease in strength. In some cases this might lead to a net decrease in energy gap.

(iii) Since ordering reduces the symmetry of the crystal and usually means that a larger unit cell must be used to describe its crystal lattice, the Brillouin zone shape will usually change and if it does its size will decrease.

(iv) Even if the Brillouin zone does not change, the electronic band structure, especially in the conduction band, may alter because of the periodicity changes. (a) The shape and potential energy of existing minima may become different. (b) Fresh minima may appear or old ones shift position in k space. (c) Some degenerate minima may split owing to the raising of degeneracy by the reduction of symmetry. (d) (a), (b) or (c) would produce changes in effective mass and therefore in the transport properties.

(v) Similar arguments indicate that the vibrational spectrum of the crystal will change. Thus there should be an appreciable change in the thermal conductivity, especially at low temperatures. It may be noted that the increase is only by a factor of two in In_2Te_3 at room temperature, although in that compound the ordering is between vacancies and indium atoms. When ordering occurs in other compounds between atoms of similar atomic weight, any increase is therefore likely to be by a factor less than two.

3. The $HgTe$–In_2Te_3 system

3.1. *Structure*

Figure 1 shows the ternary diagram of Hg, III and Te where III is either In or Ga. There are two ordered regions, one centred on the defect chalcopyrite structure $Hg\ III_2\ \square\ Te_4$ (124), the other with its centre on the pseudo-binary line at $Hg_5\ III_2\ \square\ Te_8$ (528). The

structure of 124 is known (Hahn 1955). The x-ray powder pattern of 528 indicates the space group A mm 2. This suggests that the ideal composition of this phase is in fact 428. The postulated structure for 428 shown in figure 2 is consistent with the x-ray data. Attempts to prepare the composition 428 result, however, in two phases, so that the situation is not clear, and work on this aspect is continuing.

3.2. *Material preparation*

Ingots of HgTe and $Hg_5In_2Te_8$ made from 99·99% pure elements were powdered and mixed together in the correct proportions to obtain samples at 10% intervals in composition. The melts of each sample were cooled in a uniform furnace to form ingots which were annealed at 600°C for 20 days. Samples cut from the resulting ingots were then

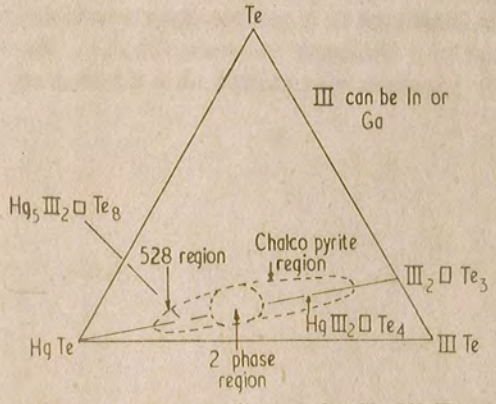

Figure 1. Ternary diagram for Hg III Te system.

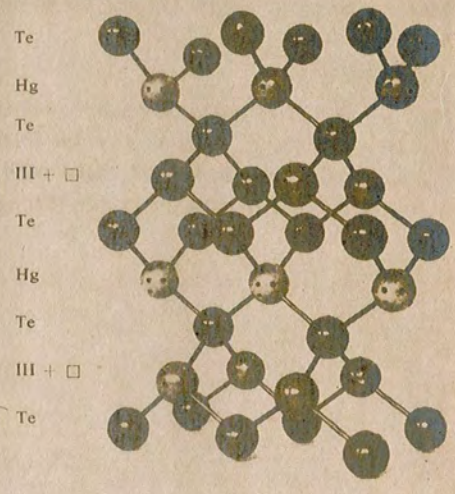

Figure 2. Suggested structure for the ideal composition $Hg_4III_2Te_8$.

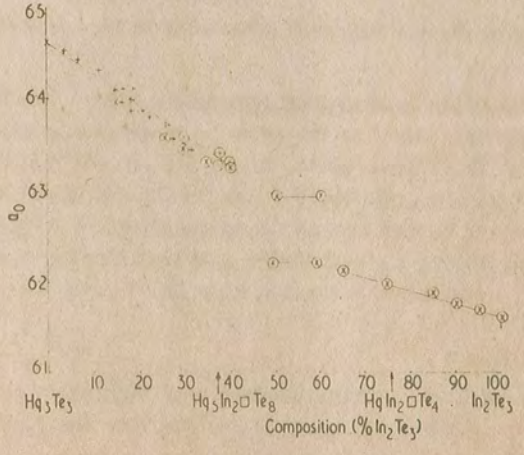

Figure 3. Lattice parameters for the HgTe–In_2Te_3 system showing present results, results of Woolley and Ray (1960) and Pamplin (1960). × J.C.W. and B.R. · B.R.P. + Present work. ○ indicates ordering.

examined optically and by x-ray powder photography. Slices adjacent to those selected for optical study were used for the electrical measurements.

Some of the ingots were not completely homogeneous and single phase, and there was evidence of a small loss of mercury from some of them. However, the slices as prepared for electrical and optical studies were homogeneous and single phase.

3.3. *Lattice parameter*

The variation of lattice parameter a_0 is plotted as a function of composition along the pseudo binary line in figure 3. The results agree well with previous work. The information was used to determine the spread in composition in non-homogeneous or two phase samples, and so to select samples for investigation of electrical propreties.

3.4. *Energy gap*

Optical measurements were taken with a Hilger and Watts large aperture spectrometer using as the detector a linear vacuum thermopile connected to a galvanometer amplifying system. Specimens from each ingot were ground to a thickness less than 100 μm. The log of the percentage transmission through each specimen was plotted as a function of

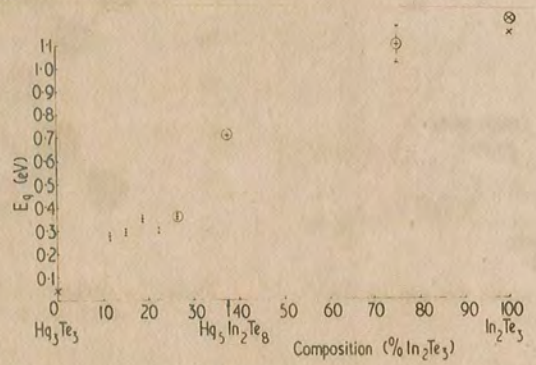

Figure 4. Energy gap as a function of composition for the system HgTe–In_2Te_3.

wavelength in the region of the fundamental absorption edge. The frequency corresponding with the energy gap was taken as the point of maximum gradient in the plot. The long wavelength limit of the apparatus was about 5·5 μm, so that the energy gaps could not be measured for specimens near HgTe. The results are shown as a function of composition in figure 4. It will be seen that all the values plotted for HgTe–In_2Te_3 compounds are higher than the line joining the end values, and that there is evidence of an inflection near 20% In_2Te_3, with a subsidiary minimum near 22·5% and maximum near 18%.

3.5. *Electrical measurements*

Measurements were made of electrical conductivity, Hall effect and Seebeck coefficient. The room temperature results for some of the alloys between HgTe and $Hg_5In_2Te_8$ are shown in the table.

It will be seen that the three compositions nearest to HgTe are n-type with high electron mobility. In the last two there are 2×10^{17} carriers per cm^3. The Seebeck coefficient

end where the x-ray photograph showed strong superlattice lines and the lattice parameter was about 6·30 Å. Another specimen from towards the other end showed only weak superlattice lines and a lattice parameter of about 6·28 Å. The two specimens therefore have very similar chemical compositions and are referred to as ordered and disordered respectively.

Both specimens had a low electrical conductivity which increased exponentially with temperature. The activation energies associated with this increase were 0·28 ev for the ordered and 0·25 ev for the disordered. Both were p-type and had large thermoelectric powers, indicating that the Fermi level was well removed from the valence band.

No Hall effect could be measured in the disordered specimen and an upper limit on the Hall mobility ($R_H\sigma$) of 40 $cm^2\ v^{-1}\ sec^{-1}$ was deduced.

The Hall effect of the ordered specimen was found to be n-type indicating a large mobility ratio μ_e/μ_h since the Seebeck coefficient was p-type.

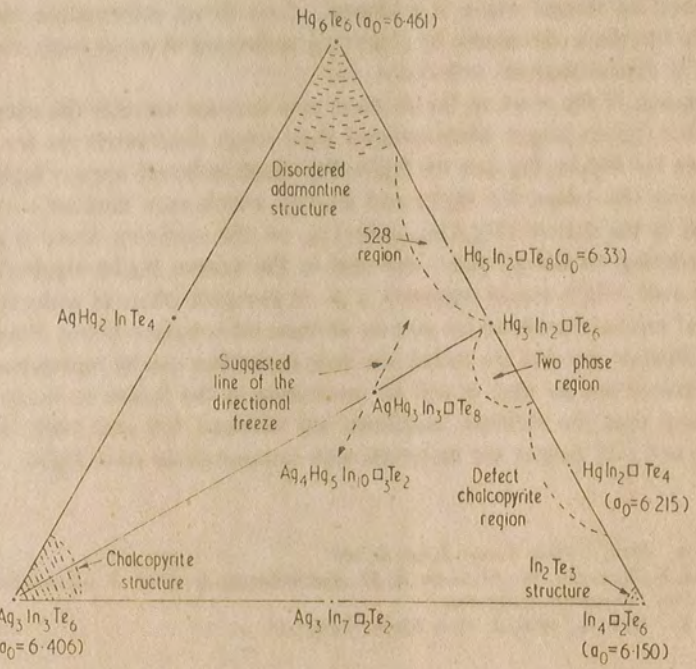

Figure 6. Pseudo-ternary diagram for some AgHgInTe alloys.

The measured value of $R\sigma$ (n-type) rose to a maximum of 530 $cm^2\ v^{-1}\ sec^{-1}$ at 325°K and then fell rapidly. A detailed analysis has not so far been completed, but it appears that although the hole mobility is of the order of unity, the electron mobility must be of the order of 1000 at room temperature.

If these materials can be doped n-type, they should therefore be of interest for practical applications.

Optical measurements indicate that the energy gaps in the two materials are 0·91 ev (ordered) and 0·83 ev (disordered).

6. Conclusions

There have hitherto been few systems known in which the effects of ordering can be studied, one of the few being the compound In_2Te_3. This material can be obtained either ordered or disordered according to the details of the heat treatment. The present work indicates that this is so also with a number of compositions in the range $(Hg_xCd_{1-x})In_2Te_8$ and $(Hg_xCd_{1-x})Ga_2Te_8$. The compound containing silver discussed in §5 gave ordered and disordered structures from different parts of the same ingot, with little difference in lattice parameter, so that the same situation probably applies to this compound also. Further investigations of these materials should greatly extend our knowledge of the effect of ordering on semiconductor properties.

The above systems

$$(Hg_xCd_{1-x})\begin{pmatrix}Ga\\In\end{pmatrix}_2 Te_8$$

and the system $HgTe$–$Hg_5In_2Te_8$ both show ranges of composition where ordering is present, followed by ranges where it is absent. Less direct information about the effects of ordering are therefore obtainable by observing variations in parameters with composition and looking for discontinuities, inflections, etc.

The main results of the work so far on these new systems are that the energy gap for the silver compound (§5) is larger when ordered than when disordered (as for In_2Te_3); that the energy gaps for $Hg_5In_2Te_8$ and for $HgIn_2Te_4$ (both ordered) appear higher than would be expected from the values for HgTe and In_2Te_3, which may indicate a consequence of ordering; that in the system $(Hg_xCd_{1-x})_5In_2Te_8$, on the contrary, there is no evidence of an effect of ordering on energy gap; and that in the system $HgTe$–$Hg_5In_2Te_8$ there is an inflection indicated which would represent a more complex effect of ordering.

The electrical measurements so far give no definite information about effects of ordering. The main conclusions are that the rather low hole mobilities can be represented by ordinary band-theory treatments, so that it will be interesting in the future to study the scattering mechanisms, and that the electron mobilities are between 100 and 1000 in many of the alloys studied, and still greater for materials with compositions near HgTe.

References

GOODMAN, C. H. L., 1958, *J. Phys. Chem. Solids*, **6**, 305.
HAHN, H., FRANK, E., KLINGER, W., STÖRGER, A. D., and STÖRGER, E., 1955, *Z. anorg. Chem.*, **279**, 241.
PAMPLIN, B. R., 1960, *Thesis* (Nottingham).
WOOLLEY, J. C., and RAY, B., 1960, *J. Phys. Chem. Solids*, **15**, 27.

indicates that these samples are slightly degenerate, so that the effective masses are approximately 0·014 times the free electron mass. These samples are disordered, and it appears that their electrical properties resemble those of HgTe.

The samples with 15–26% In_2Te_3 are p-type, with low hole mobility and carrier densities exceeding 10^{18}. The Seebeck coefficients are high, showing that the Fermi level is about $2k\,T$ above the valence band, and that the hole effective mass is approximately the same

In_2Te_3 (%)	a_0 (Å)	Eg (ev)	α (μv degc^{-1})	σ (ohm^{-1} cm^{-1})	R (cm^{2}c^{-1})	n ($6{\cdot}25\times10^{18}$ R^{-1})	$R\sigma$ (cm^2 v^{-1} sec^{-1})	Comments
37	6·338	0·71	230 p	$2{\cdot}3\times10^{-4}$	9×10^5 p	7×10^{12}	210	Ordered
26		0·36	300 p	4·9				Ordered
22	6·379	0·30	345 p		1·45 p	$4{\cdot}3\times10^{18}$	13	Faint ordering
19	6·386–6·414	0·35	290 p	15·8				Disordered
15	6·408	0·29	290 p	20	1·1 p	$5{\cdot}7\times10^{18}$	22	Disordered
11	6·430	0·28	192 p	37·5	17 n	$3{\cdot}7\times10^{17}$	630	Disordered
7	6·442		48 n	14·5	830 n	$7{\cdot}5\times10^{15}$	12 000	Disordered
4	6·453		108 n	560	30 n	$2{\cdot}1\times10^{17}$	17 000	Disordered
2			107 n	390	28 n	$2{\cdot}2\times10^{17}$	11 000	Disordered
0	6·461							

as the free electron mass. It will be noted that μ_h is much higher for $Hg_5In_2Te_8$ itself than for the solid solutions investigated, but there is not enough information at present to indicate whether the degree of ordering affects the mobility.

So far only one sample has been studied above room temperature, i.e. that with 22% In_2Te_3. This sample had a high degree of homogeneity, as indicated by the clearly resolved $CuK\alpha_1\alpha_2$ doublet, and had very faint superlattice lines. It may be classified as disordered, but clearly this composition is very near the boundary where ordering begins.

The value of σ fell slightly as T rose, together with a slight decrease in R and an increase in α. The value of $R\sigma$ fell between 290° and 410°K following very closely a $T^{-3/2}$ law. Near 410°K the Hall effect changed sign and the value of α started to fall, indicating an increasing contribution of electrons to the electrical properties. Above 500°K the value of $R\sigma$ levelled off at 110 cm^2 v^{-1} sec^{-1}, which is therefore the approximate value of the electron mobility at that temperature.

It is important to note that hole mobilities of 10 or less follow the normal laws resulting from band theory, with an effective mass of the same order as that of the free electron. Thus the ideas of narrow band semiconductors are not relevant, and it will be of interest to study the scattering processes in detail.

4. $(Hg_x–Cd_{1-x})_5\ In_2Te_8$

The ordering which exists in $Hg_5In_2Te_8$ is absent in all the specimens of $Cd_5In_2Te_8$ prepared in this investigation. $(Hg_xCd_{1-x})_5\ In_2Te_8$ is therefore another system in which it should be possible to study the dependence of ordering on composition, and the effects of ordering when it occurs. Difficulties have, however, been encountered in preparing single phase homogeneous ingots, and the only results available so far are on energy gap, as shown in figure 5. The points lie on a line joining the end values, so that there is no indication that ordering has any effect. It is present for values of x between 1·0 and 0·5.

Using gallium in place of indium, no attempts have been made to prepare ingots large enough for a complete investigation. With small samples single phase materials have been obtained at all compositions and ordering exists as far as $x = 0{\cdot}4$. At this composition the disordered state of the same material can be obtained by quenching from near the melting point. If satisfactory ingots can be made, this system will also be a useful one for the study of the effects of ordering.

Room temperature measurements on the ordered $Hg_5Ga_2Te_8$ compound show it to be p-type with $\sigma = 6 \times 10^{-3}$ ohm^{-1} cm^{-1}, $\alpha = 810\ \mu$v degC^{-1} (p-type) and $R_H = 1{\cdot}5 \times 10^4$ (p-type). This indicates a Hall mobility of 90, compared with 210 for $Hg_5In_2Te_8$ as in the table.

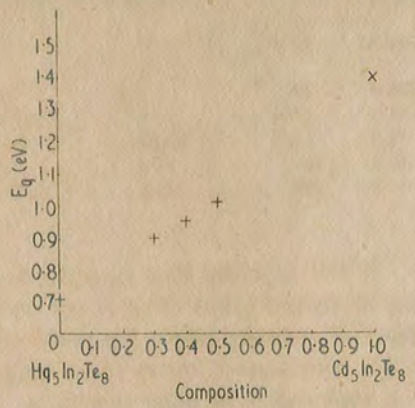

Figure 5. Energy gap as a function of composition for the system $(Hg_xCd_{1-x})_5In_2Te_8$.

5. Ordered and disordered $AgHg_3In_3\square Te_8$

The alloy $AgHg_3In_3\square Te_8$ may be derived from $Hg_5In_2\square Te_8$ by cross substitution (Goodman 1958) of equal parts of Ag and In for two atoms of Hg in the formula unit. Alternatively it may be described as the 75% : 25% alloy of the solid solution system $Hg_3In_2\square Te_6$ (the mid-point alloy of the Hg_3Te_3–$In_2\square Te_3$ pseudo binary line) and the chalcopyrite structure compound $Ag_3In_3Te_6$. The pseudo ternary diagram (figure 6) shows how it may be described in terms of compositional phase diagram theory.

A specimen was prepared from the elements in the usual way and slowly frozen in an almost uniform-temperature furnace. X-ray powder photographs showed that at one end of the ingot a disordered adamantine phase of lattice parameter 6·28 Å was produced. The other end had all the superlattice lines of the (528) compound with the same relative intensities and the same lattice parameter 6·33 Å. Since it is unlikely that ordering alone will change the lattice parameter by as much as the 1% observed, it is thought that this ingot must have frozen directionally yielding a sample of silver doped 528 at one end and a material of approximate composition $Ag_1Hg_5In_{10}\square_3Te_{22}$ at the other end. This deduction remains to be tested by chemical analysis and, it is hoped, by use of electron probe x-ray microanalysis.

Specimens were cut from the ingot at various places and were found on examination in a polarizing microscope to be single phase. They were found to contain few blow holes and seemed ideal for electrical measurements. One specimen was chosen from the ordered

CHAPTER III

Apparatus and Experimental Techniques

16.0 Introduction

The first part of this chapter deals with the synthesis, preparation and examination of the materials. This is followed by a description of the apparatus and experimental procedure to determine the lattice parameter, optical energy gap, electrical and thermal conductivity, and the Hall and Seebeck coefficients for the materials.

17.0 Furnace Technique

All the furnaces used were of the conventional electrical resistance, wire wound type designed for working at temperatures up to 1200°C. Impervious mullite tubes of 4 cm. bore and length about 1 m. were wound with 18 swg Kanthal A wire. Although the central part of the tube only needed 4 or 5 turns to the inch, the number had to be increased progressively to 10 turns per inch near the ends in order to produce a length of at least 20 cms uniform temperature. The resistance of the furnaces so wound was about 80 ohms so that the power could be taken from the mains through a rotary regavolt of 6 amps limiting current. The outer case of the furnaces were made of Sindanyo asbestos sheet and the insulation of granular vermiculite or dextramite blocks: both afforded little heat loss so that a furnace temperature of 800°C needed about half a kilowatt.

The furnace used for reacting and melting the materials was mounted on a central axis so that it could be rotated to either a vertical or horizontal position. Samples were annealed in a horizontal furnace fitted with a larger tube of bore ~ 5 cm. Considerable experimentation was needed before the correct variation in the windings was found, to produce a uniform temperature region large enough for the purpose, and it seems that this size of tube is the largest in which this can be achieved without recourse to the method of tapped windings.

The temperature variation of about 5°C in the central part of the furnace was further reduced by the use of sheaths made from 2 mm wall stainless steel tube or for temperatures above 900°C. Inconel tube, supplied by Henry Wiggins company. Inside such a sheath 15 cm long, the temperature varied by less than 1°C for the whole length. Samples which had to be annealed at 600°C were wrapped in several layers of aluminium foil (m.p. 660°C) enabling a large number to be fitted into one furnace. Those samples needing higher annealing temperatures were placed in metal sheaths.

The furnace temperatures were controlled by anticipatory transitrol instruments made by Ether Ltd who carried out routine inspections and adjustments every six months. The temperature could be held steady to a high degree of accuracy particularly inside a metal sheath.

18.0 Preparation of materials

In the preparation of all semiconductors the reduction of all unwanted impurities to insignificant levels, and the correctness of stoichiometry, is of prime importance. It was therefore necessary to take a number of steps to ensure the purity of the materials. A good description of the techniques of obtaining pure materials is given by Lawson and Nielsen (82).

18.1 Purity of the elements

In the earliest part of the work commercial Te was purified by successive distillations from a glass compartment at 450°C to a similar cooler one, under continuous vacuum provided by a rotary oil pump, the process being repeated several times until the surface of the Te appeared bright and clean, but later 99.9995 p.c. Te was obtained from Canadian Copper Refiners Ltd. Commercial Cd was purified in a similar manner. The Hg was first passed through a column of weak nitric acid and then distilled three times in the standard double column apparatus, after which treatment no impurities could be observed to be floating on the surface, which indicates an impurity level of less than a few parts per million. Other elements were purchased from Johnson Matthey & Company or from L. Light and Company in the form of small lumps, or powders, and had a purity of 99.999 p.c. or better. The black surface layer which appeared on In was removed by an HCl etch.

18.2 Synthesis of materials

As none of the elements used reacted with quartz, all the compounds and alloys were formed in transparent silica ampoules. In the case of compounds, stoichiometric quantities of the elements, having been weighed to 0.5 of a milligram, were placed in a carefully cleaned silica tube sealed at one end. The tube was then drawn to a narrow neck a little above the elements which were protected from the heat and hence oxidisation and vaporisation by a few turns of wet asbestos yarn wound on the tube. After a few hours at a pressure of less than one micron of Hg, which was provided by an oil diffusion pump coupled to a rotary backing pump, the neck was sealed leaving a wall as thick as possible at the end of the ampoule. The low pressure inside the tubes corresponds to the order of 10^{12} molecules of gas per cc and so introduces a negligible degree of impurity. Improved degassing could be achieved by gently heating the tube while on the pump, but this is not possible if Hg is present or if there is powder in the tube as both pass through the neck.

After several attempts to form ingots by quenching or slow cooling from the melt, the following method was adopted as the standard heat treatment. The constituents were reacted at about 450°C and then the compound was heated to about 100°C above the melting point. When Hg, which has a vapour pressure of 22 atmospheres at 600°C, is present there is great liklihood of an explosion if the furnace temperature is not carefully controlled and increased slowly.

As a precaution all ampoules were placed inside metal sheaths so that, in the event of an explosion, the furnace should not be damaged. All materials were kept liquid for at least six hours and were mixed by rotation of the furnace. Ingots were formed by cooling the melt at about 15°C per hour to well below the freezing point and were further cooled in the furnace to near room temperature by switching off the current. The best ingots seemed to be formed when the furnace, and hence the ampoule, were at an angle of about 20° to the horizontal. Ingots which needed further heat treatment were then transferred to the wider bore annealing furnaces. The standard annealing procedure was 60 days at 600°C.

18.3 Notes on the cutting of Ingots

The ingot size which provided the least waste of material was found to be 0.6 cm in diameter and a few cm long. Wider ingots tended to have porous central regions, and shorter ingots sometimes broke into pieces too small to be of use. Ampoules were opened by cutting off each end; the ingot could usually then be pushed out. Only certain of the alloys containing Cd showed expansion on cooling and for them the procedure adopted was to cut the silica with the ingot inside. Cutting was carried out with a 4 inch diameter carborundum wheel 0.015 cm thick, at 4,000 revolutions per minute, which was cooled by a continuous jet of soluble oil. A clear plastic cement which was easily soluble in acetone and which, after being heated a little, set hard in 15 minutes, appeared to

be the best way of fixing the ingots to 1 in. steel cylinders which were clamped magnetically to the movable table of the cutting machine. All traces of oil and glue were removed from the final samples cut from the ingots by washing in continuously distilled acetone. It is unfortunate that even with the above procedure some of the materials proved too brittle to yield good samples; this particularly applies to unannealed materials.

Each ingot was first sliced in half lengthwasy and the best sections chosen for further cuts into samples for electrical and optical work.

18.4 Grinding, polishing and microscopy

At least one cut surface in most ingots was inspected under a polarising microscope having a magnification of about 100x. A variety of polishing techniques were tried and the following was found to be the best. The freshly cut surface was further ground figure eightwise in a paste of water and grade 700 carborundum powder on a glass plate until it appeared uniform. At this point the crystal grains became apparent, each different orientation showing up in obliquely reflected light. Polishing proceeded in two stages: firstly on a beeswax lap containing the same fine carborundum and then on a similar lap containing alumina of 2 micron grain size. Finally the sample was rubbed on Selvyt cloth. A fine mirror surface could be obtained with homogeneous material although a few scratch marks still showed up under the microscope, as in figure 21a.

a) $Hg_5In_2Te_8$ Single Phase.

b) 7.5 m.p.c. In_2Te_3 Two Phase Region.

FIG. 21. MICROPHOTOGRAPHS OF POLISHED SAMPLE x 100.

Microscopic examination revealed two types of defect in the materials. Firstly, holes in the ingots showed up as dark patches as in figure 21a. It is thought that these may be due to pockets of gas remaining in the solid or small amounts of weak material which had been removed during the cutting process. It was also possible to discover a second phase in the material by its different reflectivity, provided that the regions of the second phase were large enough to be observed. Thus the two phase regions in many of the spot composition ingots of figure 21b could be observed, as could the grain boundaries in impure HgTe, which must have consisted of Te. Two phase regions could not be detected by this means in compositions at about 55 mol.p.c. In_2Te_3 in Hg_3Te_3 which by X-ray examination contained two phases of differing lattice parameters. Figure 21b shows a typical two phase region. It is taken from the extreme top of an otherwise homogeneous ingot at the composition 7.5 mol.p.c. In_2Te_3 in Hg_3Te_3. The minor phase may be HgTe or, more likely, Te. Since HgTe is single phase at all temperatures below the melting point under normal pressures (section 9.0), and since it is likely that alloys near HgTe are similar, the second phase is not a remnant of a high temperature phase.

19.0 X-ray Techniques

At least one X-ray photograph of each ingot was taken. The object of this was two fold: the lattice parameter could be calculated from the spacing of the lines, and the sharpness of the lines gave a good indication of the condition of the material.

Photographs were taken using a Debije-Scherrer powder camera fitted to a Philips X-ray Diffraction Generator which provided CuK_α radiation through a Ni filter. A narrow collimator and an exposure of 24 hours gave the best results with the very fast, fine grain film, Ilford Industrial G. Small but representative samples from the ingots were finely powdered in an agate pestle and mortar and mounted on thin glass fibres with collodion. Neither the glass nor the collodion give rise to any lines, although they do increase the background darkening especially at low angles. The overall size of the fibre plus powder was about 0.25 cm. Care was needed in the centralising of the fibre in the camera.

The sharpness of the high angle lines is influenced largely by the degree of homogeniety of the sample. Thus if in a sample, the lattice parameter varies even only slightly from one set of a few hundred atomsto the next, the overall effect leads to diffuse lines. In general, samples which had been annealed for a few weeks at a high temperature showed much improvement in the sharpness of the lines. This is shown in figure 22. Ingots showing diffuse lines even after annealing were usually rejected, or, if measurements were taken they were regarded as doubtful. Material which splits into two phases can also be analysed by X-ray diffraction provided the weakest phase is not less than about 15 p.c.: a lattice parameter can be calculated for each phase.

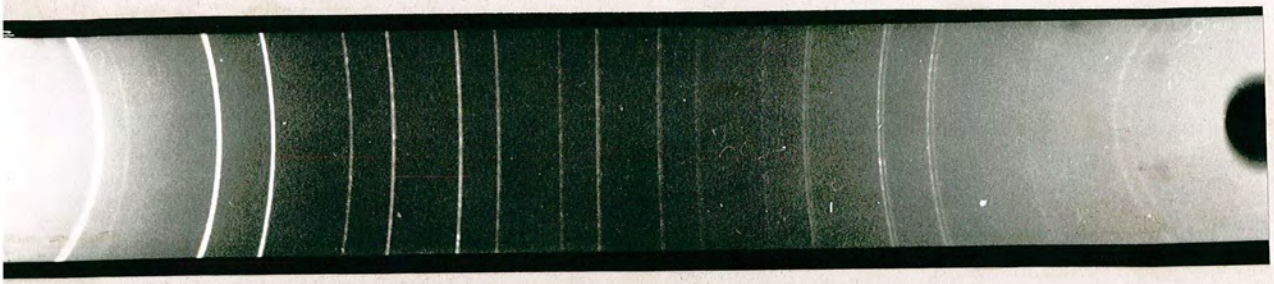

a) 17 m.p.c. In_2Te_3. Disordered Structure.

b) $Hg_5In_2Te_8$ Unannealed.

c) $Hg_5In_2Te_8$ Annealed. Ordered Structure.

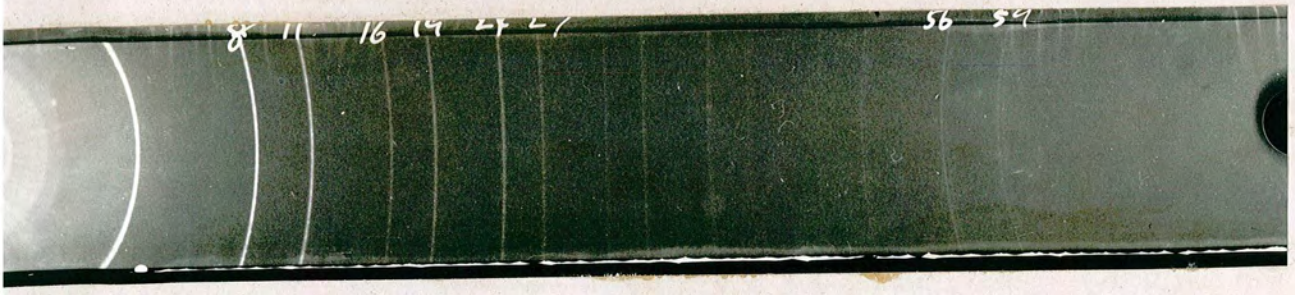

d) $Hg_5In_2Te_6$. Disordered.

FIG. 22. X-RAY DIFFRACTION PHOTOGRAPHS.

19.1 Determination of Lattice Parameter

The asymetric method of mounting the film, due to Ievins and Straumanis, has the advantage that no calibration of the camera is needed since by the measurement of both low and high angle lines, the positions corresponding to $\theta = 0^{\circ}$ and $\theta = 90^{\circ}$ can be found. After processing, the 25 x 355 mm film was attached firmly to the glass plate of a Hilger and Watts vernier film measurer so that the position of the lines could be measured to an accuracy of 0.05 mm.

Cubic lattice parameters were calculated according to the standard method (83 ch.13). At least two of the high angle doublet lines (due to the 0.25 p.c. difference in the two CuK_{α} wavelengths) which could be resolved were measured and the value of the lattice parameter calculated for each. The results were plotted against the function (83 p.190) which corrects for absorption and divergence of the X-ray beam: the value of the extrapolation to 90° was taken as the correct lattice parameter a_o. The accuracy of the determination depended mainly on the sharpness of the lines, and for well resolved high angle lines the error in a_o was reckoned to be 0.002 A.

For the cubic structure the lattice parameter a is calculated from the reflection angle θ using the Bragg equation

$$\mathrm{Sin}^2\ \theta = \frac{\lambda^2\ N}{4\ a^2} \qquad \ldots\ldots\ 48.$$

where λ is the wavelength of the radiation and N is defined from the Miller indices h, k and ℓ of the reflecting plane by the relation

$$N = h^2 + k^2 + \ell^2 \qquad \ldots\ldots 49.$$

In the zinc blende structure, being essentially face centred cubic, values of N are restricted to those where h, k, and ℓ are homogeneous. The set of strong lines which appear on a powder photograph of any material with a diamond-type structure are indexed N = 3, 8, 11, 16, 19, 24, 32, ... Usually the remaining f.c.c. lines N = 4, 12, 20, 36, ... can be seen weakly for zinc blende materials. These latter lines were visible in HgTe, but not in some of the close alloys as is shown in figure 22. The final value of N occurs for the highest value of θ less than 90°. Thus, although line 67 of the strong series could be seen in HgTe photographs, it was not present for 50 mol.p.c. In_2Te_3 in Hg_3Te_3. The calculation of the lattice parameter for the latter relied on the considerably lower angle lines N = 56, 59 and for this reason was not so accurate.

20.0 Infrared Transmission

The object of this work was the determination of the optical energy gap. The nature of the samples and the apparatus did not allow accurate determination of the absorption edge so that no knowledge could be gained about the nature of the electron energy transitions.

The energy gap is best determined if the complete absorption

edge can be plotted as a function of wavelength. This means that some transmission in the high absorption part of the spectrum must be obtained, which necessitates sensitive detection and amplification of the transmitted signal, and also samples considerably less than 100 microns thick. The production of these thin sections was considerably hampered by the brittleness of the materials, even in single crystal form.

20.1 Preparation of samples

The following procedure was found to provide adequate samples, and avoided a high number of breakages. In the region between the visible and a wavelength of 2 microns, where most of the absorption edges of the materials investigated occur, glass and most kinds of glue are still transparent, so that the thin sections could be mounted on glass slides. The glue used was Lakeside 70 which melts at about 80°C and sets into the same volume as its liquid. (This is not true of the solution types of glue which were unsuitable for this purpose). One face of a section, usually a quarter of an ingot cut lengthwise and then across, was given a high degree of polish by the method of section 18.4. This was then stuck to the thin glass slide and surrounded by three pieces of copper foil 90 microns thick. The whole was stuck to another small piece of glass so that it could be gripped for polishing. Also any defects in the section, such as porosity, could be seen when the slide was viewed against the light. The purpose of the copper foil was two-fold. In the first place,

because it is a little harder than the sample, it grinds down less fast and ensures an even thickness for the section. Secondly, when the foil reaches about 70 microns in thickness, it is easily removed from the glass slide and this gives a good indication of the thickness of the section. After the removal of the copper, the sample was polished on the beeswax lap containing carborundum 700. Thus the final section was about 50 microns thick but was still supported on the thin glass slide. For those samples whose energy gap lay further in the infrared the section had to be lifted carefully from the glass, which had been gently heated to melt the glue, placed in warmed methanol to allow the glue to be dissolved, and transferred to cover a suitably sized aperture in a metal plate. This naturally resulted in the breakage of several samples. Finally, before the sections were set up for infrared measurements, any transparent areas surrounding or within the sections were covered over with matt black paint.

20.2 Measurements

Two sources of radiation were used. For the near infrared, a 750 watt mains projector lamp (run at two thirds power for longer life) sufficed, but beyond 2 microns wavelength, it was necessary to use a Nernst filament. Measurements of transmission were taken with a Hilger and Watts large aperture spectrometer using as the detector a linear vacuum thermopile connected to a galvanometer amplifying system. Some trouble was experienced with the thermopile due mainly

to the loosening of the casing screws, and also to its extreme sensitivity to changes in the ambient temperature and to mechanical vibrations. The whole apparatus was placed on a foam rubber mat and the thermopile wrapped in cotton wool, although at times even these precautions were not adequate to prevent drift on the secondary galvanometer.

A glass prism was employed in the range up to 2 microns and the spectrum of the lamp as transmitted by a thin glass slide coated with a layer of glue was first determined. This showed a smooth curve with a maximum near 1.3 microns and a sharp dip at 1.35 microns which was thought to be due to absorption by water vapour. For certain of the samples, the monochromator slits had to be fairly wide (up to 0.5 mm) in order to observe the complete absorption edge, sothat in general the absolute value of the percentage transmission was not found. This was unimportant in the plot of the log of the percentage transmission as a function of wavelength. Interpretation of the edge as regards energy gap is given in section 6.1.

In the region beyond 2 microns wavelength the glass prism was replaced by one of rock salt, and the sections no longer mounted on glass. Because of the rapid change of transmission with wavelength due to absorption peaks in the atmosphere it was necessary to measure consecutively the transmission intensity first through the section and then through a similar sized plain aperture. This could be done provided none of the readings was sufficiently large to send the primary galvanometer beam off the prism which divides it in the

secondary circuit. In practice this limited the ratio of transmitted intensities to $1:10^4$.

The calibration of the wavelength was checked using the lines of the sodium spectrum. The first experimentwas performed on a sample of Ge. The value of 0.775 ± 0.025 eV obtained for the energy gap was slightly lower than that generally quoted but within the experimental error.

Two related factors prevented a more detailed examination of the absorption edge. As the sections could not be made thinner than about 20 microns and rarely as thin as that, it was necessary to use wide monochromator slits, which implied dispersions of up to several hundred Angstroms and a corresponding lack of definition of the edge.

21.0 Electrical Measurements

A single apparatus was designed to measure electrical conductivity, Hall and Seebeck coefficients consecutively at temperatures in the range $300^{\circ}K$ to $800^{\circ}K$. The basic design is standard and a fuller description of this type of apparatus is found in reference 12 pp.33 - 55. Details of the present apparatus can be described conveniently under three main headings.

21.1 The Sample Holder

Figure 23 shows the design of the holder which measured

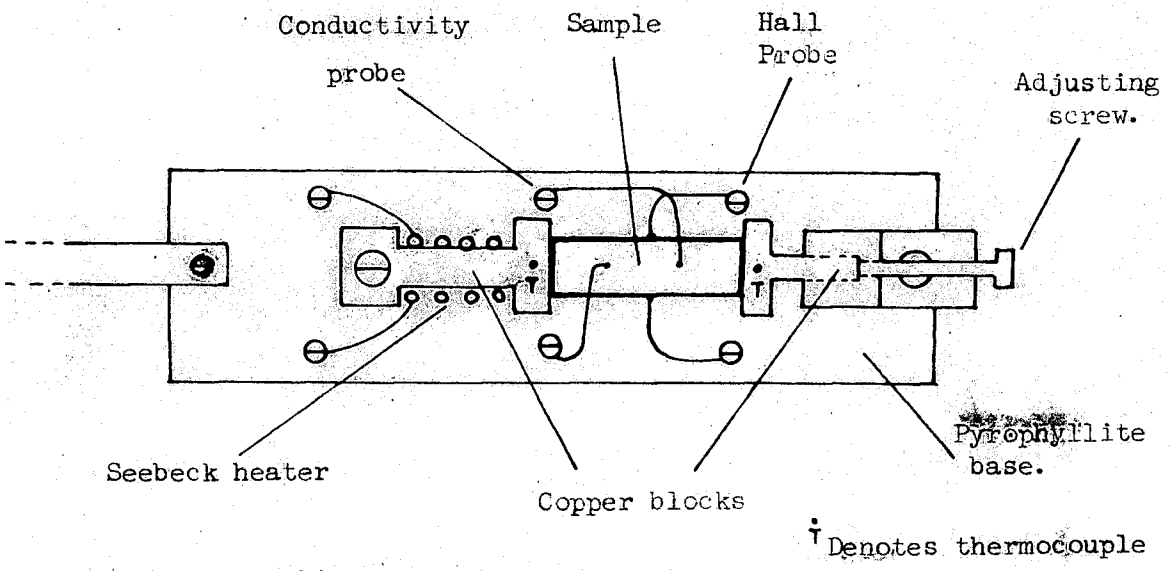

Fig. 23 The Sample Holder.

7 cm by 2 cm. The base was machined from pyrophyllite which is easily worked and has a high electrical resistivity. All probes and blocks were secured to the base by 8 or 10 B.A. nuts and bolts to which, on the reverse side of the base, copper leads sheathed in refrasil (a high temperature woven insulator) were attached. Contact between the sample and the copper blocks was maintained by pressure from the adjusting screw. This arrangement worked well provided the temperature was always increased during the experiment, and eliminated the need for elaborate spring pressure, although contact was soon lost if the temperature was decreased. The faces of the copper blocks were cleaned after each experiment. Contact to badly

finished and short samples was improved by a coating of silver dispersed in solvent MIBK, manufactured by Acheson Colloids Ltd. This practice was generally avoided because of the possible contamination of the sample.

The two conductivity and the two Hall probes were made of 0.3 mm tungsten wires etched electrolytically to points, which maintain their springiness at moderately high temperatures. Good pressure contacts could be made by bending the wires beforehand in the appropriate directions. The alignment of the Hall probes was carried out while a current flowed through the sample. The position of least standing voltage thus found did not always coincide with the geometrical opposition of the probes, and for certain of the high resistivity samples the standing voltage could not be reduced to the same order as the Hall voltage and thus had to be counteracted by a bias voltage.

The dimensions of the sample were measured with a micrometer screw gauge and the distance between the conductivity probes placed on the upper face of the sample with a travelling microscope. As the length of each sample was limited to about 10 mm by the shape of the ingot from which it was cut, the optimum rectangular cross-section was 2.5 mm x 1.5 mm. Certain samples, because of their brittleness, had to be made smaller than this, although it was never necessary to apply the correction taking into account the shorting effect of the end contacts on the Hall voltage. (12 p.45).

The hot junctions of two chromel-alumel thermocouples were placed infinely drilled holes in each of the copper blocks and fixed by small quantities of Aquadag, whilst the cold junctions were kept at room temperature. Thus both the absolute temperature and uniformity of temperature along the sample could be ascertained during the conductivity and Hall effect measurements. Alternatively, the current leads could be used in the measurement of the thermo-electric voltage set up in the sample by the 5 ohm heater wound on the upper block.

21.2 The Magnet

A medium-sized electromagnet was constructed on the premises. It was designed so that the gap between the pole pieces could be adjusted to give the maximum field that the width of the apparatus placed between the poles would allow. Connected to the DC supply of 120 volts it took a current of 11 amps and provided a maximum induction of 10,000 gauss at a 2.5 cm pole gap. To accommodate the furnace and its water cooling jacket mounted vertically between the pole pieces, the gap had to be widened to 5 cm. This lowered the induction to 6,250 gauss which, nevertheless, enabled the Hall voltage to be measured on all but some high resistance specimens through which only a low current could be passed at room temperature. In the central plane between the 7 cm diameter pole faces, the induction was uniform to within 5 p.c. over the pole area but there was a considerable increase in induction near the bevelled edges of the pole pieces. The magnet was not water cooled but could be

left on for sufficient time for each reading to be taken, without any noticeable drop in current.

21.3 Experimental Arrangement and Procedure

The sample holder was mounted on a brass rod attached centrally to a 10 cm brass plate containing three ceramic to metal vacuum seals through each of which four of the electrical leads passed. Fig. 24 shows the sample holder fitted into a silica tube that had beenwidened at one end to meet the brass plate in an O ring seal. A screw clamp enabled the pressure inside the tube to be slightly above atmospheric. Gas could be let in, or the tube evacuated via the aperture at the base of the tube. Originally, the experiments were done in vacuum to avoid oxidation of the sample and copper parts, but itwas later discovered that samples decomposed at a higher temperature in an atmosphere of argon. Before each experiment therefore, the tube was flushed with argon several times and finally filled to a pressure of 3 lb/sq. in. above atmospheric.

A Kanthal furnace was wound non-inductively round the silica tube which had first been covered with a layer of asbestos paper. A covering of alumina cement separated the windings from a narrow water cooling jacket. Readings were taken only on heating up every quarter of an hour after a current increase of 0.3 amps which provided a temperature increase of about 15°C, until a maximum temperature of about 400°C was reached at 7 amps.

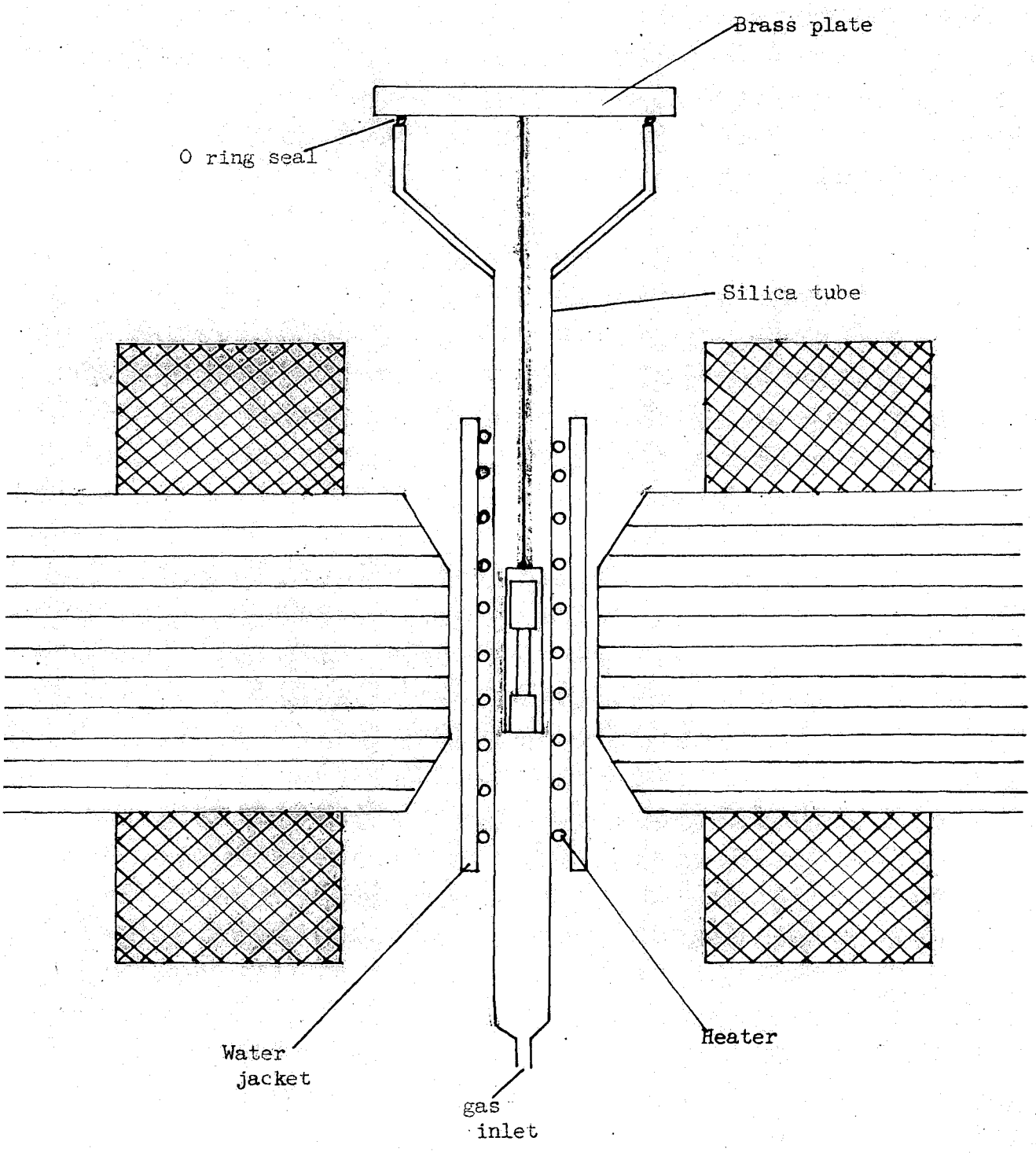

Fig. 24. Magnet and Furnace.

Electrical readings were taken on a variety of instruments. Originally all were taken on a potentiometer reading from 1 volt down to 1 microvolt, but as the off-balance current from the high resistance samples was not sufficient to deflect the galvanometer coil, the potentiometer was replaced by a Philips D.C. Microvoltmeter. The latter had an input impedance of 1 megohm on the low range, which was considerably above the highest impedance of any sample measured. It had the advantage of providing accurate readings in quick succession. To this instrument were connected in turn the conductivity probes, the Hall probes, and, after a temperature gradient had been set up, the leads from the copper blocks to measure the thermoelectric voltage.

21.31 Seebeck Coefficient

Temperatures were measured on a small potentiometer reading to 10 μV so that the possible error in the temperature difference of about 10°C was about 5 p.c., but because of the nature of the contacts to the sample the value of the Seebeck coefficient thus obtained was probably slightly lower than the actual value. The values were sufficiently large for the Seebeck coefficient of copper, 1.5 μV/°C, to be neglected. The temperature at which the Seebeck coefficient was measured was taken as the mean of the two extreme temperatures.

The Seebeck coefficient was calculated from the formula

$$\alpha = Q/\delta T \qquad \ldots\ldots 50.$$

where Q is the thermoelectric voltage in μV. developed under a

temperature difference $\delta T^{o}C$.

21.32. Conductivity

The current to the sample was provided by either a battery of 10 accumulators or a stabilised power supply. The output of the latter could be varied up to 30 volts or a maximum current of 0.5 amps and incorporated its own ammeter/voltmeter which was checked by means of a standard resistance and the microvoltmeter. In certain circumstances the power supply caused irreversible voltages to be set up on the conductivity probes and it was necessary to use the battery and a potential divider. The magnitude of the battery current was obtained from the voltage across the standard resistance. Low currents through the sample were also measured in this way.

The conductivity was calculated from the standard formula

$$\sigma = \frac{Il}{V_c} bd \qquad \ldots\ldots 51.$$

where V_c is the mean of the two voltages on the conduction probes for forward and reverse currents, l the distance between the probes, I the current, b the breadth of the sample and d the depth. All lengths are measured in centimeters and electrical quantities in practical units as is the standard practice in semiconductor work. The reversal of the current was necessary to eliminate the effects of stray thermoelectric voltages which for some samples were appreciable at room temperature. Provided the sample is homogeneous and the probes are in a region where the current density is uniform, the conductivity should be obtained to a high degree of accuracy.

21.33 Hall Effect

In the measurement of the Hall voltage not only was the current reversed but also the magnetic field; thus V_H is the mean of four readings. This procedure eliminates all errors except those due to the Ettinghausen effect (12 p. 27) and the inhomogeniety of the sample. In general the four readings showed random variation, although there were occasions when the reversal of the field produced a noticeable difference. Fluctuations in the current due possibly to defects in the contacts made the detection of the Hall voltage impossible for some samples. However, these tended to die out with increasing temperature. Where the alignment of the Hall probes was not achieved, a biasing voltage provided by a potentiometer immediately before the microvoltmeter was necessary, and unfortunately this had to be of the order of 100 times the Hall voltage for a few samples. The Hall constant was calculated from the formula

$$R = \frac{V_H \, d}{I \, B} \times 10^8 \text{ cm}^3/\text{Coulomb} \qquad \ldots\ldots 52.$$

where B the induction is measured in gauss.

The accuracy of the Hall coefficient depended on the condition of the sample and its conductivity. For homogeneous material and a high conductivity, the error was probably small, of the order of a few per cent. At temperatures where the resistivity was high and the fluctuations of the standing voltage on the probes was of the

order of the Hall voltage, the error was possibly a factor 2 or 3. Measurements that were difficult to obtain are indicated in the presentation of the results.

22.0 Thermal Conductivity Measurement

The thermal conductivity of a poor conductor is one of the most difficult properties to measure since the temperature in all the important part of the apparatus must be specified and carefully controlled. In view of the difficulties in the technology of apparatus for measurement at high and low temperatures, it was decided that an apparatus for use only at room temperature would be built. The size of the apparatus was governed by the dimensions of the samples, which were either cylinders 0.6 cm in diameter and about 0.5 cm high or of slightly larger square cross-section and not so high.

The difference in quality between a modification of the Lees' disc method of measurement and the comparison method is slight at room temperature. The absolute method was chosen because it could be used for a variety of thermal resistances without an elaborate set of standards.

Figure 25 shows the design of the apparatus. The heat source, a 1 cm diameter copper cylinder containing a 1 watt electrical heater, was secured centrally by a thin rod of perspex to the copper base. Closely surrounding the source though not touching it was a copper shield which push-fitted into the base.

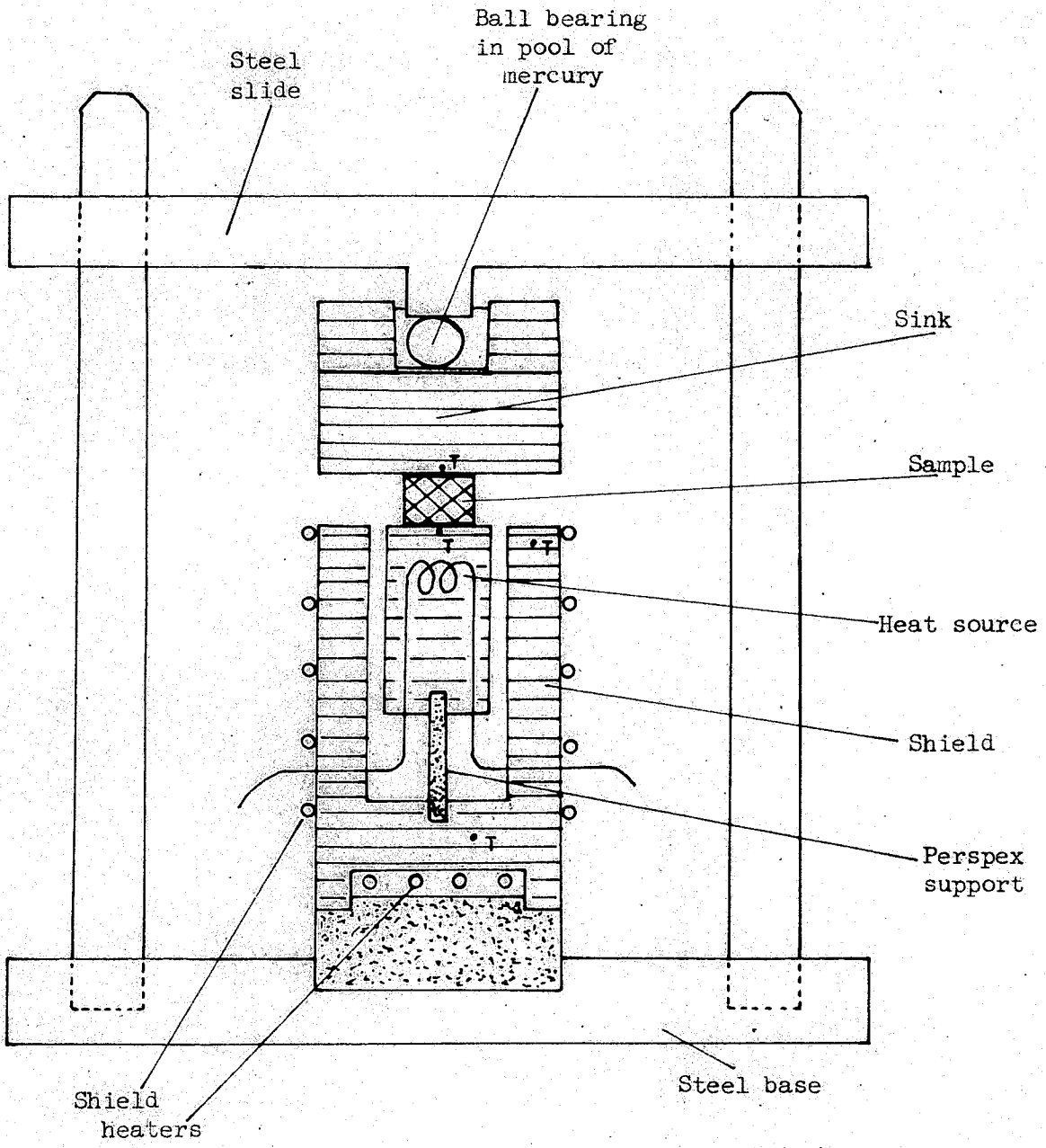

Fig. 25. Thermal Conductivity Apparatus.

Thermal insulation. Copper parts.

T Thermocouple.

Both the shield and the base were heated independently and the base was insulated from the stand by a section of sindanyo. A block of copper acted as a heat sink. Pressure on the sample was exerted by the weight of a steel slide of vertical movement through a spring loaded ball bearing to the sink. To prevent the temperature of the sink rising, heat contact to the slide was made by a pool of mercury round the ball bearing and spring. The advantage of having the apparatus this way up lies in the ease of replacing samples: only the slide and the sink need to be moved for access to the sample so that none of the delicate electrical leads are disturbed.

It is essential in this work that the thermal resistance of the contacts between the sample and the copper surfaces is negligible. The specific resistances of various types of contact are discussed by Bauerle et al. (84 p. 293). It is apparent that liquid metal contacts are far superior to others. At room temperature the most suitable liquid is a eutectic mixture of In and Ga. In common with the findings of Nielsen (85) it was observed that In reacts with HgTe to form a corrugated, dull grey surface. This defect was overcome by coating the samples with a thin layer of silver dispersion before applying the liquid.

Temperature measurements were made at the points marked T in figure 25, using calibrated copper-constantan thermocouples. By careful adjustment of the heating currents, the temperatures of the source, shield and base could be matched to within 1 per cent

of each other. All electrical leads from the source were of fine wire and passed through the shield. Thus heat losses due to radiation and conduction were minimised. The experiments were performed in vacuo to prevent convection.

Potential measurements were made on a Philips microvoltmeter. At the point where the copper current carrying leads joined the source heater, leads were connected for the measurement of the potential across the heater. The current through the heater was obtained from the voltage across a standard resistance. The thermal conductivity K was calculated from the formula

$$P = K A \delta T/L \qquad \ldots\ldots 50$$

where P was the electrical power input, A the cross-section area and L the length of the sample, and δT the temperature difference between the source and the sink. K is usually quoted in milliwatts/ cm. ^{o}C.

The principal sources of error in the measurements were thought to be due to slightly imperfect contacts to the sample and defects, such as holes, in the sample itself.

CHAPTER IV

The Properties of HgTe - In_2Te_3 and Related Alloys

23.0 Introduction

The work reported in this chapter forms the original part of the thesis. The greater part of the chapter deals with the properties of the pseudo-binary system HgTe - In_2Te_3. In the later sections effects of structural ordering in compounds of the type $II_5III_2Te_8$ is discussed.

In section 24.0 the ternary diagram Hg - Ga - Te is considered. Originally gallium was included in the alloy system instead of indium, because the thermal conductivity was expected to be lower for compositions such as $Hg_5Ga_2Te_8$ where the three elements come from different periods. Preliminary measurements of the thermal conductivity, however, showed that the difference between compounds containing indium and gallium was small. Materials containing indium were used exclusively in the later experiments because that element possesses several advantages: it is not so expensive as gallium and is much easier to handle. Also the electrical mobility in compounds containing indium is generally greater than in those containing gallium: cf. In_2Te_3 and Ga_2Te_3(63), and III-V compounds (9).

The second part of the chapter contains a discussion of the range and effects of ordering in compounds of the type $II_5III_2Te_8$. At one time it was thought that ordered and disordered material could be obtained easily, as with In_2Te_3, but a closer examination

revealed that this was not so. The substitution of Hg, Cd or $(AgIn)_{\frac{1}{2}}$ in the place of the group II element, and of In, Ga and Al for the group III element is considered as a means of producing ordered and disordered material.

24.0 The Ternary Phase Diagram Hg - Ga - Te

In order to determine the range of solid solution, a short investigation of the phase diagram of Hg - Ga - Te was made in the region near HgTe. From previous work (sect. 14.3) solid solution was known to exist between the compounds HgTe and Ga_2Te_3 except for a miscilibity gap in the centre. Two compounds had been identified on the pseudo-binary line, $HgGa_2Te_4$ and $Hg_5Ga_2Te_8$. The compound GaTe had also been identified.

Spot compositions were made up at the points marked in figure 26, which correspond to low whole number stoichiometric proportions. The melts were cooled slowly in a furnace at uniform temperature since rapid quenching caused the materials to froth, due to mercury gas escaping, and made the ingots porous.

An examination of the various samples by X-ray powder photography, and by microscopy, showed that compositions F and G which lie on the solid solution line marked in figure 26, and E which is just above the line, are single phase. Ingots A, B, C, and D were definitely two phase, one phase of which had a melting point of about 420°C and was probably associated with the eutectic points of Hg - Te and Ga - Te at about 88 atomic p.c. tellurium. The

Fig. 26.

Part of the Ternary Phase Diagram for Hg/Ga/Te.

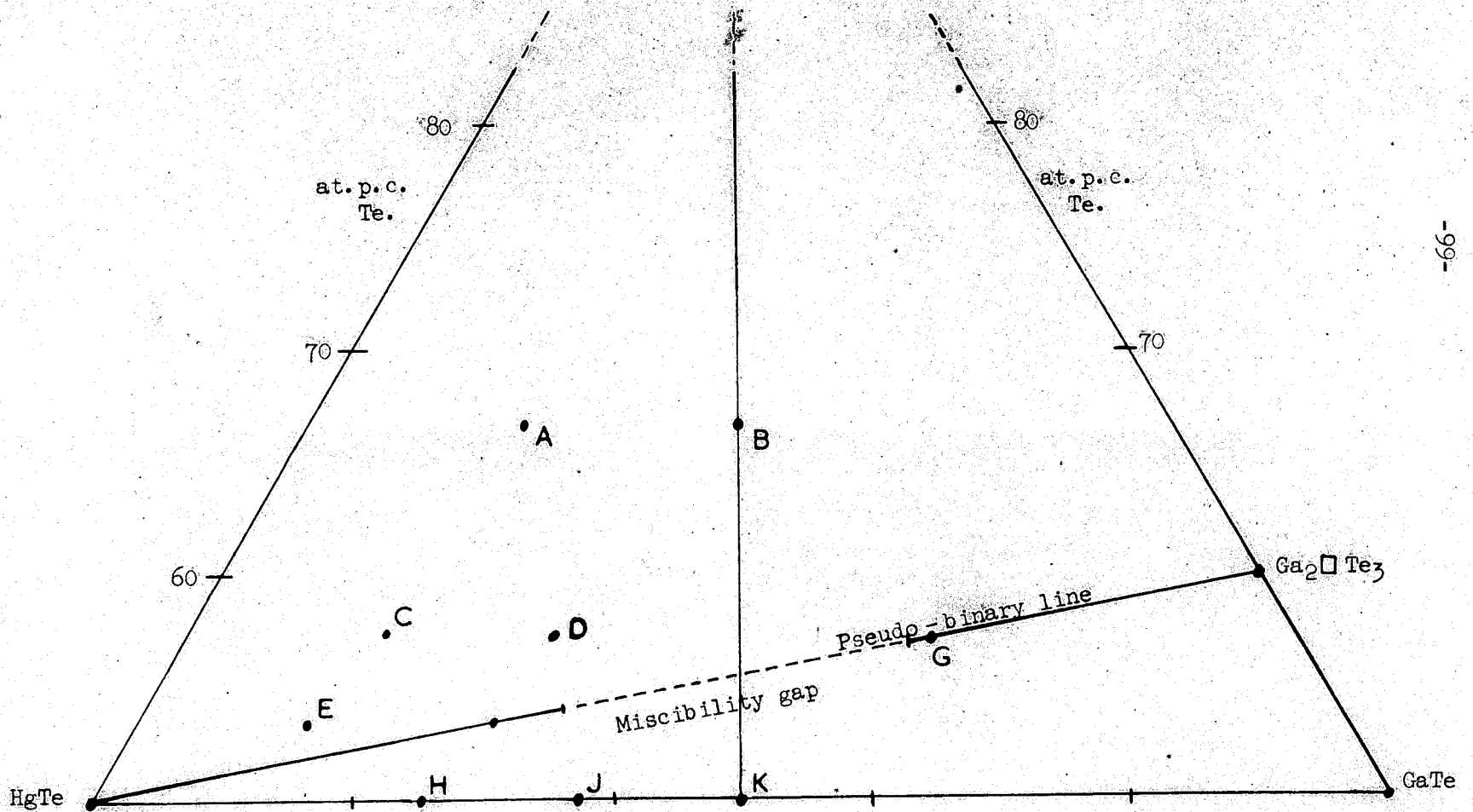

second phase present in ingots A and C had the HgTe structure with decreasedlattice parameter s, corresponding to compositions near E. In ingots B and D the zinc blende phase showed the ordering lines common to compositions near $Hg_5Ga_2Te_8$. Ingots H and J also contained the (528) ordered phase but there was much free mercury present in the ampoules. Ingot K contained material similar to $HgGa_2Te_4$ and also some liquid mercury.

In conclusion, it can be said that the solid solution which exists along the HgTe - Ga_2Te_3 line probably does not extend far above or below that line. The central region of the diagram, in common with the boundary lines Te - HgTe and Te - Ga_2Te_3, does not contain any solid solutions between Te and the zinc blende phases, but there is a eutectic near the Te vertex with a melting point of about 420°C. In particular the composition $Hg_2Ga\ Te_4$, a structure for which has been proposed by Pamplin (sect. 15.0), does not appear to be single phase.

25.0 The Pseudo-binary System HgTe - In_2Te_3

Although the absence of any differential thermal analysis on this system make definite proposals for a phase diagram impossible, the results that are discussed in this and the following sections appear to be in accordance with the phase diagram presented in figure 27. The diagram is based mainly on the results of the examination of samples annealed at 600°C. The CdTe - In_2Te_3 diagram proposed by Mason and Cook which is reproduced in figure 19, was

point D.

Fig. 27. Proposed Phase Diagram for Hg_3Te_3 - $In_2\square Te_3$.

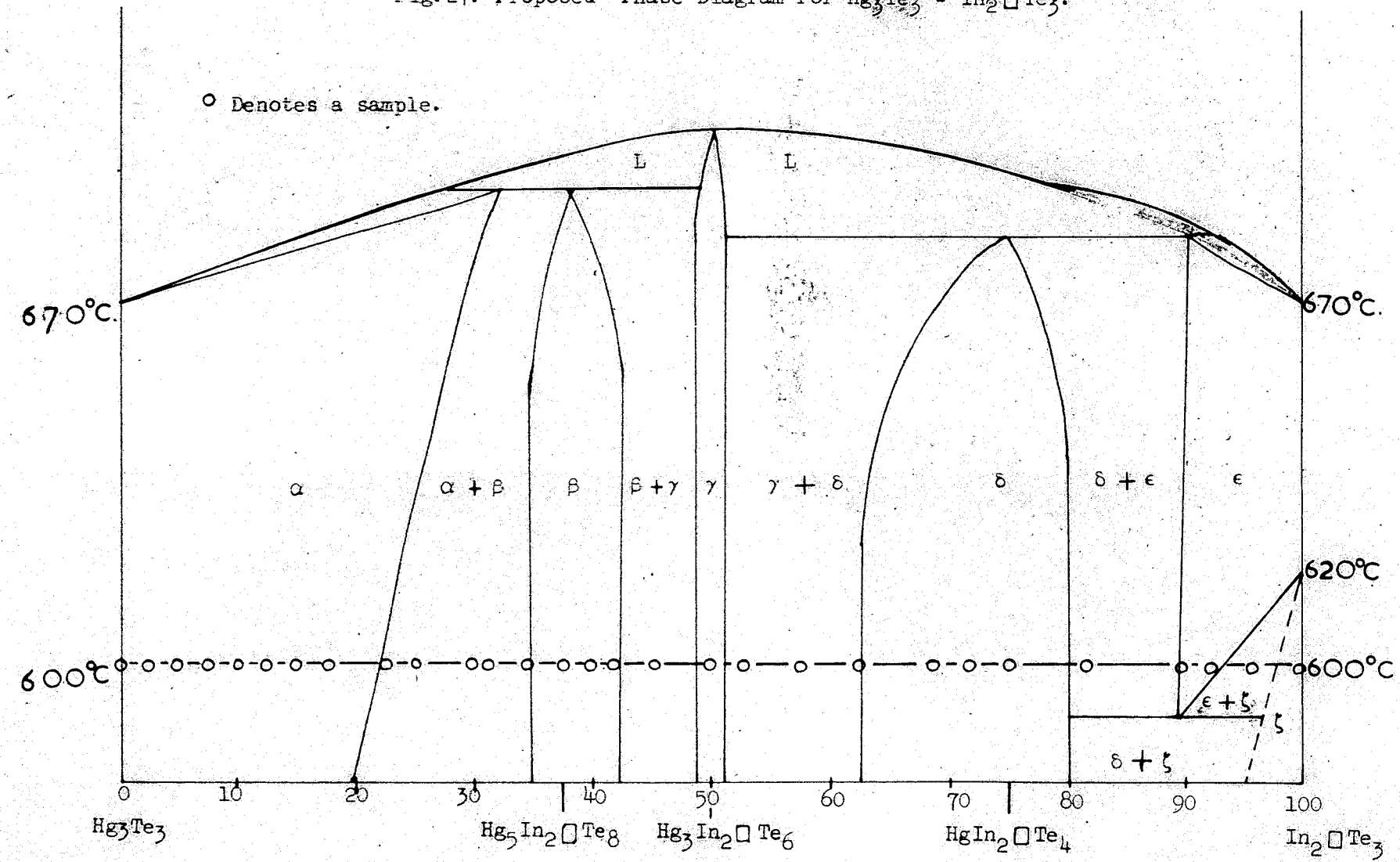

found useful. Although CdTe has a melting point of 1098°C, the phase diagrams should be similar in the In_2Te_3 half, particularly as there is a maximum in the melting point near the centre for the system involving HgTe.

The melting points of spot compositions in the region of 40 to 50 mpc appeared to be a few tens of degrees higher than that for HgTe. This implies the existence of a compound in this region, which is not peritectic as in the CdTe system. Examination of the X-ray data suggests that this compound is $Hg_3In_2\square Te_6$ with the 50 mpc composition.

Except where otherwise stated the ingots in this system were made by the following method. Firstly, large ingots of HgTe and In_2Te_3 were made according to the standard procedure (sect. 18.2). These were annealed for six days at temperatures just below the melting points. In the ampoule containing HgTe no free mercury could be seen after it had been cooled slowly. Each ingot was then ground to a fine powder and a sample taken for examination by X-ray diffraction. The correct proportions of the two powdered materials were formed into ingots by the standard method, and annealed at 600°C for 60 days. X-ray analysis showed that the lattice parameter of each ingot did not vary along the length of the ingot.

In the next section each region of the phase diagram is discussed in detail.

25.1 HgTe - 20 mpc α Phase

The HgTe type phase extends to about 20 mpc. It is characterised by extremely sharp powder photograph lines, and ingots consisted in the main of a few large single crystals. Microscopic examination showed the material to have very few holes and to be single phase except for the extreme tip of the ingot at 7.5 mpc which is shown in figure 21.

25.2 The Ordered β Phase at 37.5 mpc

The ordering lines were present with about equal intensity in all the photographs for compositions between 30 and 45 mpc, and were weakly so in those for 22.5 and 25 mpc. The high angle lines were too diffuse to allow accurate determination of the lattice parameter from photographs for 25, 30, 31, and 45 mpc. Since the lines were sharpest at 37.5 and 40 mpc, it seems likely that the phase is fairly narrow and centred on the compound $Hg_5 In_2 \square Te_8$, the 37.5 composition.

Melts of this latter composition were directionally frozen at a rate of about 0.3 cm per hour. The resulting ingots were well formed and contained single crystals of large surface area but only a few mm. thick. The X-ray photographs of the first and last ends to freeze showed diffuse lines, so that the change in lattice parameter could not be measured, although it must have been small. The electrical properties varied considerably down the ingot, one end being strongly n-type and the other nearly intrinsic. It seems likely that the

phase is formed peritectically and ingots become homogeneous on annealing.

The region between 20 and 35 mpc is two phase in the sense that the ordering is not complete. This led to a blurring of the high angle lines but not to resolution into two distinct sets of lines. The region around 45 mpc is two phase in the same manner.

25.3 The Disordered γ Phase at 50 mpc

An ingot made by direct reaction from the elements at the composition 50 mpc In_2Te_3, which corresponds to the compound $Hg_3In_2\square Te_6$, yielded a sharp set of diffraction lines prior to annealing. This suggests that the compound is formed direct from the melt at a maximum in the solidus. Since the ingot was too porous to be of use for electrical measurements, although there were some single crystals on the surface, it was powdered, reformed and annealed for 30 days at 600°C. Compounds treated in this way invariably formed solid ingots the second time.

Contrary to the findings of Woolley and Ray (sect. 14.3), this composition was not found to be ordered, and was thought to be similar in structure to the α phase. It is difficult to explain the difference, since the annealing temperature was lower than that of Woolley and Ray, and consequently the disordered phase cannot represent a high temperature phase as in In_2Te_3. The lattice parameters are in agreement.

25.4 The Central Miscibility Gap

The two phase region, with distinct lattice parameters, exists between about 51 and 62 mpc. As the percentage increases the ordering lines of the δ phase become more apparent. None of the ingots in this range were prepared for measurement except that at 52.5 mpc which was used in the study of thermal conductivity.

25.5 The δ Phase

The phase with the chalcopyrite ordered structure appears to exist between about 62 and 80 mpc and is probably centred on the compound $HgIn_2\square Te_4$, which is discussed in section 14.3. A directional freeze at this composition yielded similar results to the one at 37.5 mpc, though without the single crystals. It is probable that the composition, as with $CdIn_2Te_4$, is peritectic. Because of the difficulties of obtaining good material and taking measurements, no attempt was made to determine the electrical properties at compositions between the miscibility gap and In_2Te_3.

25.6 The In_2Te_3 Phase

The X-ray results were found to be in accordance with the phase diagram proposed by Mason and Cook for the system involving cadmium, which is reproduced in figure 19. The data from their phase diagram for the high percentage end is therefore incorporated in figure 27.

25.7 A Note on the HgTe - Ga_2Te_3 Phase Diagram

Woolley and Ray found that the central miscibility gap was much wider, ranging from 42 to 73 mpc Ga_2Te_3 (sect. 14.3). In a directionally frozen ingot of the 37.5 mpc composition, Pamplin (81) found that the lattice parameter could be calculated accurately and did not change appreciably along the ingot. These facts indicate that the maximum in the solidus may occur at the composition $Hg_5Ga_2Te_8$.

26.0 Lattice Parameter

The lattice parameters for all the materials made between HgTe and 50 mpc In_2Te_3 were calculated and are presented in figure 28. The results are in agreement with those of previous workers, and are more extensive. Since most of the electrical and thermal properties were measured only in this range, it was decided not to extend the lattice parameter measurements beyond 50 mpc.

The method of obtaining the lattice parameter, and the accuracy, is discussed in section 19.1. The low values at 30 and 31 mpc in figure 28 indicate that this region may either have been two phase one phase of which did not show up in the X-ray photographs, or that the ingot had lost a considerable amount of mercury.+ The low value at 37.5 mpc is for an ingot to which an excess of indium had been added: therefore it almost certainly contained more In_2Te_3 thereby reducing the lattice parameter. The general pattern of the lattice parameter suggests that the number of vacancies is directly proportional

+ See appendix I.

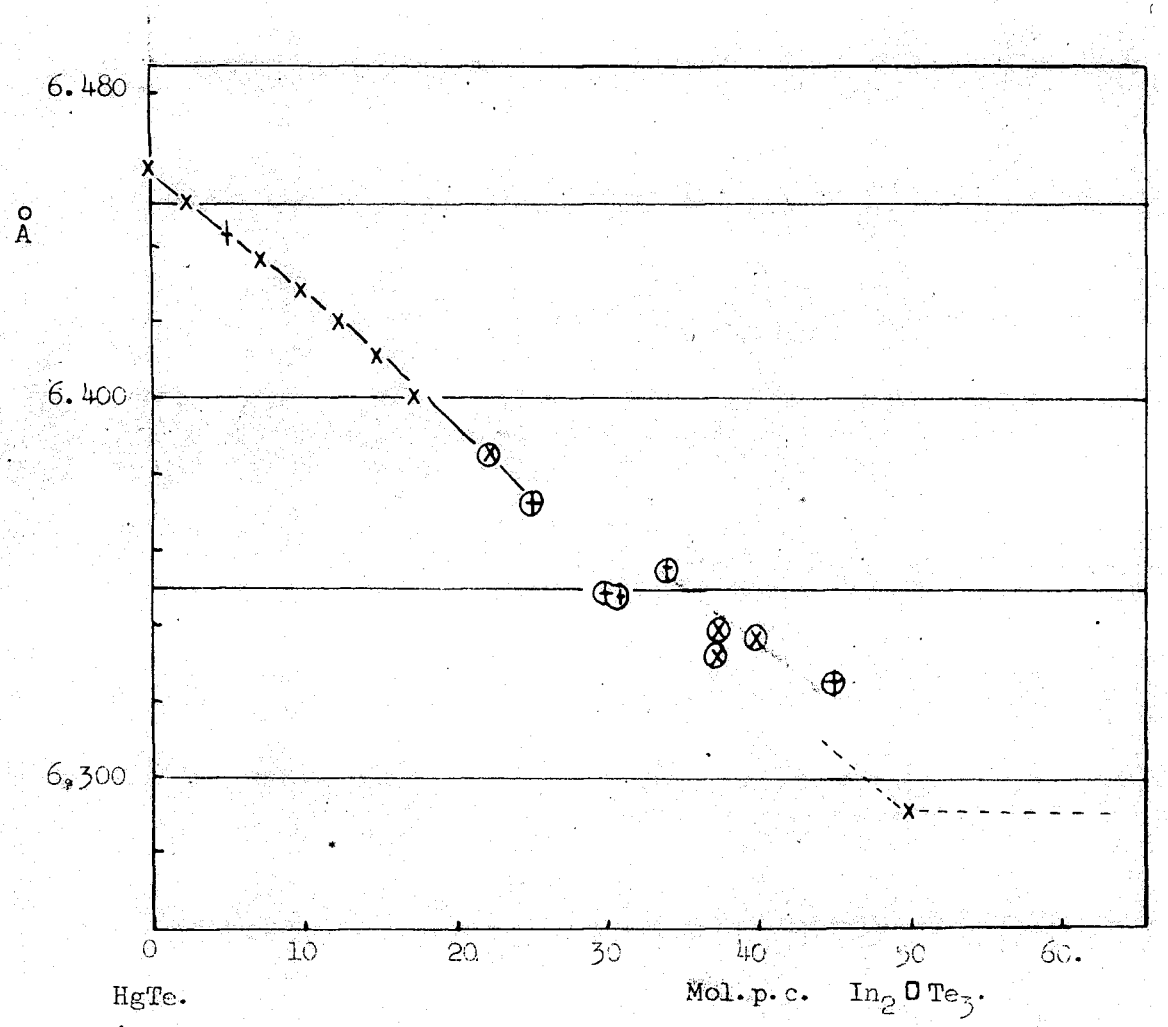

Fig. 28 Lattice Parameter a_o.

x indicates an accurate measurement.

ǂ indicates diffuse lines on the X-ray photograph.

⊙ indicates ordering lines present.

to the indium concentration, though there is no way of checking this. Accordingly, the vacancy concentration is 3.3 at.p.c. at 20 mpc and 6.25 at.p.c. at 37.5 mpc In_2Te_3. The point where indium ceases to act as an impurity in HgTe and the first vacancies are formed, has not been determined.

27.0 Optical Energy Gap

The results of the measurements of the absorption edge are presented in figure 29.

The estimated error in the measurement is indicated by the length of the vertical lines at each value. With the higher percentage compositions the error is large because the samples were in too poor a condition for complete measurement of the absorption edge. Below about 0.33 eV the uninterrupted beam through the apparatus dropped greatly in intensity, and below about 0.1 eV it was impossible to measure the transmission through the sample.

The value of the energy gap for ordered In_2Te_3 only was measured in this present work. The value for the disordered material was obtained by assuming the same difference as reported by Evans (87). The absorption curves, plotted against photon energy are reproduced in figures 30 and 31.

An interesting feature of the graph is the platform between 20 and 30 mpc at 0.35 eV, which was hinted at in the previous work (sect. 15.0). This corresponds to the two phase region between the HgTe solid solution and the ordered phase. The former continues to

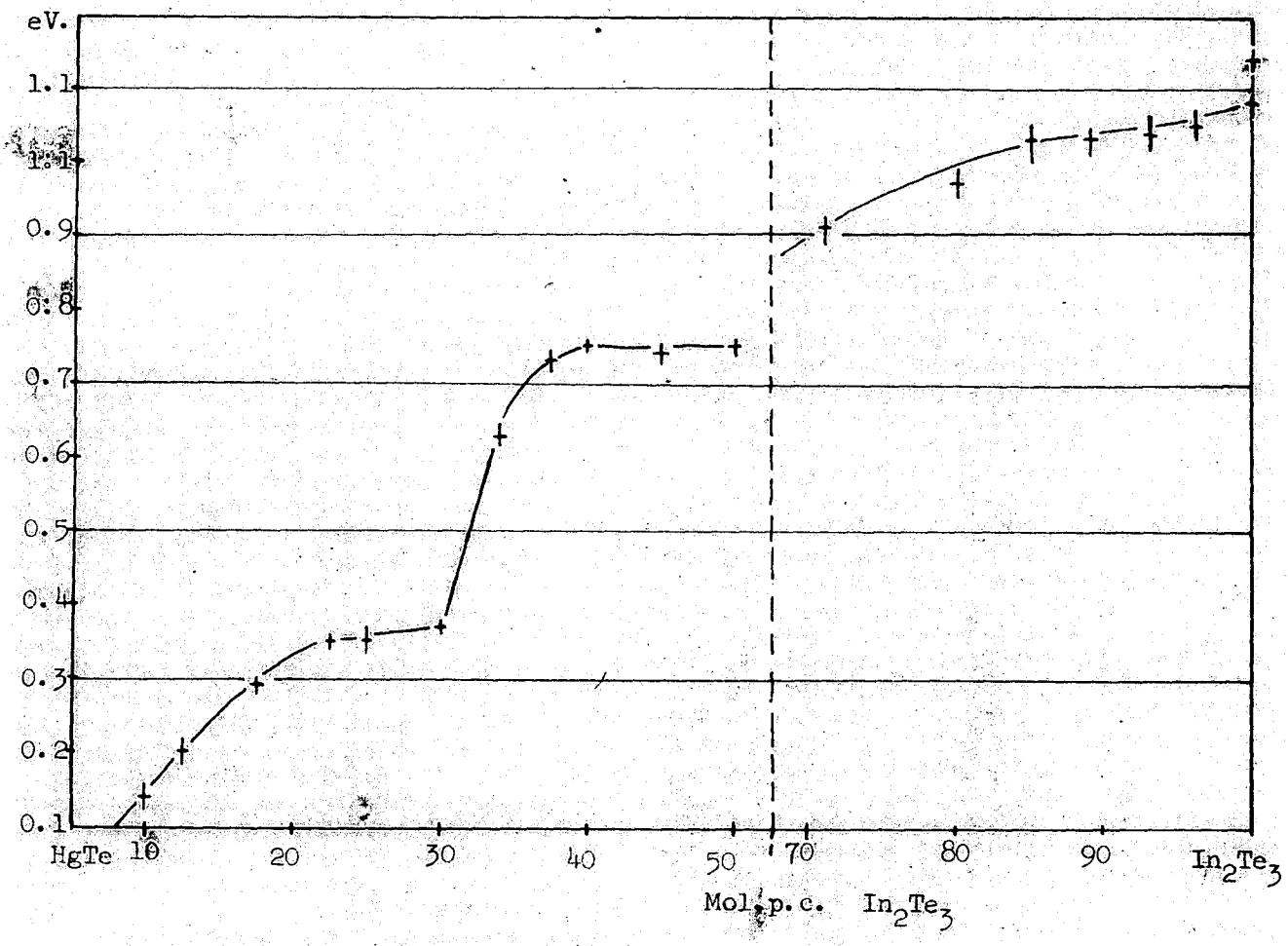

Fig. 29. Optical Energy Gap E_g.

absorb at lower energies than the latter. The values at 37.5 and 40 mpc are slightly above the general trend, which may indicate that the ordering of the structure increases the energy gap, as in In_2Te_3.

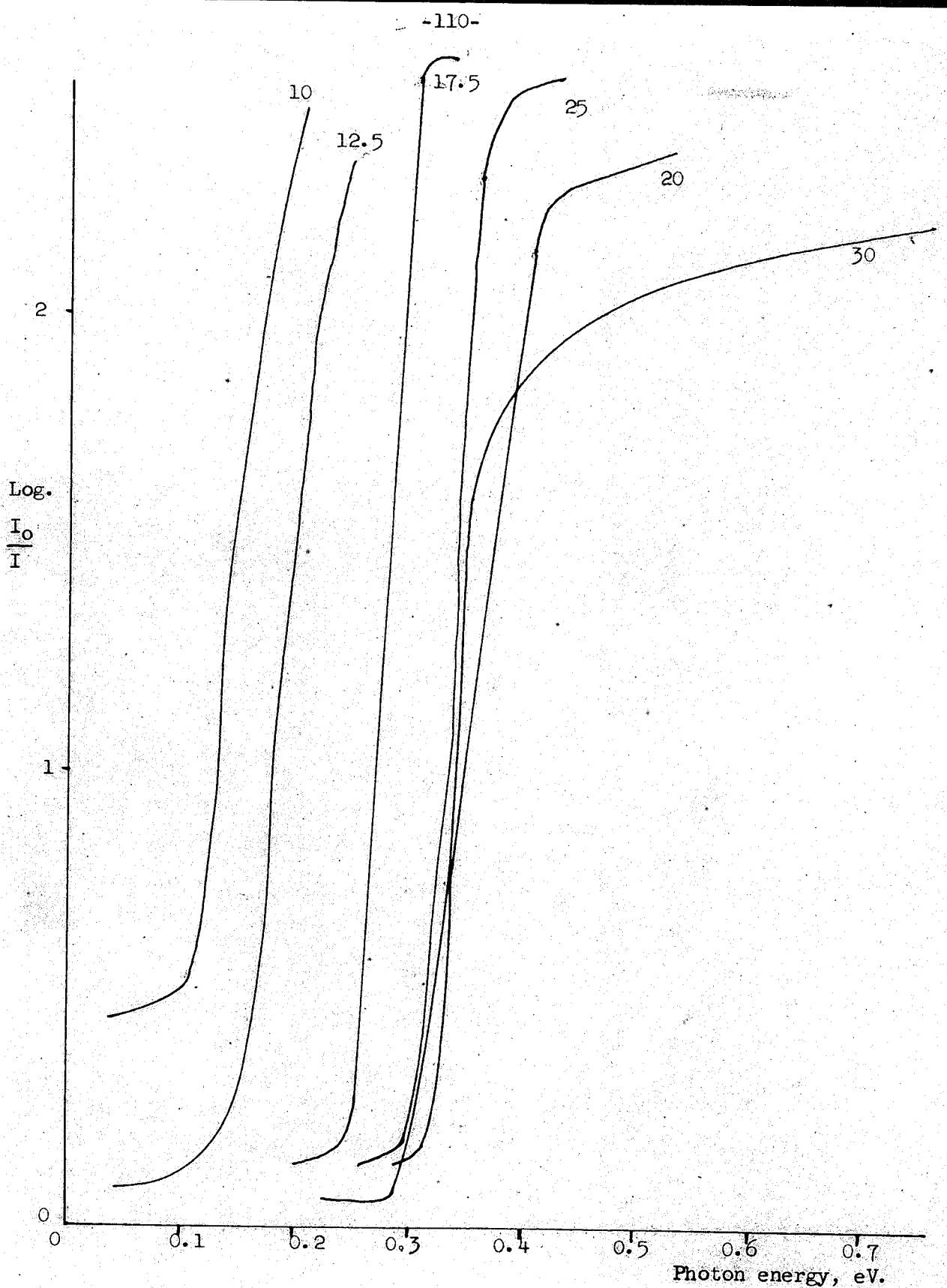

Fig. 30. Infrared Absorption, 10 mpc. to 30 mpc. In_2Te_3.

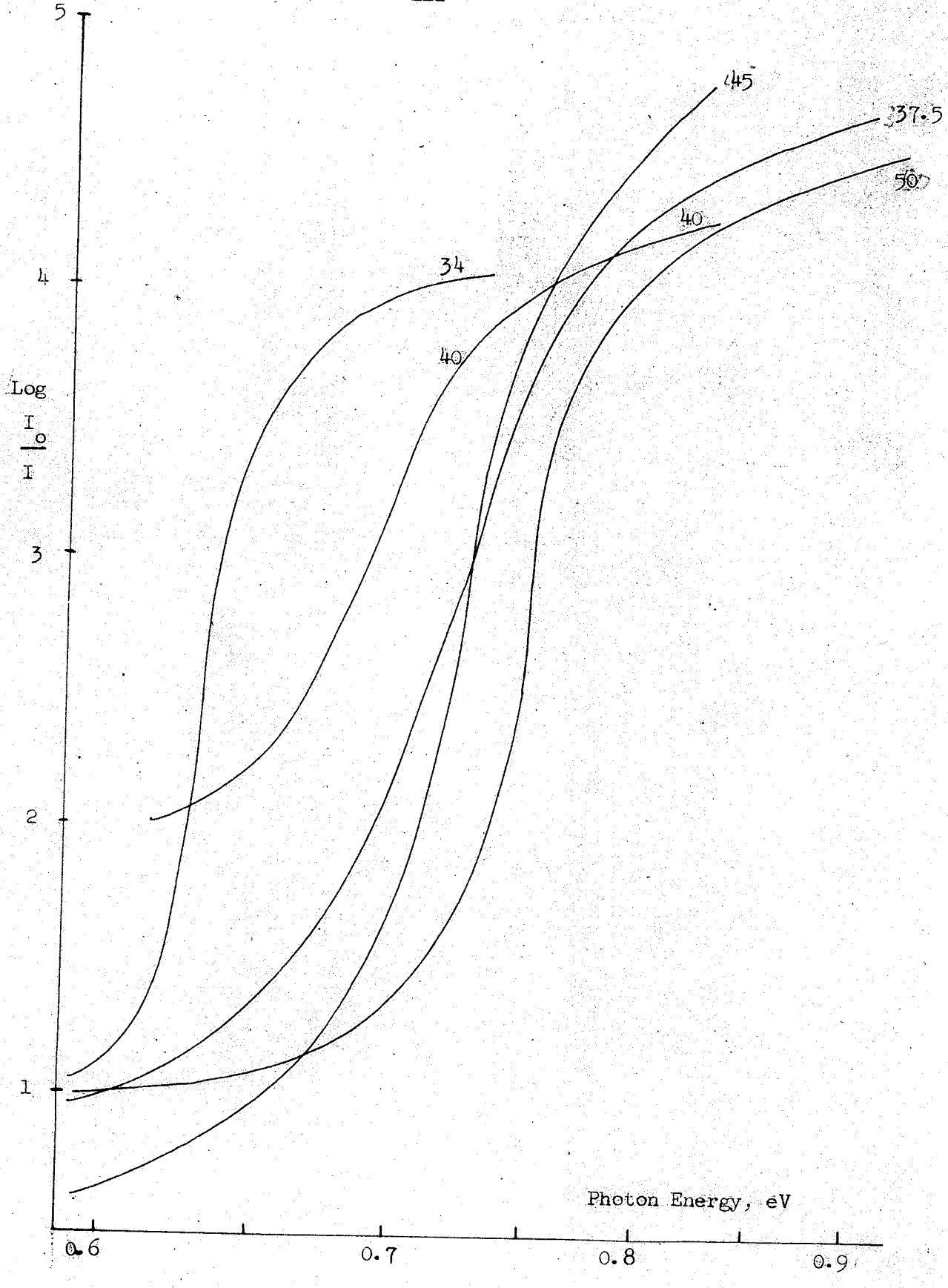

Fig. 31. Infrared Absorption, 34 m.p.c. to 50 m.p.c. In_2Te_3

28.0 Thermal Conductivity

The results of the measurement of thermal conductivity for the first half of the system are presented in figure 32.

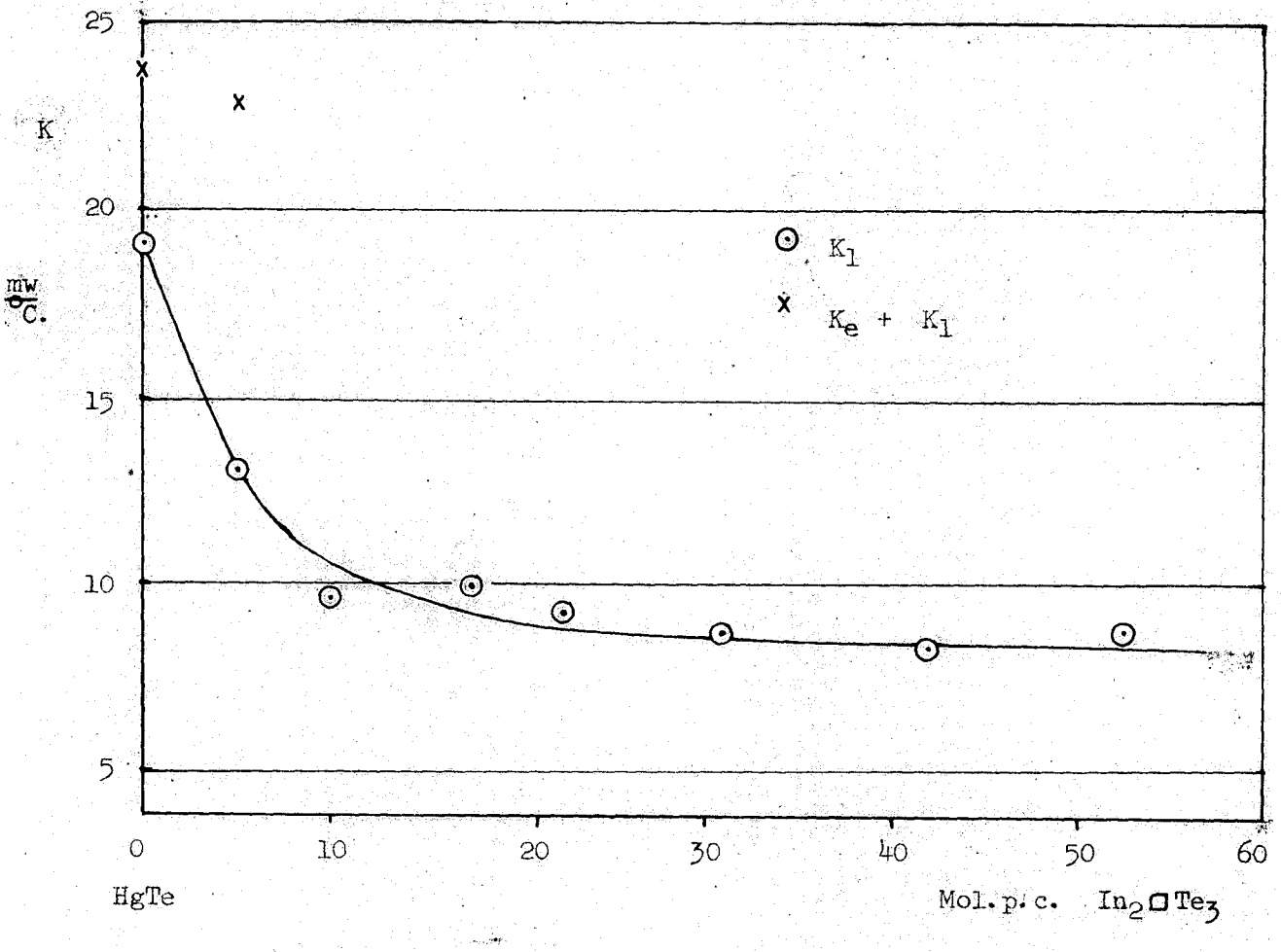

Fig,32. Thermal conductivity, K.

Since the electrical conductivity falls considerably with increasing concentration of In_2Te_3, the electronic component of the thermal conductivity is negligible for all but the first two samples. The non-degenerate value for the Lorenz number has been

used, in the calculations, though, since the materials are to a certain extent degenerate, the value of the lattice component of the thermal conductivity may be a little too high.

The thermal conductivity of In_2Te_3 has been discussed in section 13.4. Values reported are 6.8 and 11.2 mw/cm.^{o}C for the disordered and ordered material respectively. It is probable therefore that after the drop between HgTe and 10 mpc the thermal conductivity remains almost constant for the rest of the alloy system. This result is surprising because an increase in the number of vacancies should affect the scattering of phonons and reduce the thermal conductivity. It is possible that the mean free path of the phonons is of the same order as the interatomic distance and, consequently, the minimal value of the thermal conductivity is reached at a low vacancy concentration. However, Rosi et al. (88) have reported values of the thermal conductivity in the system $AgSbTe_2$ - PbTe which correspond to an effective mean free path less than the interatomic distance.

29.0 Electrical Properties

Measurements of the electrical conductivity, Hall and Seebeck Coefficients were made on a number of samples with compositions between HgTe and 50 mpc. In_2Te_3. The results are presented and discussed under separate headings corresponding to the various regions of the phase diagram.

Samples in the region up to 15 mpc show behaviour similar to that of HgTe, i.e. they are n-type at room temperature with a high carrier concentration and a fairly high mobility. The mobility decreases with increasing indium concentration. Most of the samples from 17.5 to 34 mpc, discussed in detail in sect. 29.2, were p-type, changing to intrinsic at about 500°K. The maximum in the negative Hall coefficient was used to find the mobility ratio. Values for the mobilities, effective masses and intrinsic carrier concentration were also determined.

In the remaining part of the range, from 35 to 50 mpc, the samples appeared to be either n-type extrinsic, or p-type with low carrier concentration. The effect on the electrical properties of the ordering which occurs at about 40 mpc, is discussed in section 31.0.

29.1 HgTe - 15 mpc

All the samples in this range show properties similar to those of HgTe. The limit of the region, therefore, depends much on the condition of the samples and in the preliminary work (sect. 15.0) the material prepared was p-type at 11 and 15 mpc. In the later batch of ingots, larger and more homogeneous, the first p-type ingots appeared at 17.5 mpc. The physical condition of these later ingots was generally good, and measurements could be made to a high degree of accuracy. The lines on the X-ray photograph for the 5 mpc composition were not as sharp as those for all the other samples in the region, which indicates that this particular ingot was not

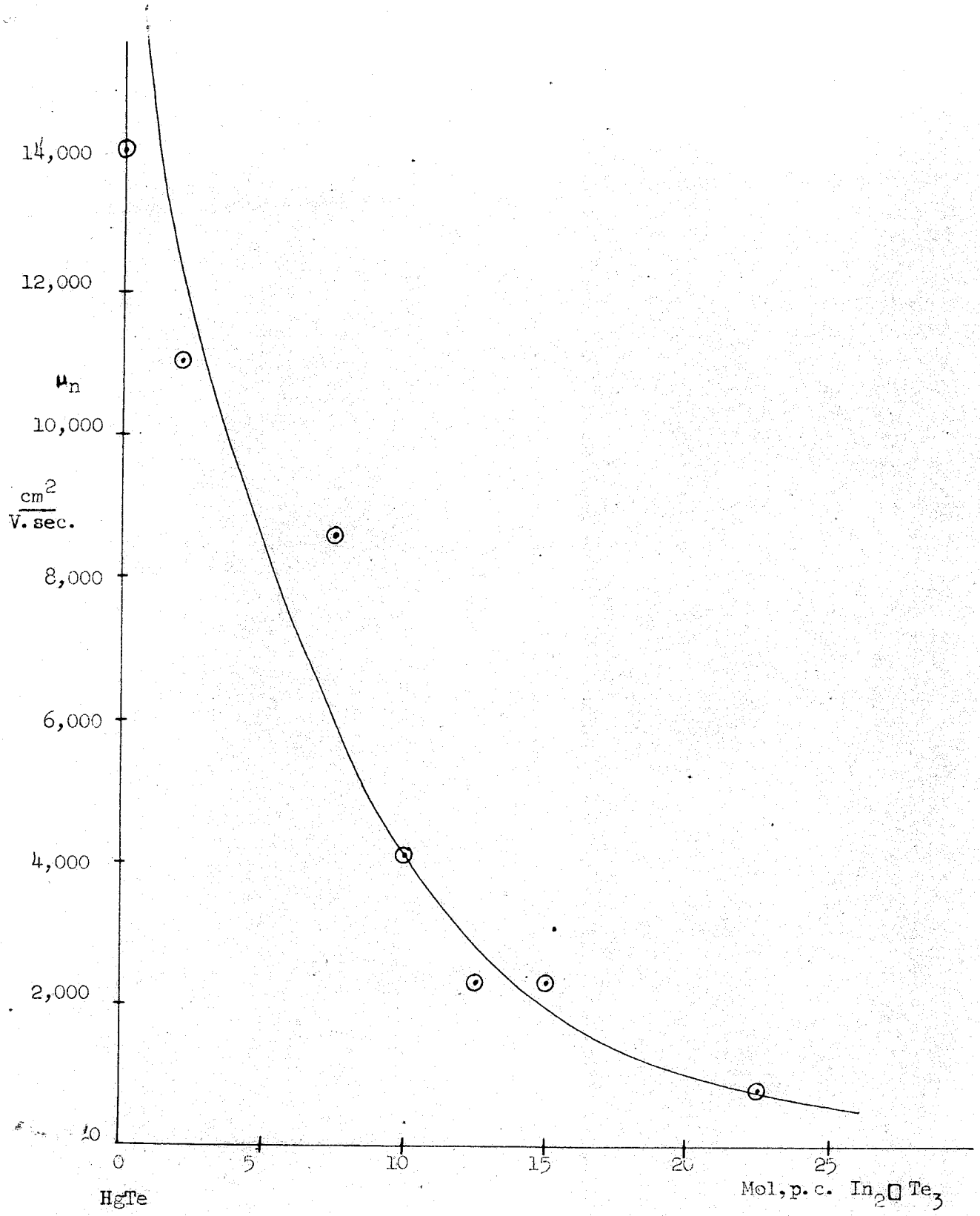

Fig. 33. Variation of electronic mobility μ_n with composition.

The values of μ_n for samples annealed in mercury vapour are considerably greater than those given here.

completely homogeneous. The surface of the ingot at 2.5 mpc was dull grey, not bright as with the rest, indicating the presence of impurities.

The room temperature properties of the samples in the region up to 15 mpc are presented in table 3.

mol.p.c.	a_o	α	σ	R	σR	n	Opt.E_g
In_2Te_3	Å	$\mu V/^oC$	Mho/cm	cm^3/C	$cm^2/Vsec$	per cm^3	eV
0	6.460	-119	670	-20.6	13,900	3×10^{17}	-
2.5	5.450	-43	2,920	-2.05	6,000	3×10^{18}	-
5	6.44	-40	2,170	-2.36	5,100	2.6×10^{18}	-
7.5	6.437	-106	2,620	-31.5	8,250	2.0×10^{17}	-
10	6.428	-73	900	-4.6	4,150	1.3×10^{18}	0.14
12.5	6.420	-65	11.9	-200	2,380	3.12×10^{16}	0.2
15	6.411	-80	470	-5	2,350	1.25×10^{18}	-

Table 3 Electrical Properties of HgTe - 15 mpc In_2Te_3.

No obvious trends appear in the results. By comparison with the previous table of results (sect. 15.0 p.248), the mobilities of the 2.5 and 5 mpc samples are low, which is probably due to the presence of impurities and the inhomogeneity mentioned earlier. Assuming higher values for the mobility at these points, it seems likely that the electron mobility falls in the manner shown in figure 33. The electron mobilities of samples with concentrations of In_2Te_3 greater than 17.5 mpc onwards were less than 600 $cm^2/V.sec$. This corresponds

to the observed variation of mobility with composition in the HgTe - CdTe system (28).

It seems probable that the non-parabolic conduction band in HgTe (sect. 10.1), associated with the high mobility and the semimetallic properties, is replaced at about 15 mpc by a band in which the effective mass is higher. The conduction band is also displaced relative to the valence band so that the energy gap becomes positive, with direct transitions of about 0.3 eV. The relative positions of the valence bands may remain unaltered. The high concentration of electrons in the range 0-15 mpc also supports this argument. When the band overlap disappears, the material can be made p-type ~~extrinsic~~ at room temperature. In fact the samples above 15 mpc were strongly p-type, although all were made by the same method from the same original components and should therefore contain the same impurities.

The variation with temperature of Hall effect and conductivity indicates that all the materials with compositions up to 15 mpc, except for 12.5 mpc, are n-type extrinsic with constant or slowly varying Hall coefficient at temperatures down to 77°K. Low Seebeck coefficients are associated with high carrier densities. The Fermi level lies between 0.5 and 1.5 kT above the conduction band, indicating a degree of degeneracy. Approximate calculations, using non-degenerate statistics, for the effective mass of electrons show that the ratio is of the order of 10^{-2}, as in HgTe.

29.11 Scattering Mechanism

In samples with 2.5, 5, 10 and 15 mpc In_2Te_3 the Hall coefficient was constant over a range of temperature sufficiently large to enable logarithmic plots of the variation of Hall mobility with temperature to be made. The graphs are reproduced in figure 34. The slope of the best straight line through the points for each sample corresponds to an exponent in the equation

$$\mu = \mu_o T^a \qquad \ldots\ldots 51.$$

The observed values of a, given in table 4, with the exception

mpc. In_2Te_3	2.5	5	10	15
a	-1.45	-1.65	-1.4	-1.1

Table 4 The exponent a, from the temperature variation of mobility.

of that for 15 mpc, indicate that the scattering at room temperature and above was predominantly by acoustic mode lattice vibrations.

Below room temperature the mobility generally rose to a maximum and then fell slightly, indicating that the scattering was changing in character, probably to ionised impurity scattering. For the sample at 2.5 mpc an approximate straight line was obtained between 77°K and 300°K, the slope of which corresponded to a = +1.

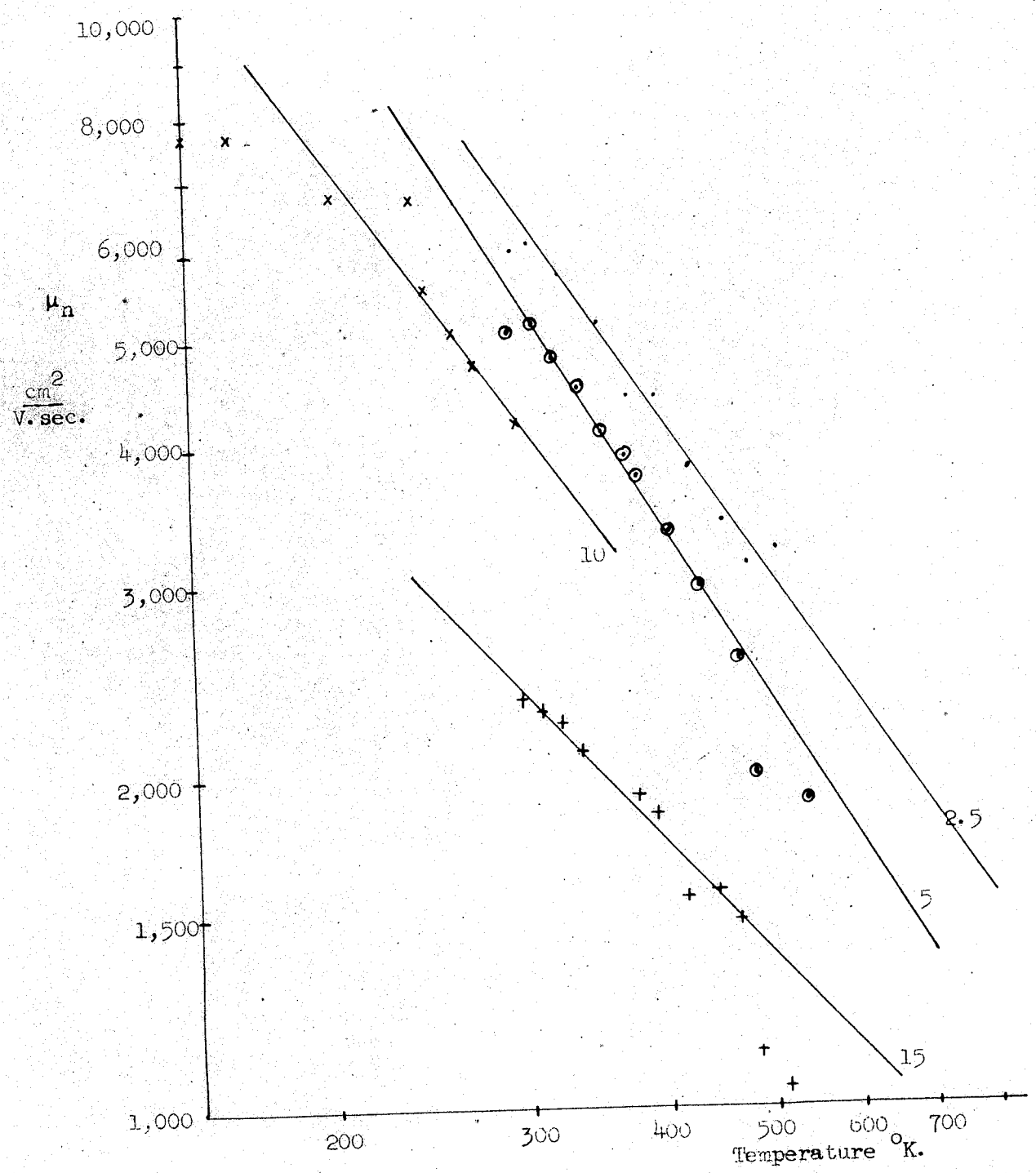

Fig. 34. Mobility v. Temperature.

• 2.5 mpc. × 10 mpc.

⊙ 5 mpc. + 15 mpc.

29.12 Samples annealed in Mercury vapour

The work of Rodot and that of Giriat, reported in section 10.0, shows that the mobility of HgTe can be greatly increased by annealing the samples in mercury vapour. Some of the samples whose properties had been measured were annealed at 250°C in evacuated tubes containing a small amount of Hg, but unfortunately many of them proved too brittle to withstand the treatment. Measurements were taken on specimens at 2.5 and 5 mpc. After the annealing the mobility had increased by about 10 p.c. at room temperature, and about 30 p.c. at 77°K. The number of carriers, which remained constant with temperature, had increased by about 40 p.c. These results indicate that the annealing has some effect, though the increase in the carrier concentration is surprising. A much fuller programme of such heat treatment is needed.

29.2 The Region 17.5 to 35 mpc

This region marks the onset of the ordered phase. The ordered lines on the X-ray photographs show up weakly at 22.5 mpc and 25 mpc and strongly at 30, 31 and 34 mpc. The diffuseness of the lines suggests that samples between 25 and 35 mpc are not homogeneous, and the region is thought to be two phase (sect. 25). The electrical results appear to be in accordance with this interpretation.

Most of the ingots in the region were polycrystalline of small grain size, and, although it was possible to cut good samples

from the centres, the outer layers of the ingots were porous. The samples appeared homogeneous when viewed under the microscope except for that at 34 mpc which was slightly porous throughout. The ingots of 22.5 and 17.5 mpc were in better condition than the others.

Most of the samples in this region exhibited similar electrical properties. The conductivity was of the order of 10 mho/cm and the Seebeck coefficient about +300 $\mu V/^{o}C$. The Hall coefficient indicated that holes were the predominant carriers near room temperature and for some materials the coefficient was constant over a range of temperature. The samples became intrinsic above about $500^{o}K$. The conductivity, Hall and Seebeck coefficients are plotted against the inverse of temperature for samples at 17.5, 22.5, 25, 30, and 34 mpc in figures 35 to 39 in the temperature range $300^{o}K$ to $600^{o}K$.

The readings have been analysed on the model of a simple energy band semiconductor discussed in Chapter I.

29.21 The Mobility Ratio

The equation

$$R_{max} = \frac{(b - 1)^2}{4b} R_q \qquad \ldots\ldots 36.$$

of section 5.1 was used to determine the mobility ratio for each of the samples. The results are presented in table 5.

The calculation relies on the constancy of the number of holes in the impurity range near room temperature. The Hall effect is constant for all samples except for 17.5 and possibly 30 mpc. For

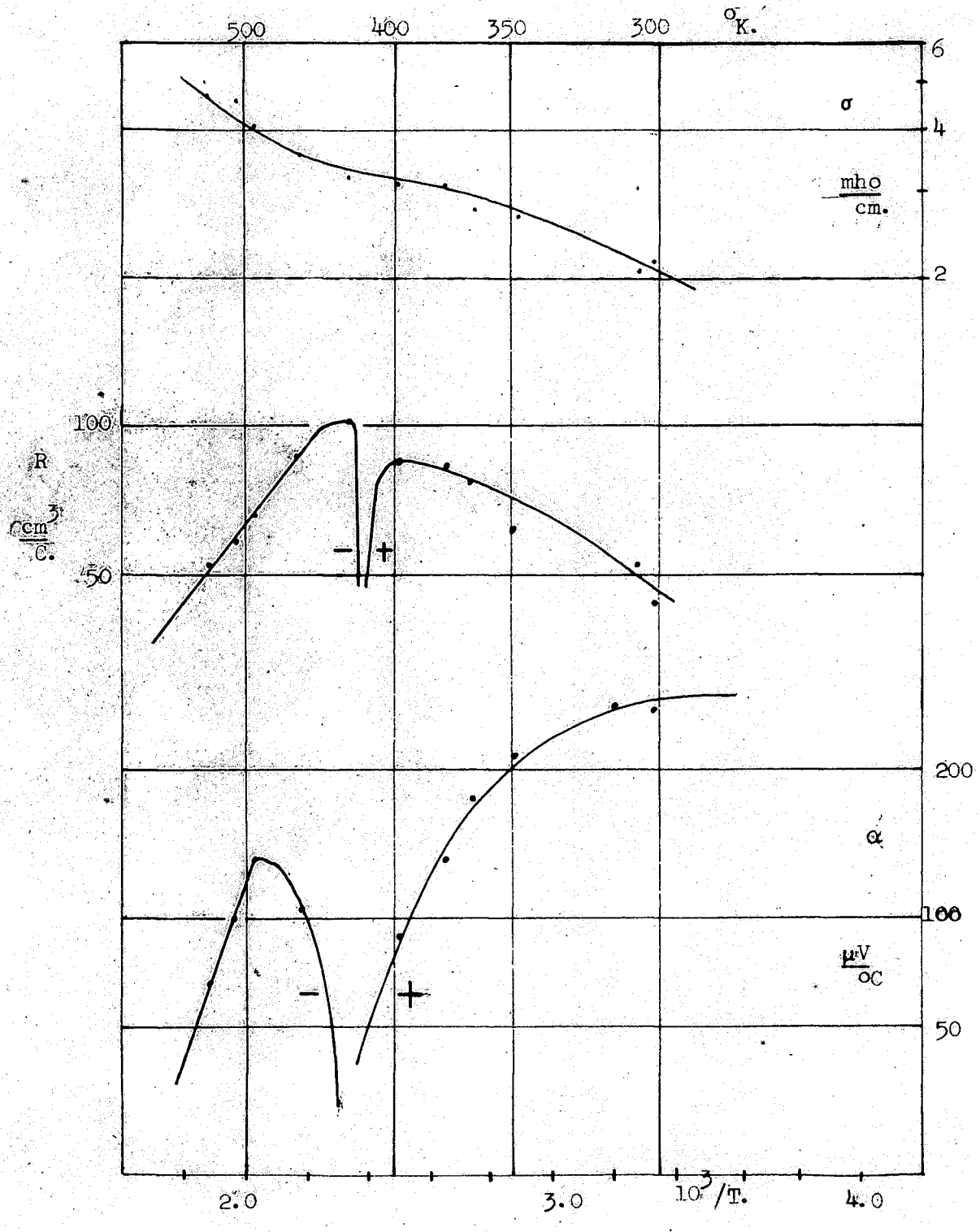

Fig. 35. Conductivity σ, Hall Coefficient R and Seebeck Coefficient α v. 1/T at 17.5 mpc,

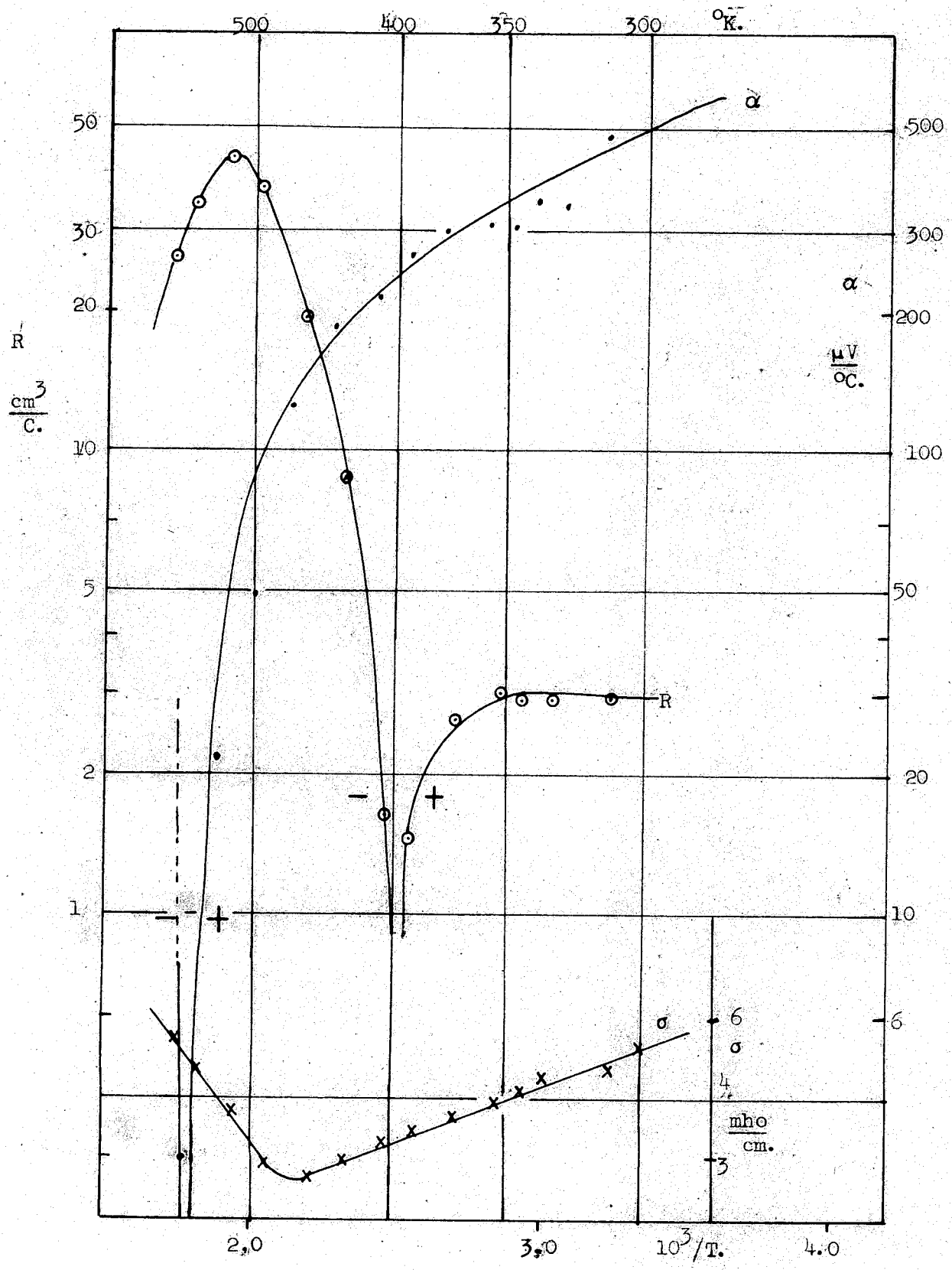

Fig. 36. Electrical Results at 22.5 mpc.

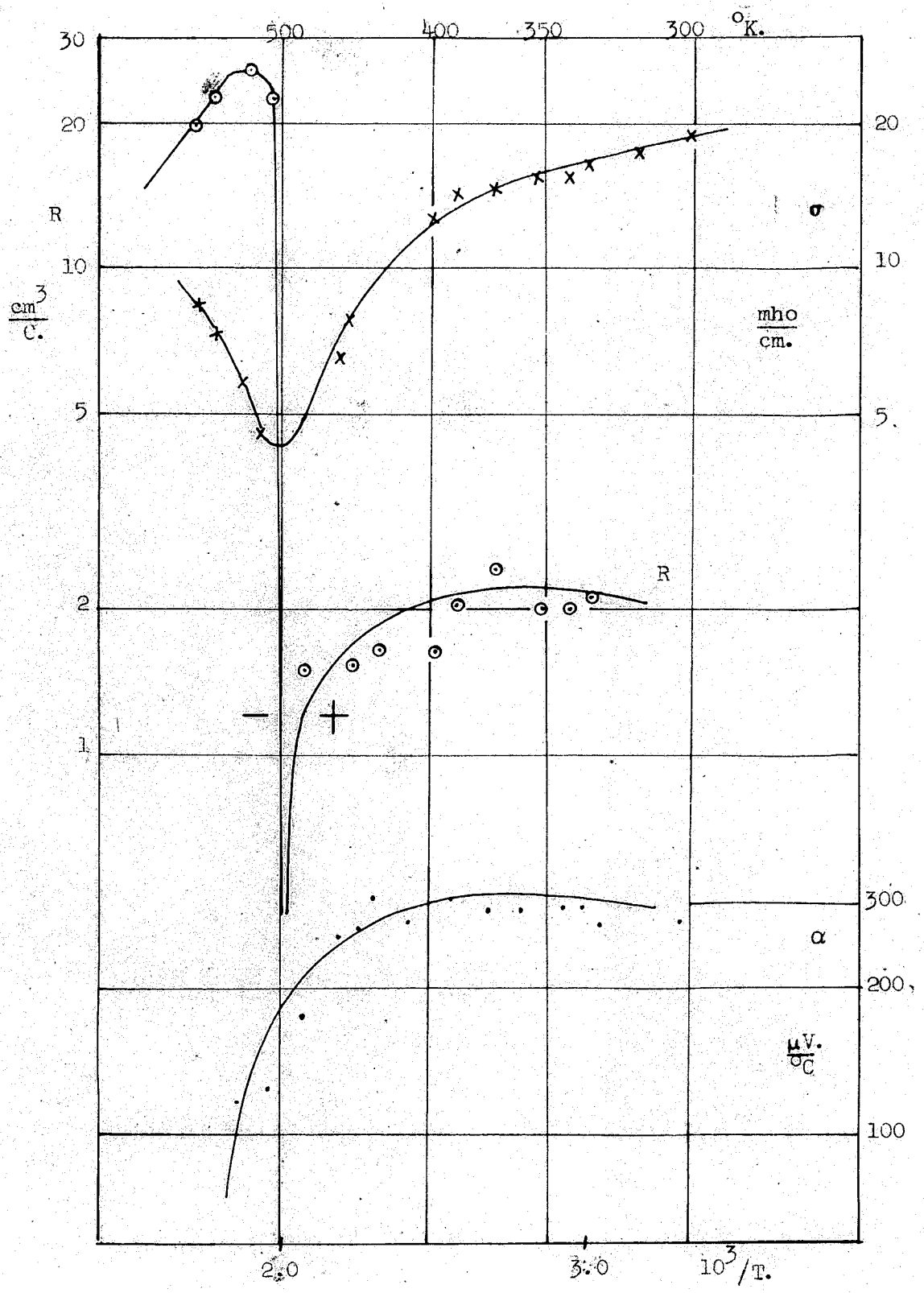

Fig.37. Electrical Results at 25 mpc.

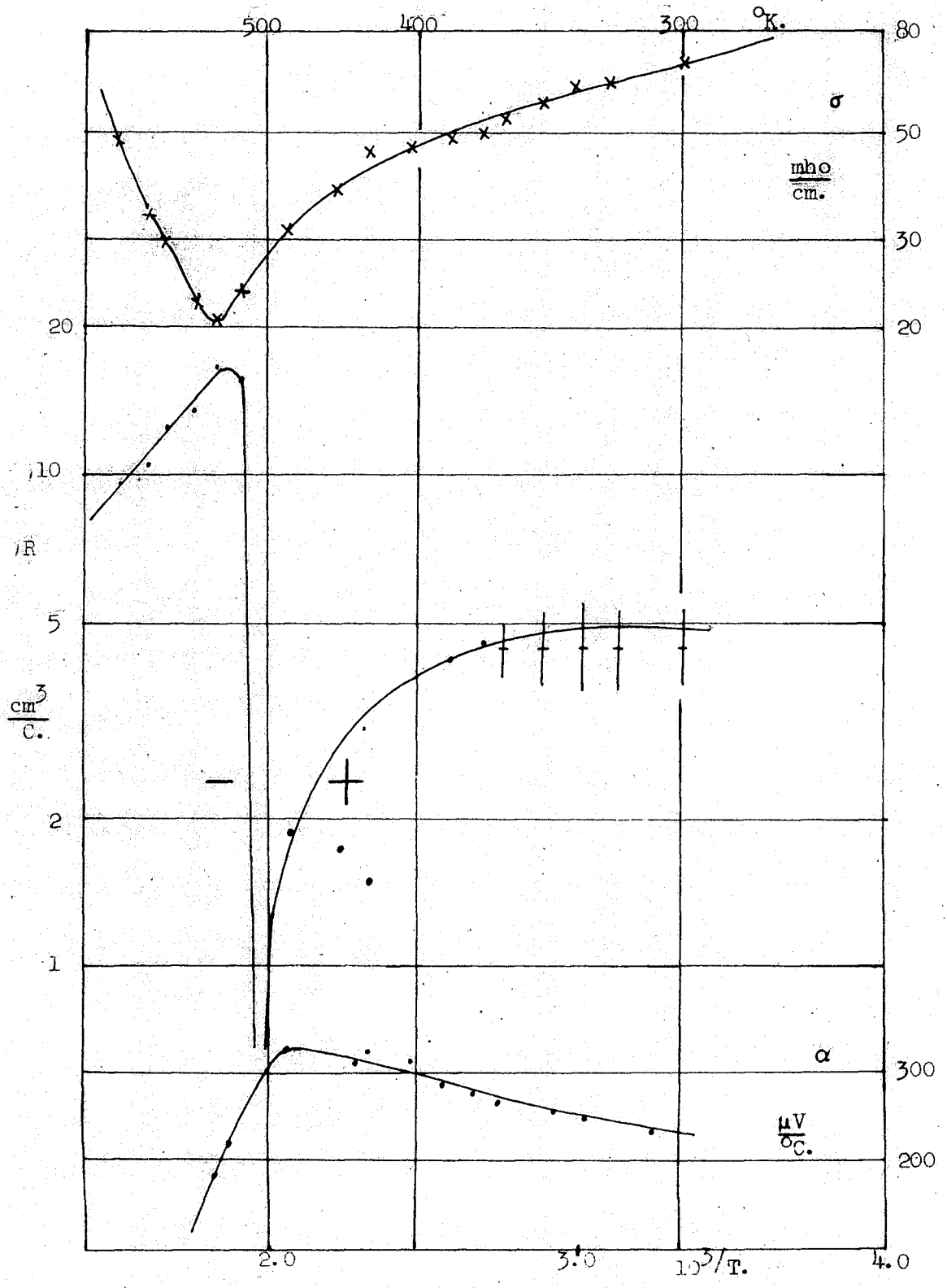

Fig. 38. Electrical Results at 30 mpc.

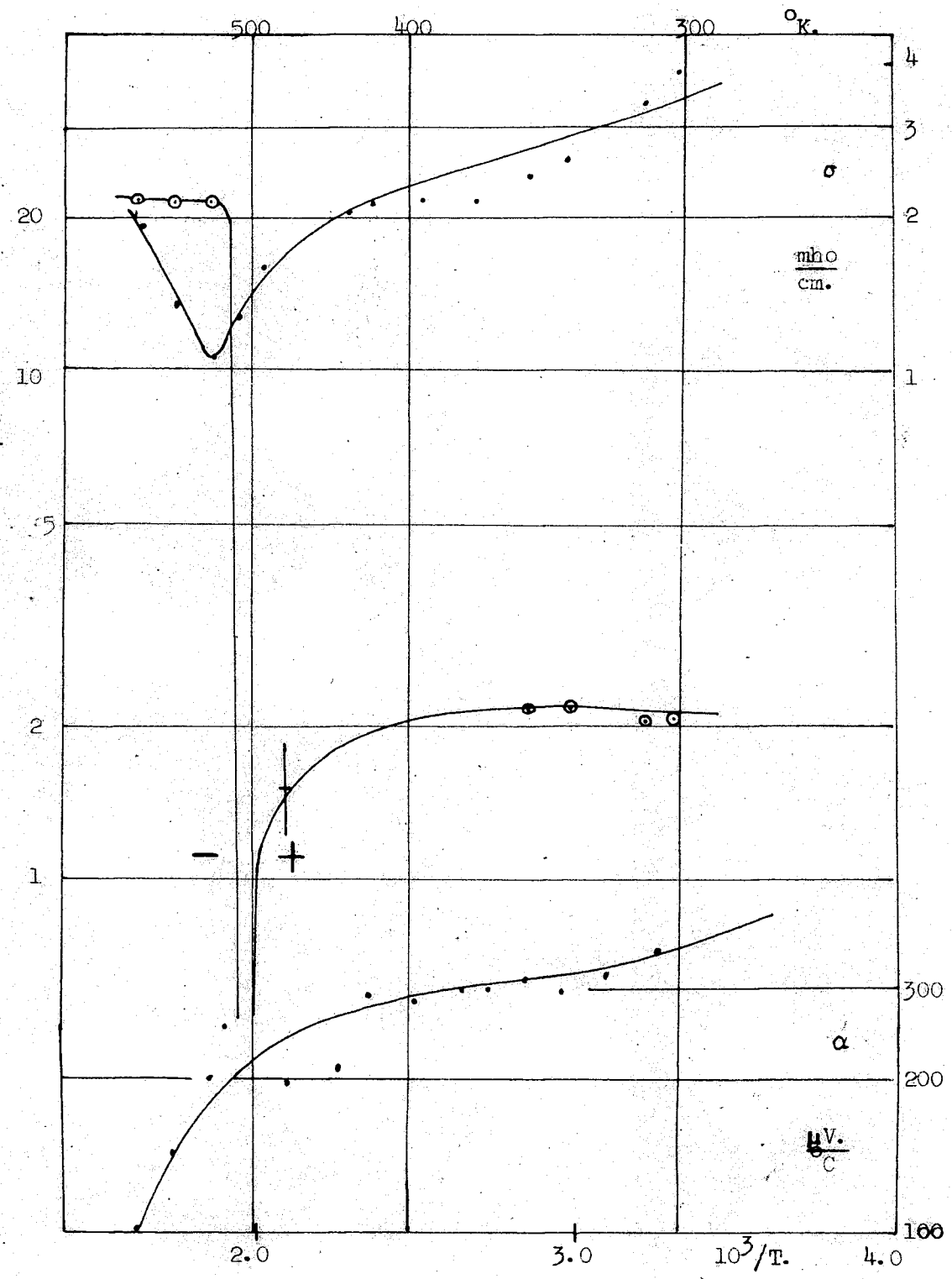

Fig. 39. Electrical Results at 34 mpc.

	17.5	22.5	25	30	34	mpc
R_{max}	-102	-43	-25.4	-17	-22*	cm^3/C
R_q	+45*	+3.0	+2.2	+4.5*	2.2*	cm^3/C
b	10*	59	48	17*	42*	
Temp.	430	520	530	548	550*	^oK

* Indicates an approximate value

Table 5 Mobility ratio. 17.5 to 34 mpc.

the latter sample readings at room temperature couldnot be obtained accurately. It can be seen that the mobility ratio for these two is lower than that for the other samples.

The conductivity is also useful in indicating the state of the carrier density. If the number of impurity carriers is constant then the conductivity falls slightly with increasing temperature since the mobility must also drop if lattice scattering predominates, until the intrinsic carriers become important and cause the conductivity to increase rapidly with temperature. This type of variation is observed for all samples excapt 17.5 mpc. where the conductivity is increasing in the region near room temperature where the Hall coefficient is also increasing positively with temperature. Such behaviour is difficult to explain on the basis of active donors and acceptor impurities and may imply defects in the material.

It may be concluded that the mobility ratio in this region is about 40, possibly falling with increasing vacancy concentration. Values for the mobility ratio in HgTe are generally higher than this, though they have been determined at lower temperatures (sect. 10.4).

29.22 Mobility

Above the negative Hall maximum the materials appear intrinsic with electrons as the predominant current carriers. The mobilities in this range, calculated from the product $R\sigma$ and the above values of b, are presented in table 6. The temperatures given are the lowest at which the material is intrinsic.

	17.5	22.5	25	30	34	mpc
Temp.	593	550	560	600	580*	^{o}K
$R_i\sigma_i$	215	200	162	36.4	30*	$cm^2/V.sec$
μ_n	240	203	165	38.6	31*	"
μ_p	23.4	3.45	3.5	2.24	0.73*	"
$300^{o}K$ μ_p	100	13.5	35	30	8	"

Table 6. Mobilities in the range 17.5 to 35 mpc.

The product $R\sigma$ at room temperature, which may be taken as the hole mobility, is given in the sixth line of the table.

The values of μ_n for 17.4 and 22.5 mpc at high temperature are considerably lower than those of 12.5 and 15 mpc at the same temperature which supports the view that the band structure changes at about 15 mpc. The values indicate that the mobility drops with increasing In_2Te_3 concentration. This may be due to the increasing concentration of vacancies, or, as seems likely, to an increase in the concentration of the ordered phase when the In_2Te_3 content exceeds about 20 mpc. Only one sample in this region, 31 mpc turned out to be n-type. The carrier concentration was 1.7×10^{17} per cm^3. The electronic mobility was 500 $cm^2/V.sec$ at room temperature dropping to 250 $cm^2/V.sec$ at 600°K. These values are considerably higher than the values for the 30 mpc sample which was p-type. It is possible that the conducting phase in the n-type sample was the ordered phase which had been strongly doped. A fuller discussion of this sample is given in section 29.3.

29.23 Intrinsic Activation Energy

The slope of the graph of log R v. 1/T in the short temperature range above the Hall maximum has been used to determine the activation energy E_a. If E_a varies with temperature then the value determined by this method is that at absolute zero (3 P.321). Although the materials begin to decompose at these temperatures, the agreement between E_a and the room temperature optical energy gap E_g indicates that the bulk of the material has not been greatly affected. The results are presented in table 7.

	17.5	22.5	25	30	34	mpc
E_a	0.3	0.29	0.33	0.31	-	eV
E_g	0.29	0.35	0.35	0.37	0.65	eV

Table 7. Activation energy and optical energy gap

29.24 Carrier concentration and Effective Mass

Table 8 gives the intrinsic carrier concentrations at the negative Hall maximum, calculated by extrapolation of the intrinsic Hall coefficient line. The value of b is too large to have any noticeable effect in the value of n_i obtained from equation 31 using the Hall coefficient.

	17.5	22.5	25	30	34	mpc
Temp.	430	520	530	546	550	^oK
R_i	120	-43	-28	-17	-22	cm^3/C
n_i	$5.2x10^{16}$	$1.45x10^{17}$	$2.2x10^{17}$	$3.7x10^{17}$	$2.8x10^{17}$	per cm^3
$m_n m_p/m^2$ from E_g	0.030	0.065	0.095	0.21	7.4	
$m_n m_p/m^2$ from E_a	0.054	0.032	0.056	0.11	0.053	

Table 8. Intrinsic Carrier Density and Effective Mass Product

Using equation 21 the effective mass product $m_n m_p/m^2$ can be determined from values for n_i and the energy gap. In lines 5 and 6 of table 8 the results of the calculations using first the optical

energy gap E_g and then the intrinsic activation energy E_a. The latter is more likely to be the correct one to use. In particular, at the composition 34 mpc, E_g = 0.65 eV gives an impossibly large value for the product. Unfortunately, the intrinsic range for this sample could not be reached. However, if it is assumed that the material is two phase and that the conducting phase is similar to those of the other samples, then a similar value for E_a may be taken. It can be seen from table 7 that the activation energy of the phase is about 0.3 eV. and the substitution of this value gives a realistic value for the product. The values in the sixth line of table 8 are therefore to be taken as the best values for the effective mass product.

29.25 Seebeck Coefficient

In all samples the Seebeck coefficient is observed to change from positive to negative values in the region of the negative Hall maximum, which is the normal behaviour for p-type material. The reduced Fermi level η', as in figure 13, is obtained from the Seebeck coefficient by means of equation 38. Using this value for η' and the extrinsic carrier density q from the Hall coefficient, a value can be determined for the hole effective mass ratio at room temperature. The results of these calculations are presented in table 9.

	17.5	22.5	25	30	34	mpc
η'	1.2	2.05	1.35	1.22	1.46	
Temp.	300	336	330	370	330	^{o}K
α	+270	+350	+300	+270	+270	$\mu V/^{o}C$
q	1.3×10^{17}	2.2×10^{18}	2.9×10^{18}	1.4×10^{18}	2.9×10^{18}	per cm^3
m_p/m	v. low	0.53	0.29	0.067	0.30	
m_n/m	-	0.061	0.19	-	0.18	

Table 9. The Fermi level and Effective Masses

It can be seen that the samples at 17.5 and 30 mpc whose Hall coefficients were not constant and whose mobility ratio was considerably lower than those of the other samples, have values for m_p/m which are definitely too low. In the seventh line of the table the values for m_n/m have been calculated using the values of the product in table 8, line 6 on the assumption that the effective mass does not change greatly with temperature.

Although these results are not very conclusive, it seems likely that in the composition range 17.5 to 35 mpc. the effective mass ratio for electrons is about 0.1, and the hole effective mass ratio about 0.3. The electron effective mass is therefore considerably larger than that for HgTe and corresponds to the lower mobility.

29.26 Conclusion

There are two possible interpretations of the results for the materials in the range 17.5 to 35 mpc In_2Te_3. If solid solution

really exists between the HgTe and the ordered phases, and the observed inhomogeneity is due to incorrect heat treatment, then the electrical results, particularly the decreasing mobility, must be interpreted on the basis of increasing vacancy concentration. This does not explain the constant values for the activation energy and for the optical energy gap observed in part of this range.

However, the more probable interpretation, as the X-ray diffraction photographs indicate, is that the region between 22.5 and 35 mpc is two phase. The 20 mpc phase, having a lower activation energy is naturally the more conductive, unless the ordered phase at 40 mpc, in which, as will be shown later, electrons have a higher mobility, is extrinsic and therefore conducts more. Thus the observed optical energy gap at 34 mpc is that of the ordered phase, while there is still sufficient of the 20 mpc phase with an activation energy of 0.3 eV to be the effective conductor. The decrease in mobility with increasing percentage In_2Te_3 arises naturally from the defects due to the increasing amount of the ordered non-conducting phase. Nevertheless, the X-ray and optical examinations indicate that the two phases are not sharply resolved.

Since the mobilities are lower and the electron effective mass higher than those for the HgTe type phase, support is given to the idea that the high mobility, non-parabolic conduction band of HgTe is replaced by one of lower mobility in the region of 15 mpc In_2Te_3.

29.3 The Ordered Region 37.5 to 45 mpc

Samples in this range show the ordering pattern of lines on the X-ray diffraction photographs very strongly and of about equal intensity throughout the range. The high angle lines were sharpest at 37.5 mpc, the compound $Hg_3In_2Te_6$, and diffuse at 45 mpc. All samples used for electrical measurements appeared homogeneous when viewed under the microscope except that for 45 mpc which was slightly porous, although some of the earliest ingots produced in this range were definitely two phase. Single crystals up to a few mm in size were often found, particularly on the free surfaces of the larger ingots at 37.5 mpc. It is thought that large single crystals of this composition may be grown using the method discussed by Mason and Cook.(78) for peritectic compounds.

Since the 50 mpc ingot had a disordered structure and the one at 45 mpc was slightly inhomogeneous (sect. 25), it seems likely that the latter material was not single phase but contained a little of the disordered phase. It should be possible to grow single crystals of the compound $Hg_3In_2Te_6$ by any of the standard techniques.

The electrical results for the samples in this region do not fit into a straightforward pattern. While some appear definitely n-type and one definitely p-type at room temperature, others have a large positive Seebeck coefficient coupled with a large negative Hall coefficient. Each of the three types will be discussed in detail.

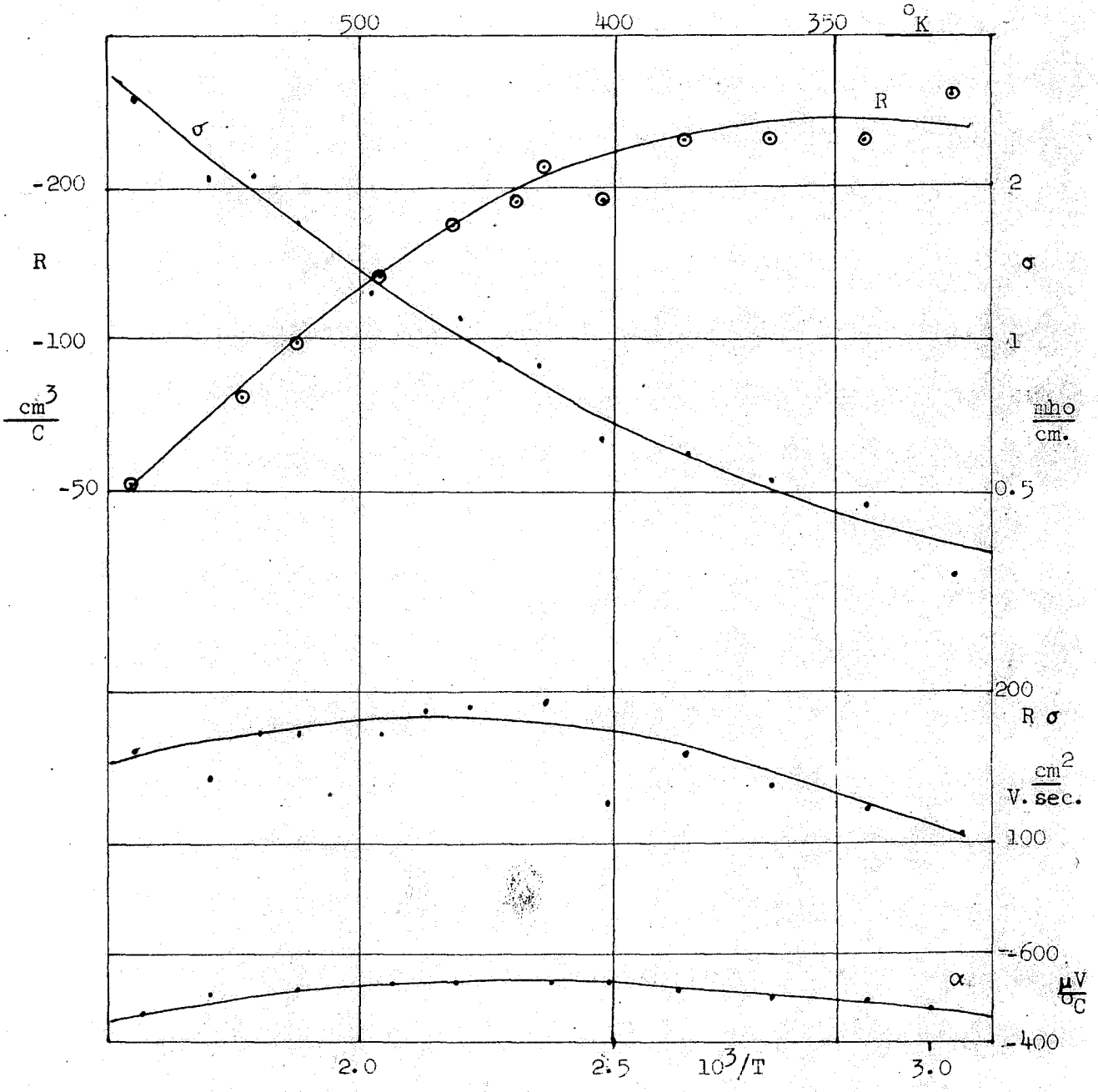

Fig. 40. Electrical Results. First end to freeze of directionally frozen ingot at 37.5 mpc.

29.31 n-type Material

The first end to freeze of a directionally frozen ingot at 37.5 mpc produced n-type material with about 10^{16} carriers per cm^3. The X-ray powder photograph indicated that the material was not very homogeneous so that an accurate value for the lattice parameter could not be obtained. When viewed under the microscope the sample appeared single phase and non-porous. Being unannealed, it was rather brittle.

The electrical results for this sample are presented in figure 40. The variation of the conductivity and Hall coefficient indicate that the number of electrons increased slightly with temperature reaching about 10^{17} per cm^3 at $600^{\circ}K$. This is still in the extrinsic range, if the optical energy gap of 0.73 eV is assumed as the energy gap at this temperature. The approximately constant value of 500 $\mu V/^{\circ}C$ for the Seebeck coefficient confirms these findings.

The reduced Fermi level obtained from the Seebeck coefficient is 3.8 which makes the Fermi level -0.01 eV at room temperature. Electrons are the predominant carriers so that the product $R\sigma$ gives the value of the electronic mobility. The maximum in the mobility, 180 $cm^2/V.sec$, occurs at about $430^{\circ}K$ showing that lattice scattering is not dominant. Since the X-ray examination shows that the material is not completely homogeneous, it is probable that the value of the mobility is low compared to that which may otherwise be obtained.

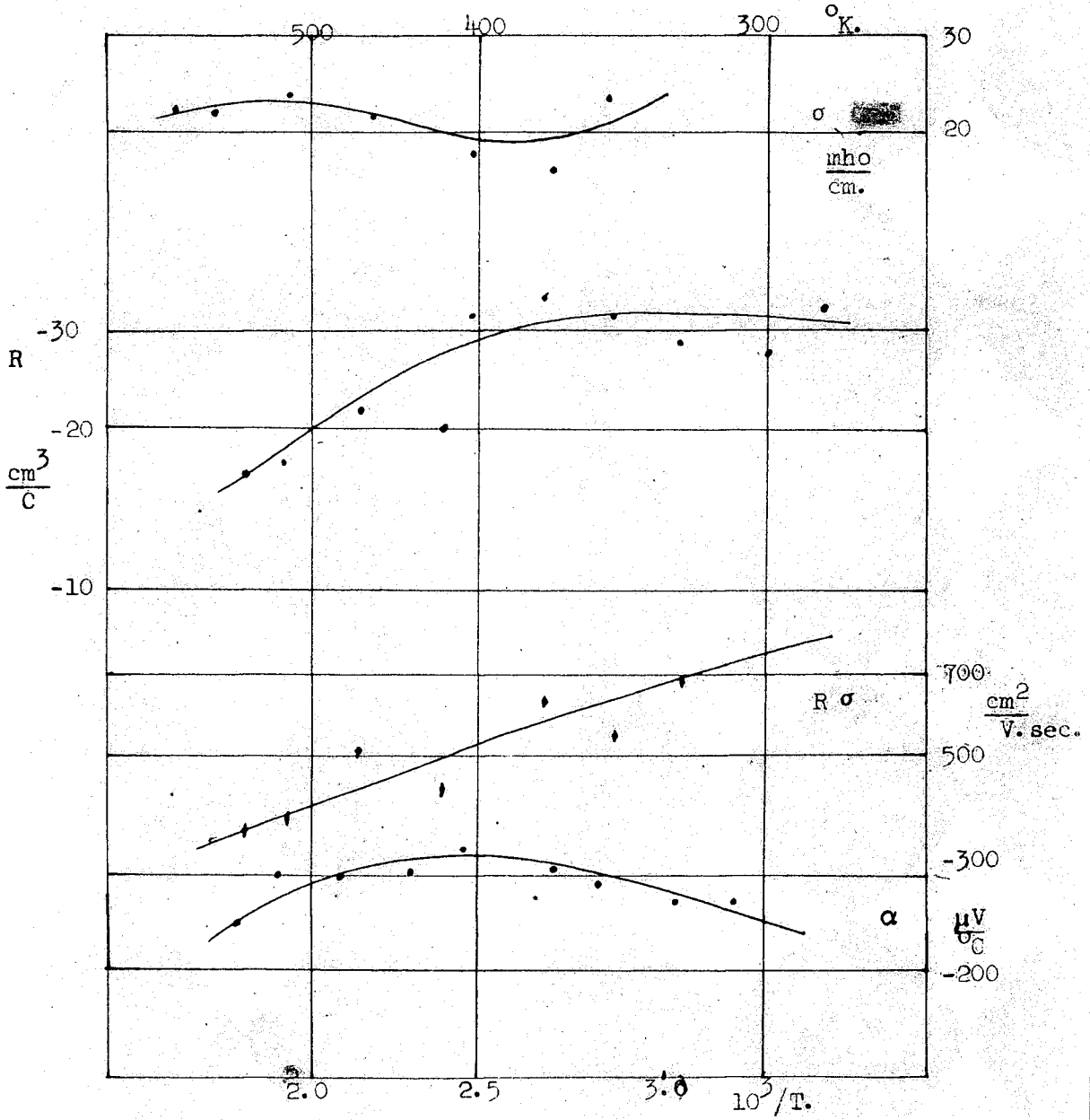

Fig. 41. Electrical Results at 37.5 mpc. Indium Rich.

The calculations of the effective mass ratio are presented in table 10 for two values of the scattering parameters.

Temp.	s	m_n/m
370°K	+ 1/2	0.1
	- 1/2	0.07
555°K	+ 1/2	0.16
	- 1/2	0.081

Table 10. Effective mass ratio for electrons 37.5 mpc.

In view of the mobility variation with temperature, the negative values for s would appear to give the more realistic values for m_n/m.

Another n-type sample was obtained by increasing the indium content of an otherwise 37.5 mpc composition (sect. 26.0). The material appeared single phase and homogeneous. At room temperature the carrier concentration was about 2×10^{17} per cm^3.

The electrical results are presented in figure 41. The scatter of points in these graphs and also in the logarithmic plot of mobility make definite conclusions impossible. The slope of the mobility graph indicates that scattering is probably by lattice vibrations. The electron effective mass ratio, calculated using $s = + 1/2$ is given in table 11.

The results are therefore in agreement with those obtained for the previous sample with $s = + 1/2$.

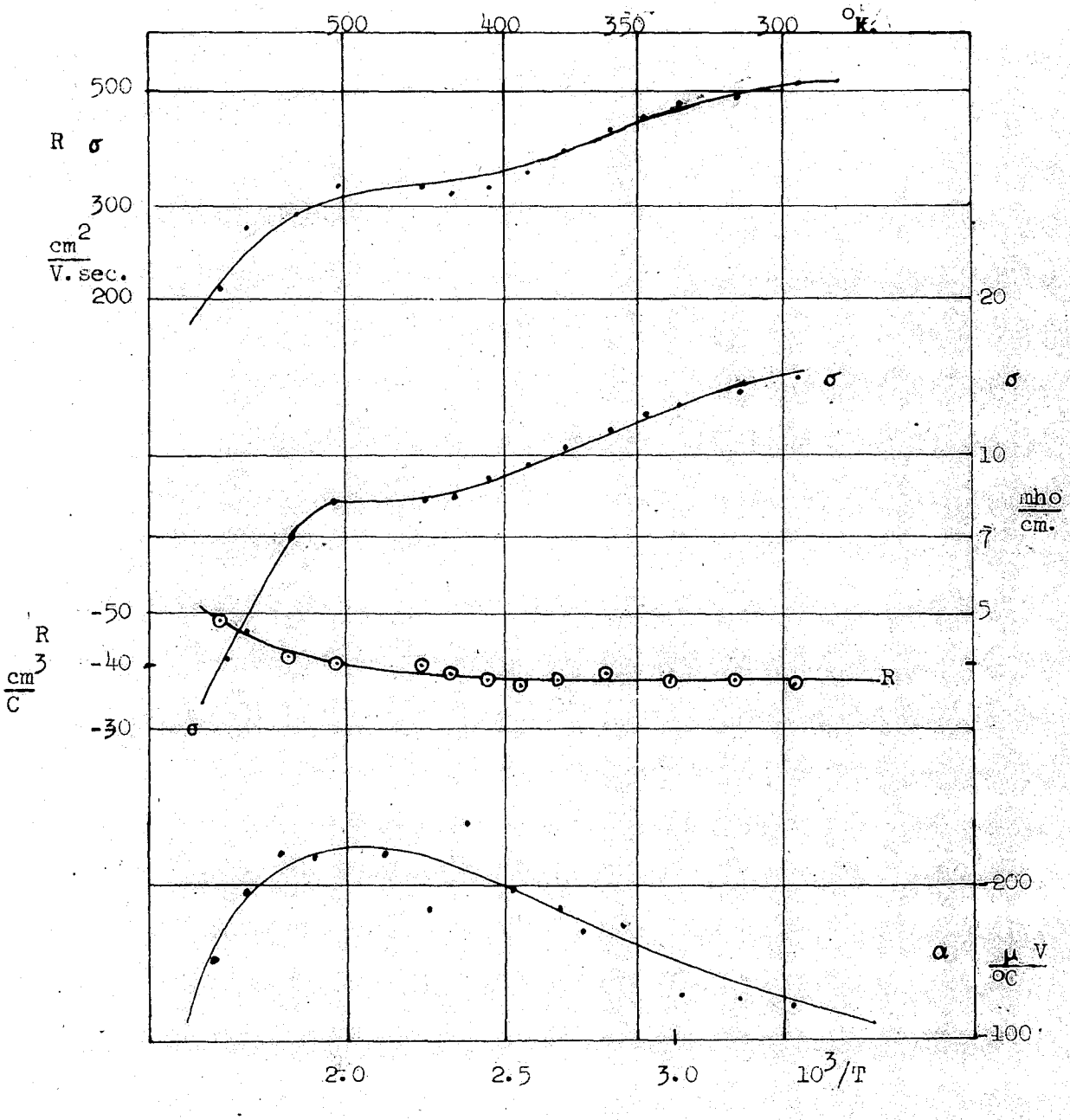

Fig. 42. Electrical Results at 31 mpc.

Temp.	m_n/m
330°K	0.071
500°K	0.087

Table 11. Effective Mass ratio for electrons. Indium Rich 37.5 mpc.

The third sample to be considered in this section is that of 31 mpc mentioned in section 29.22 where it was suggested that the material was two phase and doped n-type. Since the ordered phase has the higher mobility by a factor of 2 or 3, it is probably the most conductive. The electrical results are presented in figure 42. The room temperature value for the electron concentration is 1.7×10^{17} per cm^3. Where the Hall effect is constant, from 300°K to 450°K, the mobility varies as $T^{-1.55}$, indicating lattice scattering. Above 500°K the results appear anomalous and may be due to changes in the condition of the sample. The results for this sample are similar to those for the samples at 37.5 except that the Seebeck coefficient is considerably lower. It is of course possible that both phases are conducting in the 31 mpc ingot and the lowering of the Seebeck coefficient may be due to this.

29.32 p-type and Intrinsic Material

The majority of samples in this region had low carrier concentrations and correspondingly low conductivities. At room temperature the measurement of Hall coefficient and conductivity was often difficult and sometimes impossible.

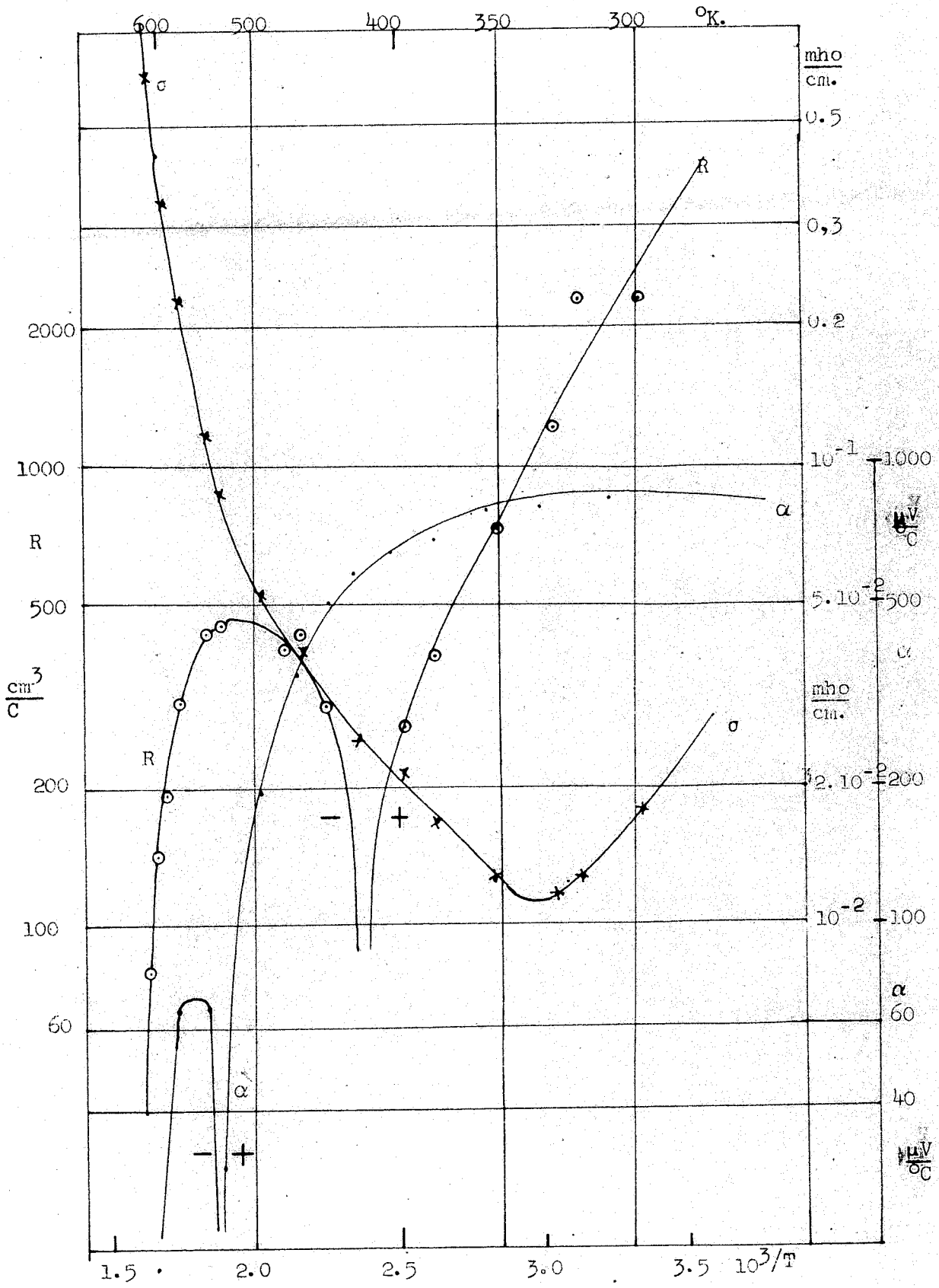

Fig. 43. Electrical Results at 45 mpc.

The electrical results for the p-type sample at 45 mpc are shown in figure 43. The continuous variation of the positive Hall coefficient precludes a calculation for the mobility ratio. However, if it is assumed that the Hall coefficient levels off at or just below room temperature, giving a carrier concentration of 2×10^{15}, then the mobility ratio should be equal to 2 at the negative maximum at 530°K.

It is apparent from the variation of the Hall and Seebeck coefficients above the negative Hall maximum that, although there may be a short intrinsic range, the sample deteriorates rapidly at these temperatures. Assuming intrinsic conditions at 580°K, the mobilities are $\mu_n = 140$ and $\mu_p = 70$ cm²/V.sec, although at room temperature the product $R\sigma$, possibly the hole mobility, is only 30 cm²/V.sec. Low values for the mobility are to be expected since this ingot was not homogeneous. Approximate calculations for the effective mass ratios give the value for electrons and for holes at about 0.3.

Two samples at 37.5 mpc and one at 40 mpc made by different processes, have several characteristics in common. The Hall coefficient is large and negative at room temperature and falls rapidly with increasing temperature as the conductivity rises, while the Seebeck coefficient is positive at room temperature and changes sign at a higher temperature.

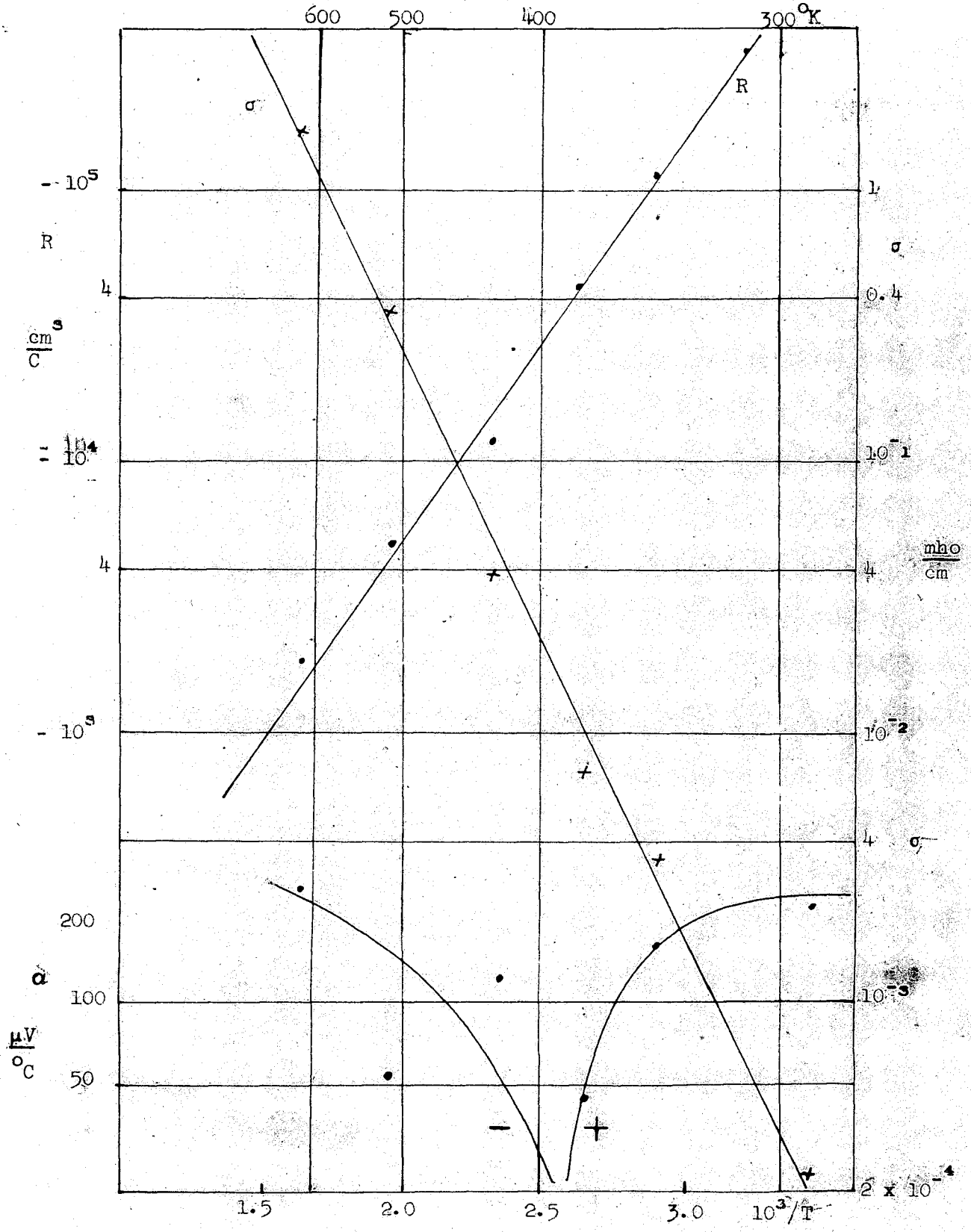

Fig. 44. Electrical Results. Last end to freeze from a directionally frozen ingot at 37.5 m.p.c.

This behaviour is difficult to explain on the basis of the simple theory. It is possible that a combination of mixed conduction and a low value for the mobility ratio, perhaps even less than one, is the explanation. A complex band structure may also be the cause. The possibility that the material is two phase cannot be ruled out as there is no definite X-ray or microscopic evidence against this. Since the samples were aggregates of a few single crystals, electron conduction may have taken place at grain boundaries, while the bulk of the grains were p-type. Further work on single crystal material is clearly needed.

However, for the present purpose, the materials are considered single phase and the electrical properties typical of the bulk. A sample cut from the last end to freeze of the directionally frozen ingot mentioned in section 29.31 gave the electrical results shown in figure 44. The variation of Hall effect and conductivity suggest that the material is intrinsic, although the Seebeck effect does not change sign until 390°K. The slope of the $\log. RT^{3/2}$ v. 1/T graph which is linear to about 500°K indicates an activation energy of 0.58 eV. The number of carriers at room temperature, assuming the material is intrinsic and has a mobility ratio of 2, is 1.25×10^{13} per cm^3. Using these values, the product of the effective mass ratios is 0.035. If the same calculation is performed using the value of the optical energy gap $E_g = 0.74$ eV, then the value of 1.0 is obtained for the product. It seems likely therefore that the material is

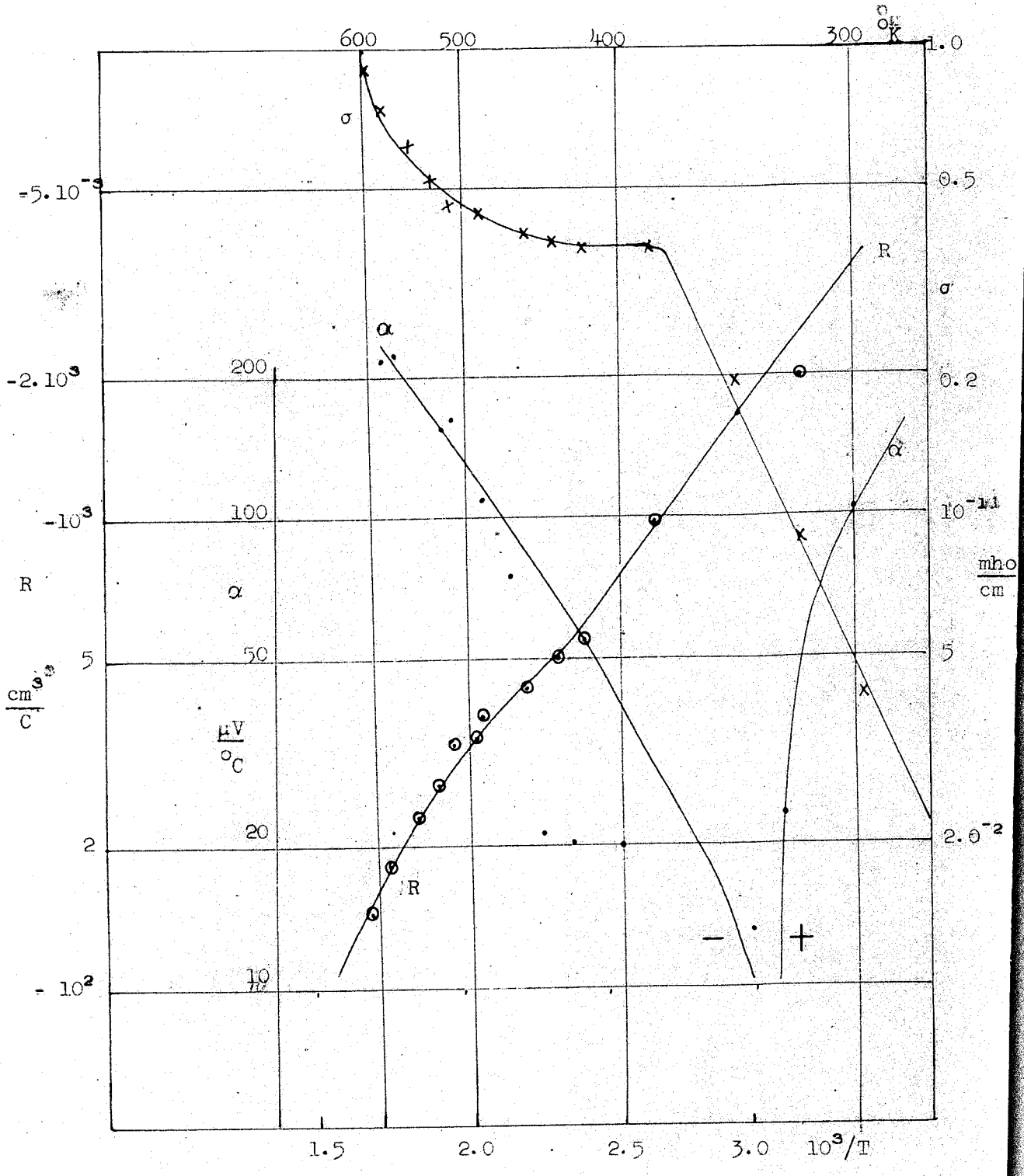

Fig. 45. Electrical Results at 37.5 m.p.c.
Sample annealed for 6 days at 600 °C.

intrinsic with an activation energy of 0.58 eV involving indirect transitions and that the direct energy gap, as determined by the optical absorption, is 0.74 eV. The product Rσ at room temperature is about 300 $cm^2/V.sec$. Under the above assumptions this makes the mobilities $\mu_n = 600$ and $\mu_p = 300$ $cm^2/V.sec$.

The electrical properties of the second sample at 37.5 mpc, formed by the standard method from the elements and annealed for six days at 600°C, are given in figure 45. The Seebeck coefficient changes sign at 345°K. The initial activation energy is 0.31 eV, and that above 500°K is 0.55 eV. If the material is assumed to be intrinsic above 500°K then this sample appears similar to the one above. Below 500°K the measurements were not reproducible and it seems likely that there was some conduction by a second phase probably along grain boundaries.

A sample at 40 mpc, given the standard heat treatment, gave the electrical results shown in figure 46. The Seebeck coefficient changed sign at 460°K. The plot of $\log. RT^{3/2}$ v. 1/T did not yield any definite linear portions; the activation energy obtained from the slope varied from about 0.37 eV to 0.7 eV between 300°K and 500°K respectively. Calculated values for the intrinsic carrier density at 500°K are possibly better explained in terms of an activation energy of 0.58 eV rather than the optical energy gap. The results for this sample are not conclusive.

B

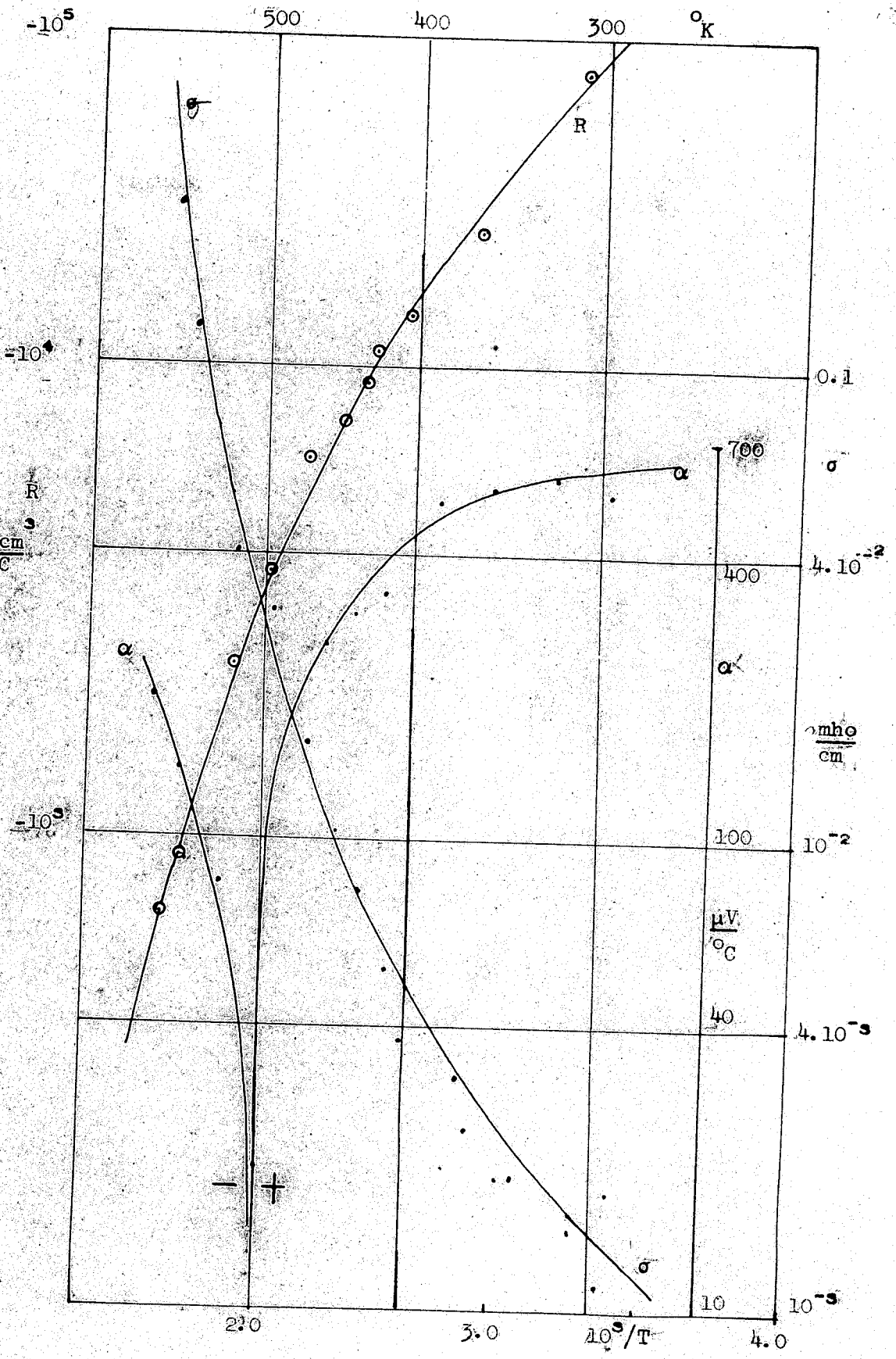

Fig. 46. Electrical Results at 40 m.p.c.

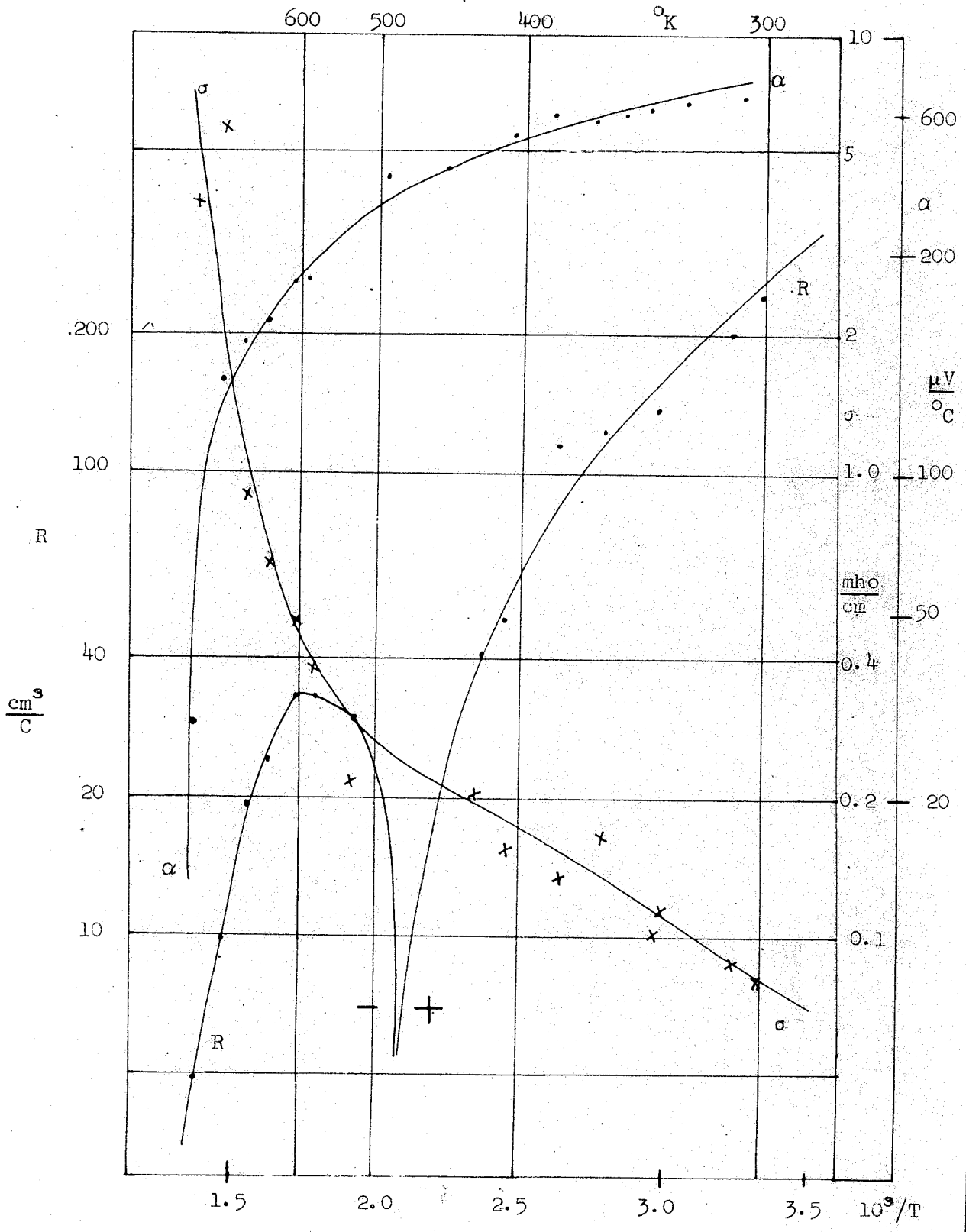

Fig. 47. Electrical results at 50 m.p.c.

29.4 The Disordered Compound at 50 mpc

The maximum in the solidus is thought to occur at the composition $Hg_3In_2Te_6$ whose structure was found to be disordered (sect. 25.3).

The electrical results for a sample cut from the annealed ingot are presented in figure 47. The Hall coefficient indicates that the material is extrinsic being p-type near room temperature and changing to n-type at about 580°K. The Seebeck coefficient does not change sign at the negative Hall maximum but at a higher temperature at which the sample was probably decomposing.

It is not possible to obtain a value for the mobility ratio, although the large and positive Seebeck coefficient and the variation of the Hall coefficient indicate that b cannot be very large. If it is assumed that the material is p-type at room temperature, then the hole mobility is about 18 $cm^2/V.sec$ and if $b = 3$ the value for the electron mobility is 54 $cm^2/V.sec$. At temperatures above the Hall maximum, the product $R\sigma$ is about 17 $cm^2/V.sec$. Consequently, if this is taken as the electron mobility the hole mobility is about 5 $cm^2/V.sec$. In comparison with these for the ordered compound discussed in the previous section, those values for the mobilities are several times lower. This effect is most likely due to the disordering of the atoms and vacancies in the metallic sublattice.

A hole effective mass ratio of 0.39 was calculated from the values of the Hall and Seebeck coefficients at room temperature.

29.5 The Reproducibility of Results

The two topics dealt with in this section are the reproducibility of results with different samples, and the effect of the heat treatment given to samples in the course of the electrical measurements.

There is general agreement between the preliminary set of results (sect. 15.0) and the later set. Differences may be due to several causes. Ingots made up under different conditions naturally have varying carrier densities due to the random inclusion of small amounts of impurities. The degree of homogeneity and the size of the crystal grains also effect the transport properties. The effect of the correct heat treatment in mercury vapour on HgTe has been reported in section 10.0.

Since all the measurements reported in Chapter IV of this thesis were made on polycrystalline material, it is to be expected that measurements on single crystals will be different. In particular the mobility in monocrystalline material, correctly annealed, should be increased, though the energy gap and effective mass should not havealtered.

The second topic is more relevant to this thesis. Under atmospheric pressure, HgTe begins to decompose at about 550°K, but In_2Te_3 can withstand higher temperatures (63). A sample of the 40 mpc composition was held at 600°K for several hours under the conditions of the electrical measurements. Upon examination the

sample was found to have decomposed in the following manner. The remaining part of the sample was composed of a mixture of the 40 mpc composition and In_2Te_3, while on the surrounding sampleholder were deposited small globules of Te. After prolonged treatment at the same temperature on another specimen it was reduced to a hollow shell.

Measurements on any one sample were generally reproducible after heat treatment to 550°K, though it was necessary sometimes to remove the surface layer before remeasurement. The very low conductivities and the correspondingly large Hall coefficients of some materials in the composition range 35 to 50 mpc could not always be regained after such treatment. Some measurements were taken at about 600°K, but, as stated in the relevant sections, they are of doubtful validity.

30.0 Summary of Results HgTe - In_2Te_3 System

Phase		α Disordered		β Ordered	γ Disordered	δ Ordered	
Mpc In_2Te_3		10	22.5	37.5	50	75	
a_o		6.428	6.385	6.338	6.29	6.19[x]	Å
Optical E_g		0.14	0.35	0.73	0.74	0.97*	eV
Activation E_a		-	0.29	0.58*	-	-	eV
b		50*	59	2*	3*	1.4[+]	
μ_n	300°K	4150	800*	600*	54*	-	$\frac{cm^2}{Vsec}$
	550°K	-	203.	300*	17	200[+]	
μ_p	300°K	83*	13.5	300*	18	-	$\frac{cm^2}{Vsec}$
	550°K	-	3.45	150*	5*	140[+]	
m_n/m		0.01*	0.06	0.07	-	-	
m_p/m		-	0.5	0.5*	0.4	-	
K		9.6	9.4	9*	8.8	-	$\frac{mw}{cm\,°C}$

x Measurements by Woolley and Ray (76).

+ Results of Busch et al. (80) see sect. 14.3.

* Indicates approximate value.

Table 12. The properties of the principal phases.

The more important results on the system Hg_3Te_3 - 50 m.p.c. In_2Te_3 are presented in table 12. The electrical and optical results appear to be in accordance with the phase diagram shown in figure 27. These findings need confirmation from differential thermal analysis and electrical measurements on single crystal material which has been annealed in mercury vapour.

Apart from the effect of the ordering which occurs at compositions of 37.5 and 75 m.p.c., the reduction of the electronic mobility with increasing concentration of In_2Te_3 is probably associated with the increase in the energy gap and possibly also with the increasing number of vacancies which act as additional scattering centres. The variation of optical energy gap with composition is much as to be expected in such a system although there is a steep increase in the region of the ordered composition at 37.5 m.p.c.

The results indicate that the band structure changes in the following manner. At about 15 m.p.c. In_2Te_3 the non-parabolic conduction band associated with the low effective mass of the alloys near HgTe is replaced by a broader band of lower mobility. The overlap in energy responsible for the semi-metallic characteristics of HgTe is also removed at about 15 m.p.c. In the region of 20 m.p.c. the optical energy gap and the activation energy appear to correspond at about 0.3 eV. It is probable therefore that the electron energy transitions are direct. The transitions may also be direct in the compound at the 50 m.p.c. composition with an energy gap of 0.74 eV. There are indications that a band of higher electronic mobility, giving indirect transitions of about 0.58 eV., is present in the ordered

compound at 37.5 m.p.c. The optical energy gap, corresponding to the direct transitions, has the value 0.73 eV.

31.0 The Effects of Ordering in the System $Hg_3Te_3 - In_2Te_3$.

The three ordered compositions are $Hg_5In_2\square Te_8$ at 37.5 m.p.c., $HgIn_2\square Te_4$ at 75 m.p.c. the structure of which is chalcopyrite, and $In_2\square Te_3$ which may be obtained both ordered and disordered. The compound $Hg_3In_2\square Te_6$ at 50 m.p.c. was found to be disordered. The proportions of vacancies to lattice sites for the three ordered compounds are 6.25, 12.5 and 16.67 per cent respectively. It is expected therefore that the effects of ordering will be more noticeable where the vacancy concentration is higher. The properties of In_2Te_3 have been reviewed in section 13.

31.1 Energy Gap.

In an alloy system of complete solid solution, the energy gap may follow a linear law over at least part of the range. Figure 29 page 109 shows that, were it not for the ordered composition and the two phase region preceding it, the energy gap would have been linear to 50 m.p.c. In the region of the ordered compound at 37.5 m.p.c. the values of the energy gap lie considerably above this straight line for disordered material. This indicates that the energy gap is increased by the ordering of the structure as in In_2Te_3. Any increase in energy gap in the region of 75 m.p.c. is obscured by experimental error and an insufficient number of measurements. (Some ingots in this region were destroyed during annealing). An increase in energy gap is to be expected on ordering because of the reduction in entropy and the resulting increase in strength of some of the bonds (Section 15, p.245).

31.2 Electronic Mobility

The ordering of the two compounds at 37.5 and 75 m.p.c. has a pronounced effect on the electron and hole mobilities, whose values may be suitably compared with those for the disordered materials at 22.5 and 50 m.p.c. as shown in table 12. A degree of disorder in the lattice produces additional scattering centres and thus lowers the mobility.

The mobility ratio at 37.5 m.p.c. is very much lower than that at 22.5. Consequently, although the electron mobilities are similar (in spite of the doubling of the optical energy gap), the mobility of the holes is much greater for the ordered compound. Both the mobility ratio and the optical energy gap are similar for the ordered compound at 37.5 m.p.c. and for the disordered compound at 50 m.p.c., but the hole and electron mobilities are a great deal larger for the former. The values for the effective masses given in the table suggest that the differences in mobility are due to scattering processes; in this context it would be very desirable in future work to determine m_n at 50 m.p.c. Alternatively, the increase may be due to a change in band structure.

The compound at 75 m.p.c., investigated by Busch et al. (80), shows similar results. In spite of the increase in the energy gap above that of the 50 m.p.c. composition, the mobilities are greater for the ordered compound.

31.3 Thermal Conductivity.

There were not enough suitable specimens for a complete study of the thermal conductivity in the region of the ordered composition. The

results obtained however, do not indicate any appreciable change in the conductivity due to ordering. As was reported in section 13.4 the thermal conductivity of In_2Te_3 is almost doubled in the ordered material.

31.4 Thermoelectric Applications.

The effect of the ordering of the compound $Hg_5In_2Te_8$ is to increase the electron and hole mobilities above the values for the disordered material, without increasing the thermal conductivity appreciably. This indicates that ordering is advantageous for thermoelectric applications for which a high value of the term $\frac{\mu m^{x\,3/2}}{K}$ is required, where m^x is the effective mass.

32.0 Compounds of the Type $II_5III_2\square Te_8$.

Compounds of type have been investigated by several workers. It has become apparent that the ordered structure occurs only when the group II element is mercury, and the group III element is indium or gallium. During the work for this thesis, attempts were made to form the compound $Hg_5Al_2Te_8$ which resulted in several explosions. An ingot was finally produced using extremely slow cooling, but was found to be two phase by microscopic and X-ray analysis, one phase of which was HgTe.

Woolley and Ray (76, 79) found that solid solution existed between compositions of this type and the corresponding II - Te compound when the group III element was indium or gallium and the group II element, cadmium or zinc. No ordered structures were reported for the 528 compositions. Mason and Cook (sec. 14.2) found that the composition $Cd_5In_2Te_8$ occurred in a two phase region.

32.1 $(Hg_{1-x}Cd_x)_{x.5}In_2\square_2Te_8$

In an attempt to produce ordered and disordered material of the same chemical composition ingots were made for the above system at intervals of x = 0.1 from the correct proportions of the compositions at x = 0 and x = 1. Difficulty was experienced in producing ingots at x = 0.4 and x = 0.5 since these appeared to expand on cooling, and if cooled too quickly, cracked the ampoules at temperatures of about 200°C below the freezing points. The materials were annealed for 60 days at 600°C and then cooled slowly to room temperature. The ingots were all polycrystalline and porous to an extent that samples could not be obtained for electrical measurements, although thin sections were cut for infrared transmission studies.

X-ray powder photographs were taken of samples at each composition. The high angle lines at values of x = 0.3 to x = 0.8 were slightly diffuse indicating a degree of inhomogeneity in these samples: the remaining samples were all homogeneous. Microscopic examination showed that all the materials were single phase. The degree of ordering of the structure appeared equally strong in all samples between x = 0 and x = 0.5, but was very slight at x = 0.6. It seems possible that given the correct heat treatments samples at about x = 0.55 could be obtained both ordered and disordered. This was not confirmed.

The results of calculations for the lattice parameter are presented in figure 48. It is noticed that the values of a_o at x = 0.3, 0.4 and 0.5 were considerably larger than the general trend of values. This

agrees with the observed expansion of these ingots on cooling.

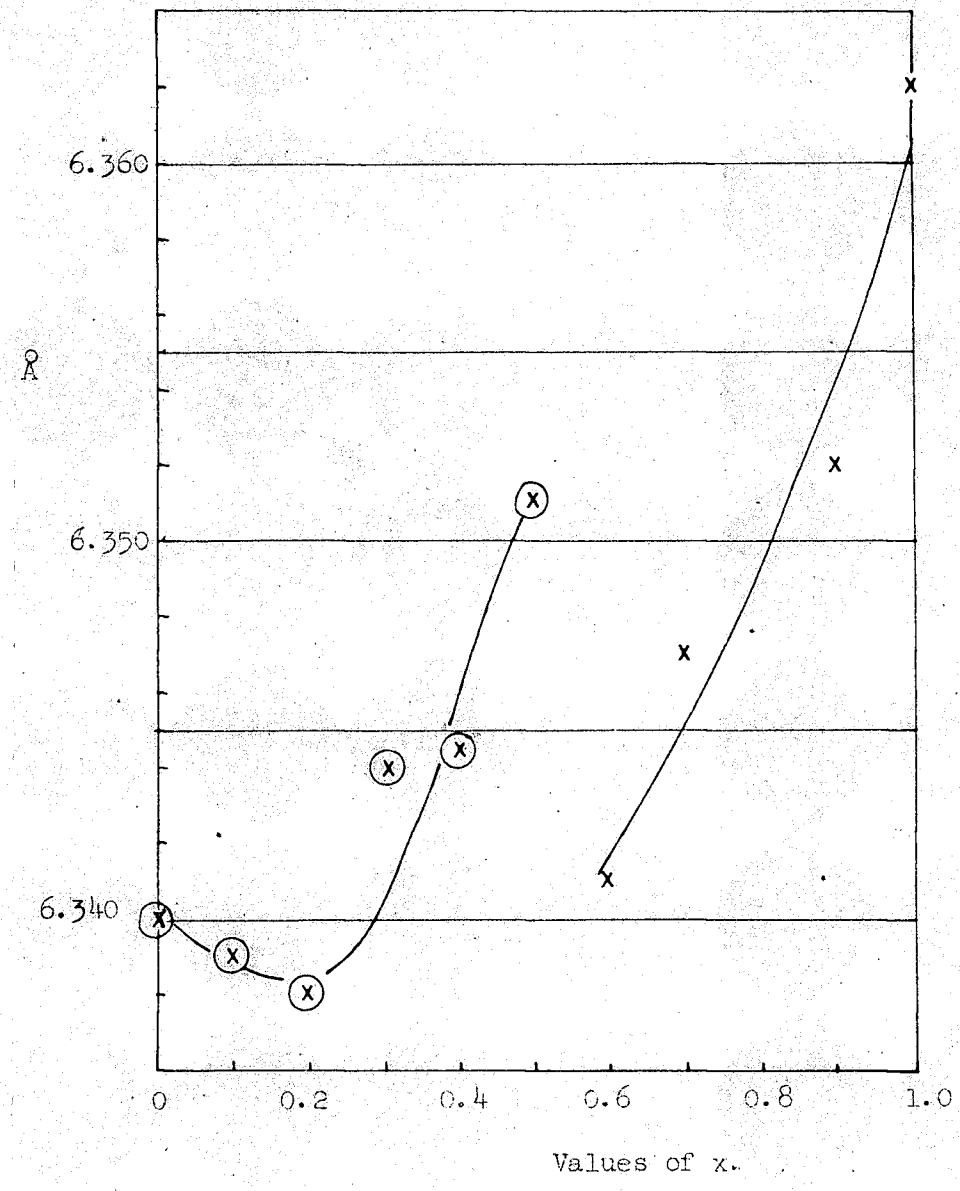

Fig. 48. Lattice Parameter, $(Hg_{1-x}Cd_x)_5In_2Te_8$.

(X) Indicates ordering present.

The absorption edge, determined from the infrared transmission, is shown in figure 49 for each value of x. The accuracy of the measurements towards the cadmium end is not very great due to the difficulty in obtaining suitable sections. It is not possible to deduce any effect of the ordering which ends abruptly between x = 0.5 and x = 0.6.

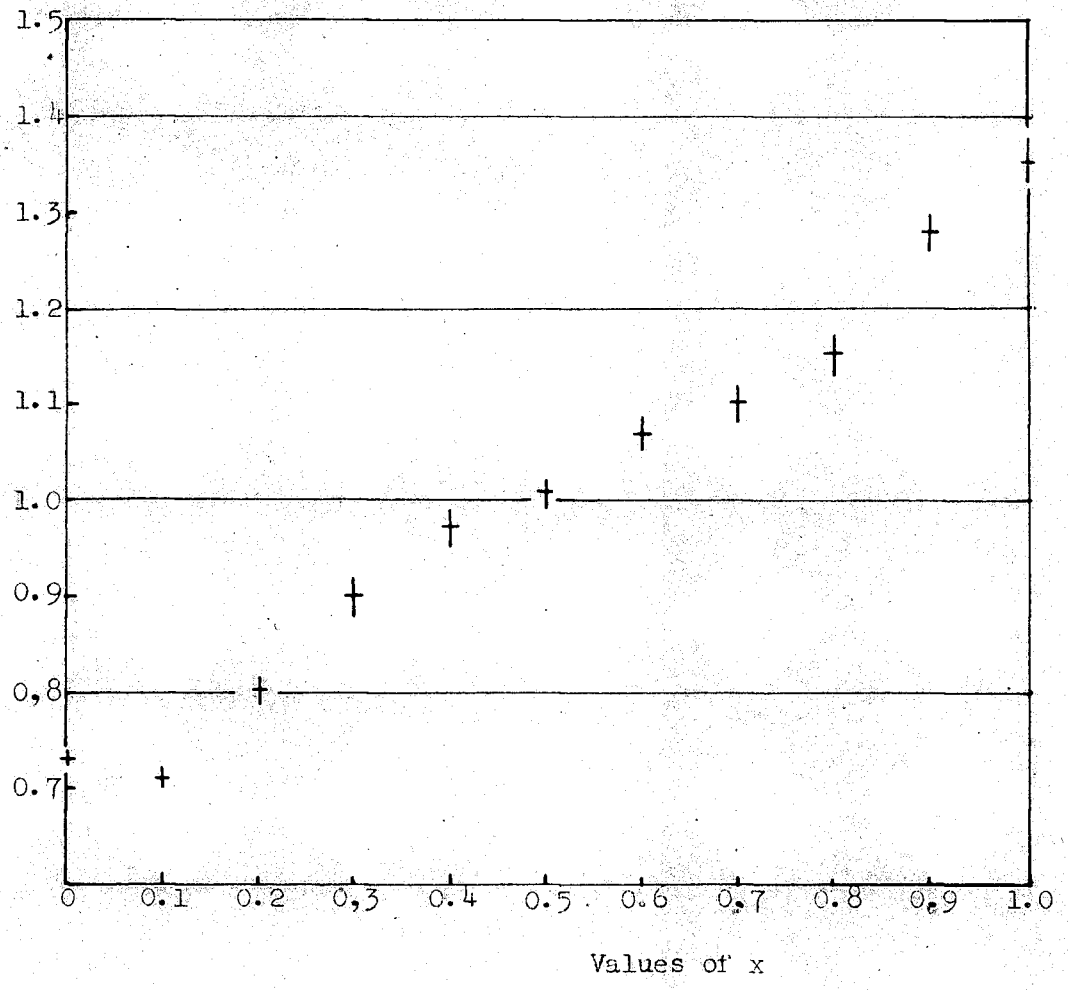

Fig. 49, Optical energy gap, $(Hg_{1-x}Cd_x)_{\frac{5}{3}}In_2Te_8$.

32.2 $(Hg_{1-x} - In_{\frac{x}{2}} Ag_{\frac{x}{2}})_5 In_2 \square Te_8$.

Following the method of cross-substitution used by Goodman (89), the cadmium was replaced by AgIn in the compositions discussed in section 32.1. The ingots were made from the correct proportions of the compositions x = 0 and x = 0.5 since the ingot of the composition corresponding to x = 1 was two phase even after a period of anneal at 600°C. All samples were given the standard heat treatment and none showed the expansion on cooling observed in the cadmium materials.

The results of the calculations for the lattice parameter are shown in figure 50 for x = 0 to x = 0.5. All the X-ray photographs contained well resolved high angle lines, except for that at x = 0.3. This particular ingot had broken during the annealing period so that measurements had to be taken on an unannealed sample. The ordering lines were strongly present at x = 0 to x = 0.3 and weakly so at x = 0.4. The sample at x = 0.5 was completely disordered. No other measurements were made on this system apart from those of the preliminary investigation reported in section 15.0.

The physical condition of the ingots in this system and the sharpness of the lines on the X-ray photographs of annealed material suggest that single crystals could be obtained easily to provide samples for electrical measurements.

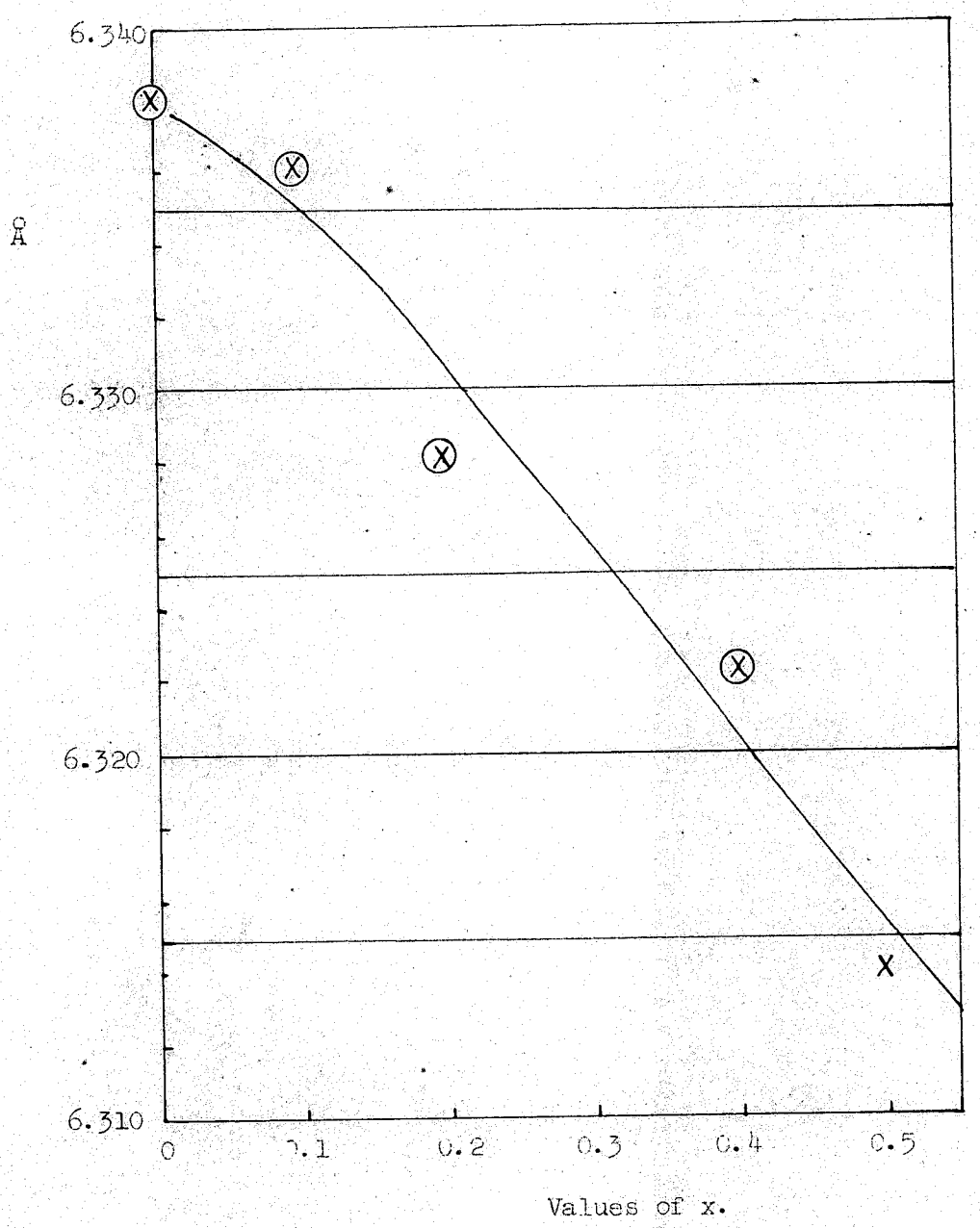

Fig.50. Lattice Parameter, $(Hg_{1-x}Ag_{\frac{x}{2}}In_{\frac{x}{2}})_5In_2Te_8$.

⊗ Indicates ordering present.

33.0 Conclusion: Suggestions for Further Research.

The work presented in this thesis shows that, far from being a simple alloy system, HgTe - In_2Te_3 contains at least five regions of solid solution of which three have ordered structures. The electrical, optical and X-ray properties are in accordance with the phase diagram given in figure 27. In section 31 the effects of the ordering in the system were considered and shown to be quite marked in the electron and hole mobilities and the optical energy gap but not in the thermal conductivity.

As mentioned in the text, there are several instances where further research on the alloy system would be rewarding. The main topics are listed below.

(i) Confirmation of the phase diagram is needed from differential thermal analysis.

(ii) The production of single crystals should be possible for the phases HgTe - 22.5 m.p.c., 37.5 m.p.c., 50 m.p.c., and 75 m.p.c. As some of these are probably peritectic, the method of Mason and Cook is applicable (78).

(iii) The production of material of controlled purity by annealing in mercury vapour may lead to samples with increased values of the mobilities. Doped material could also be produced by varying the stoichiometry slightly or by adding impurities. The variation of Seebeck effect and conductivity with carrier density would be interesting from the thermoelectric point of view.

(iv) Better optical apparatus and thinner sections obtained from

single crystals would lead to higher resolution in the infrared absorption. It may be possible to observe indirect transitions.

(v) The crystal structure of the ordered compound at 37.5 m.p.c. could be determined from the X-ray analysis of single crystals.

(vi) The effect of surface conduction needs to be determined for samples of high resistivity. Single crystals are important for ~~all~~ all electrical measurements on such material to avoid the effect of conduction at grain boundaries.

(vii) Further study of the effective masses and the variation of mobility with temperature may determine whether the structural ordering effect is due to a decrease in scattering centres or a change in the band structure.

(viii) The electrical and optical measurements have yet to be made on the systems involving cadmium and silver. Either system may be used in the study of the effects of ordering, although good ingots of the latter system are more easily obtained.

Appendix I.

The Analysis of Samples.

Previous workers have found that a loss of up to 10 per cent mercury occurred in samples with high mercury content (76,79). As the cost of analysis of samples is large, it was decided that, in the first instance, only four of the samples used for this thesis would be analysed. The four chosen were widely spaced in composition and were not all made from the same ingots of HgTe and In_2Te_3. They were all annealed at 600°C for 60 days.

Sample m.p.c.		Hg	In	Te
12.5	calc.	44.5	4.3	51.2
	anal.	44.7	4.2	51.1
30	calc.	36.8	10.5	52.7
	anal.	36.1	10.7	53.2
40	calc.	32.2	14.3	53.5
	anal.	32.2	14.3	53.5
50	calc.	27.3	18.2	54.5
	anal.	27.3	18.2	54.5

Table 13. The Analysis of Samples in atomic per cent

The analysis was carried out by Johnson, Matthey and Company Ltd., Table 13 shows the results of the analysis compared to the percentage calculated from the nominal chemical composition. There is in general

very good agreement between the analytical and the calculated values, consequently, it was decided that the analysis of further samples was unnecessary. Only the sample at 30 m.p.c. shows an appreciable loss of mercury, though this is only 0.7 per cent. It seems likely that the period of anneal of 12 days used by Woolley and Ray, though it was sufficient to produce homogeneity, was not long enough for all the free mercury to be reabsorbed into the ingot.

References

1. Evans R.C. Crystal Chemistry. 2nd. Ed. 1946.
2. Drabble J.R. and Goodman C.H.L. J. Phys. Chem. Solids. 5. 142. 1958.
3. Smith R.A. Semiconductors. 1959.
4. Mooser E. and Pearson W.B. Progress in Semiconductors. 5. 1960.
5. Kleinman L. Proc. Int. Conf. Semiconductor Phys. Exeter. 552. 1962.
6. Slater J.C. Quantum Theory of Matter. 1951.
7. Hannay N.B. (Ed.) Semiconductors. 1959.
8. Smith B.A. Wave Mechanics of Crystalline Solids. 1961.
9. Hilsum, C. and Rose-Innes A.C. Semiconducting III-V Compounds. 1961.
10. Pincherle L. Proc. Int. Conf. Semiconductor Phys. Exeter. 541. 1962.
11. Krömer H. Progress in Semiconductors. 4. 1960.
12. Putley E.H. The Hall Effect and Related Phenomena. 1960.
13. Lax B. and Mavroides J.G. Solid State Physics. 11. 1960.
14. Lax B. Proc. Int. Conf. Semiconductor Physics. 265. 1962.
15. Ehrenberg W. Proc. Phys. Soc. A. 63. 75. 1950.
17. Ioffe A.F. Physics of Semiconductors. 1957.
18. Drabble J.R. and Goldsmit H.J. Thermal Conduction in Semiconductors. 1961.
19. Tauc J. Int. Conf. Semiconductor Phys. Exeter. 333. 1962.
20. Moss T.S. Optical Properties of Semiconductors. 1959.
21. Cardona M. J. Appl. Phys. Suppl. 32. 2151. 1961.
22. Gasson D.B. J. Sci. Inst. 39. 78. 1962.

23. Herman F. et al. Progress in Semiconductors. 2. 1957.

24. Hansen M. and Anderko K. Constitution of Binary Alloys. 1958.

25. Delves R.T. and Lewis B. J. Phys. Chem. Solids. 24. 549. 1963.

26. Dana E.S. Descriptive Mineralogy. 6th Ed. 64. 1909.

27. Ray B. Thesis Nottingham 1960.

28. Lawson W.D. et al. J. Phys. Chem. Solids. 9. 325. 1959.

29. Blum A.I. and Regel A.R. Zhur. Tekh. Fiz. 21. 316. 1951.

30. Nikolskaya E. and Regel A. Zhur. Tekh. Fiz. 25. 1352. 1955.

31. Tsidil'kovski I.M. Sov. Phys. Tech. 2. 1622. 1957.

32. Elpat'evskaya O.D. and Regel A.R. Sov. Phys. Tech. 2. 35. 1957.

33. Carlson R.O. Phys. Rev. 111. 476. 1958.

34. Lagrenaudie J. J. Chim. Phys. (French) 55. 175. 1958.

35. Bell R.L. J. Elect. Contr. 3. 487. 1957.

36. Black J. et al. J. Elect. Chem. Soc. 105. 723. 1958.

37. Harman T.C. et al. J. Phys. Chem. Solids. 7. 228. 1958.

38. Rodot H. and Triboulet R. C.R. Acad. Sci. (French) 254. 852. 1962.

39. Quilliet A. et al. Proc. Int. Conf. Semiconductor Phys. Exeter. 711. 1962.

40. Giriat W. To be published in Brit. J. App. Phys. 1963.

41. Rodot H. and Rodot M. C.R. Acad. Sci. 248. 937. 1959.

42. Rodot H. and Rodot M. C.R. Acad. Sci. 250. 1447. 1960.

43. Harman T.C. and Strauss A.J. J. App. Phys. Supp. 32, 2265. 1961.

44. Harman T.C. et al. Phys. Rev. Lett. 7. 403. 1961.

45. Strauss A.J. Proc. Int. Conf. Semiconductor Phys. Exeter 703. 1962.

46. Kane E.O. J. Phys. Chem. Solids. 1. 249. 1957.

47. Blair J. and Smith A.C. Phys. Rev. Lett. 7. 124. 1961.

48. Kafalas J.A. et al. J. Phys. Chem. Solids. 23. 1541. 1962.

49. Sorokin O.M. Sov. Phys. Sol. St. 2. 2091. 1961.

50. Braithwaite J. Pure Phys. Soc. B.64. 274. 1951.

51. Kruse P.W. et al. Infra-red Phys. 2. 53. 1962.

52. Quilliet A. et al. J. de Phys. et Rad. 23. 93. 1962.

53. Cardona M. and Harbeke G. J. App. Phys. 34. 813. 1963.

54. Cardona M. and Greenaway D.L. Phys. Rev. (to be published).

55. Ioffe A.V. and Ioffe A.F. Sov. Phys. Sol. St. 2. 719. 1960.

56. Rodot M. et al. J. App. Phys. 32. 2254. 1961.

57. Brach B. Ya. Sov. Phys. Sol. St. 3. 786. 1961.

58. Wright G.B. et al. Phys. Rev. 125. 1534. 1962.

59. Shneider A.D. and Gavrishchak I.V. Sov. Phys. Sol. St. 2. 1865. 1961.

60. Woolley J.C. and Ray B. J. Phys. Chem. Sol. 13. 151. 1960.

61. Blair J. and Newnham R. Metal. Soc. Conf. 12. 393. 1961.

62. Holmes P.J. et al. J. Phys. Chem. Sol. 23. 1. 1962.

63. Woolley J.C. and Pamplin B.R. J. Elect. Chem. Soc. 108. 874. 1961.

64. Zhuze V.P. et al. Sov. Phys. Sol. St. 2. 2857. 1960.

65. Petrusevich V.A. and Sergeeva V.M. Sov. Phys. Sol. St. 2. 256. 1961.

66. Woolley J.C. et al. J. Less Comm. Metals. 1. 362. 1959.

67. Zaslavskii A.I. and Sergeeva V.M. Sov. Phys. Sol. St. 2. 2545. 1960.

68. Woolley J.C. et al. J. Phys. Chem. Sol. 19. 147. 1961.

69. Ioffe A.F. J. Phys. Chem. Sol. 8. 6. 1959.

70. Woolley J.C. et al. J. phys. Chem. Sol. 16. 138. 1960.

71. Kiosse C.A. et al. Izv. Mold. fil. AN SSSR No. 3 (69) p.3. 1960.

72. Woolley J.C. et al. J. Phys. Chem. Sol. 19. 147. 1961.

73. Gasson D.B. Int. Conf. Semiconductor Phys. Exeter 681. 1962.

74. Greenaway D.L. and Cardona M. Int. Conf. Semiconductor Phys. Exeter 666. 1962.

75. Hahn H. et al. Z.anorg.Chem. 279. 241. 1955.

76. Woolley J.C. and Ray B. J. Phys. Chem. Sol. 15. 27. 1960.

77. Thomassen L. and Mason D.R. J. Elect. Chem. Soc. 106. 206. 1959.

78. Mason D.R. and Cook J.S. J. App.Phys. 32. 475. 1961.

79. Woolley J.C. and Ray B. J. Phys. Chem. Sol. 16. 102. 1960.

80. Busch G. et al. Halbleiter und Phosphore 470. 1958.

81. Pamplin B.R. Thesis. Nottingham 1960.

82. Lawson W.D. and Nielsen S. Preparation of Single Crystals 1958.

83. Henry N.F.M., Lipson H. and Wooster W.A. The Interpretation of X-ray diffraction Photographs. 1960.

84. Hackes R.R. and Ure R.W. Thermoelectricity. 293. 1961.

85. Nielsen S. Brit. J. App. Phys. 10. 380, 1959.

86. Goryunova N.A. et al. Fizika. 7. 1962.

87. Evans J. Thesis. Nottingham 1961.

88. Rosi F.D. et al. RCA Review 22. 82. 1961.

89. Goodman C.H.L. J. Phys. Chem. Solids. 6. 305. 1958.